Development of a 400 Level 3C Clamped Downhole Seismic Receiver Array for 3D Borehole Seismic Imaging of Gas Reservoirs

Final Report:

October 1, 2001 – September 30, 2006

Björn N.P. Paulsson

September 30, 2006

DOE Contract: DE-FC26-01NT41234

Paulsson Geophysical Services, Inc.
1215 West Lambert Road
Brea, CA 92821-2819

Phone: 562-697-9711 x 101, Cell: 310-489-5594
Fax: 562-697-9773

E-mail: bjorn.paulsson@paulsson.com
Website: www.paulsson.com

DISCLAIMER

ABSTRACT

Borehole seismology is the highest resolution geophysical imaging technique available today to the oil and gas industry for characterization and monitoring of oil and gas reservoirs. However, the industry's ability to perform high resolution 3D imaging of deep and complex gas reservoirs using borehole seismology has been hampered by the lack of acquisition technology necessary to record large volumes of high frequency, high signal-to-noise-ratio borehole seismic data. This project took aim at this shortcoming by developing a 400 level 3C clamped downhole seismic receiver array, and accompanying software, for borehole seismic 3D imaging. This large borehole seismic array has removed the technical acquisition barrier for recording the data volumes necessary to do high resolution 3D VSP and 3D cross-well seismic imaging.

Massive 3D VSP® and long range Cross-Well Seismology (CWS) are two of the borehole seismic techniques that promise to take the gas industry to the next level in their quest for higher resolution images of deep and complex oil and gas reservoirs. Today only a fraction of the oil or gas in place is produced when reservoirs are considered depleted. This is primarily due to our lack of understanding of detailed compartmentalization of oil and gas reservoirs.

In this project, we developed a 400 level 3C borehole seismic receiver array that allows for economic use of 3D borehole seismic imaging for reservoir characterization and monitoring. This new array has significantly increased the efficiency of recording large data volumes at sufficiently dense spatial sampling to resolve reservoir complexities. The receiver pods have been fabricated and tested to withstand high temperature (200° C/400° F) and high pressure (25,000 psi), so that they can operate in wells up to 7,620 meters (25,000 feet) deep. The receiver array is deployed on standard production or drill tubing. In combination with 3C surface seismic or 3C borehole seismic sources, the 400 level receiver array can be used to obtain 3D 9C data. These 9C borehole seismic data provide both compressional wave and shear wave information that can be used for quantitative prediction of rock and pore fluid types.

The 400-level borehole receiver array has been deployed successfully in a number of oil and gas wells during the course of this project, and each survey has resulted in marked improvements in imaging of geologic features that are critical for oil or gas production but were previously considered to be below the limits of seismic resolution. This added level of reservoir detail has resulted in improved well placement in the oil and gas fields that have been drilled using the Massive 3D VSP® images. In the future, the 400-level downhole seismic receiver array is expected to continue to improve reservoir characterization and drilling success in deep and complex oil and gas reservoirs.

TABLE OF CONTENTS

LIST OF FIGURES

LIST OF TABLES

EXECUTIVE SUMMARY

This project successfully developed and commercialized a 400 level 3C borehole seismic receiver array consisting of five 80 level 3C arrays which can be deployed in one well or simultaneously in five wells. As of September 30, 2006 these borehole seismic arrays had been deployed together or individually in about 30 different wells. The technology developed in this project has recorded the 20 largest Massive 3D VSP® surveys in the oil and gas industry. With a couple of exceptions, every survey recorded with the 80 – 400 level arrays is a larger survey than what has been recorded during any other survey by any other borehole seismic tool.

INTRODUCTION

This project was undertaken to develop a borehole seismic array and companion software for advanced 3D/4D 3C VSP imaging of complex natural gas reservoirs. This document reports on the development of a 3C borehole seismic array comprised of 5 cables, each 3,657.6 – 6,096 meters (12,000 – 20,000 ft) long with 1,219.2 meters (4,000 feet) long active array sections, which can be deployed separately or as a continuous 6,096-meter (20,000-foot) array. A long borehole seismic array is essential to economically record enough data to do 3D VSP imaging or large data volume cross well imaging.

In the past borehole seismic arrays have been deployed using seven conductor wireline technology. A seven conductor wireline has a limited data band width, limited mechanical strength and are limited to operations in wells which are vertical or nearly vertical. These limitations put severe restrictions on the number of receivers that can be deployed on a wireline based array. Today, the maximum number of receivers that can be deployed on a wireline based array recording data with 2 ms sampling rate is about 20. The tubing deployed downhole array developed by P/GSI and discussed in this report can in principle deploy several thousand receiver levels overcoming the limitations with wireline deployed borehole receiver arrays.

COMPLETED TASKS

The following tasks were completed during the course of the project:

Task 1.0 -- Design of Receiver Array:

The receiver array design was completed successfully. The project team designed the array to work with wellhead pressure control equipment. The cables and the geophone pods were designed to include 400 receiver levels. The 400 level array was designed using five separate cables, each with 80 receiver levels. Each receiver level was designed as a geophone pod containing 3 component geophones. The P/GSI project team designed the tubing, geophone pod housings, deployment equipment, winches, geophone pods, and the system used to transport the 400-level receiver array to the field.

P/GSI designed the 400 level borehole seismic array using P/GSI's existing borehole seismic array as a starting point. The cable was updated using a new thermal plastic material and the geophone pods were manufactured in steel rather than polyurethane. We have redesigned the 3rd generation cables and tested the 3rd generation prototypes of the new array to a temperature of 200° C (400° F) and 12.20607 kg/cm2 (25,000 psi).

It was necessary to identify and select temperature components that could operate reliably in the range of 150° C (300° F) to 200° C (400° F) to achieve capability of operating in deep wells, up to7,620 m (25,000 ft). Some of the components were commercially available and could be immediately incorporated into the high temperature array. High temperature geophones that operate to a temperature of 200° C (400° F) are available from several manufacturers.

To ensure that the array would work with wellhead pressure control equipment, the project team conducted interviews with operators of gas fields to gain a full understanding of the required functions of the array to be acceptable for deployment in a well with high temperatures and pressures. The resulting design has a well head feed-through mechanism that simultaneously holds the production tubing and the cables. This system allows for recording data in a well that is pressurized.

The project team designed the analog cables for the 400 level 3C receiver arrays. The analog cables contain a twisted pair for each geophone, so the cable design is capable of transmitting data over 9,144 m (30,000 ft) long cables. The 9,144 m (30,000 ft) of analog data transmission has met with general acceptance among geophysicists that have been consulted on this key issue. In surface seismic surveys, analog lines as long as 15,240 m (50,000 ft) were and are routinely used. The borehole is furthermore a very quiet environment electrically so very little noise couples into the arrays. The lead-in cable with 126 twisted pairs in our first array was 3,048 m (10,000 ft) long with no apparent degradation in data quality.

The cable design was modified to accommodate 276 twisted pairs, up from the previous 126 pairs, using magnet wire that connects the geophones in the geophone pods with the digitizing electronics on the surface. This design change was accomplished without changing the outside diameter of the cable. The 276 twisted pair cable allow us to deploy 80 3C levels, 240 channels, on one cable. The geophone pod design was changed to include a steel housing and steel end caps. These changes increase significantly the pressure rating of the geophone pods. The pressure rating of the new design is12.20607 kg/cm2 (25,000 psi), confirmed by testing – a high enough rating for a receiver array deployment to a depth of 18,288 m (60,000 ft) in water. The 3rd generation pods have been successfully cycle tested to a pressure of 12.20607 kg/cm2 (25,000 psi) at 200° C (400° F) without any leaks or failures.

P/GSI designed the tubing required for deploying the 400 level geophone array. A 4.2164 cm (1.660") tubing was selected using a EUE type tubing, 10 Rd threads and an N80 material. There are stronger specialty steels if deeper deployment and higher strength is required.

The geophone pod housings were designed to protect the geophone pods during the deployment of the array, and to contain the clamping mechanisms for the geophone pods. The project team designed the geophone pod housings to be able to handle an axial load of 49,895.1607 – 54,431.0844 kg (110,000 – 120,000 lb). In a test, a preliminary design failed at a load of 44,452.05226 kg (98,000 lb). P/GSI also designed all the deployment equipment to safely deploy the receiver arrays in gas wells. These equipment components include: sheave wheels designed to guide the cables from the winches to the well, work plate for safely working over the well, specialized tools for attaching the cables to the geophone pod housings, a new bottom assembly for the array, a new top assembly to control and regulate the clamping of the geophones, a new centralizer to protect cable splices, and a new cable protection sub designed to protect the cable through blow-out preventers.

P/GSI designed the spools for the geophone pod cables. The new spool has a sturdy frame which allows lifting and handling the unit without risking damage to the cable. The spool design also incorporated a foot switch that allows one person to both operate the spool and control the cable spooling. The spools can hold up to 7,620 m (25,000 ft) of cable.

P/GSI also designed the field unit used to transport the 400 level receiver array system to the field. The field unit allows secure transport and handling of the equipment to the field and serves as the operator's cab, with power, heating, and cooling.

Task 2.0 -- Manufacture of Receiver Array:

The receiver array was manufactured in two stages. Initially, P/GSI had five sub arrays manufactured by a subcontractor for the 400 level analog receiver array. This first set of cables was flawed, and it was necessary for P/GSI to redesign the cables to overcome these flaws. The re-designed cables are referred to as P/GSI's 3rd generation cables.

In order to verify the specification of the arrays P/GSI tested prototypes of the new components to a temperature of 204.45° C (400° F) and 12.20607 kg/cm2 (25,000 psi). After testing the prototypes of the 3rd generation arrays, the 3rd generation cables were built.

P/GSI manufactured the tubing required for deploying the geophone array, the geophone pod housings, the deployment equipment, the winches for the cables and geophone pods, and the system used to transport the 400 level receiver array systems to the field.

Task 3.0 – Development of Processing and Imaging Software:

P/GSI developed advanced data processing and imaging software modules to handle the 9C borehole seismic data. The processing system is closely linked to the acquisition system with interfaces that allow for communication with other systems in a secure and speedy manner.

P/GSI developed a data flow management sequence and infrastructure for 9C data volumes. The software framework is based on a multi-threaded object flow, which allows for fast parallel as well as pipelined computation on suitable computer hardware. The software infrastructure keeps track of the data types, origins, and destinations.

P/GSI developed the data analysis modules to perform 9C data processing, including modules for 9C wave field separation; modules for 3D velocity model estimation; and modules for 3D imaging. These modules have been incorporated into P/GSI's proprietary borehole seismic processing system.

Justification for Removal of Field Demonstration

In the original contract between P/GSI and DOE, we had planned to conduct a field demonstration of the borehole receiver array, after design, manufacture, and initial testing were completed. However, the field demonstration became unnecessary because a number of successful field demonstrations were completed using P/GSI's receiver array system in commercial surveys for industry. The completion of successful field tests with industry removed the need for the project to proceed to a formal demonstration phase.

RESULTS AND DISCUSSION

During 2002, the first year of this project, P/GSI successfully completed the engineering design, assembly and the initial testing of the 400 level 3C borehole seismic array. Paulsson Geophysical was directly responsible for the design of the deployment system. The deployment system is designed to work with analog, digital or optical cables. The 2nd generation cables purchased for this project are analog and were based on a design used for standard seismic land cables as far as data transmission was concerned.

During the entire project P/GSI continued to develop the software for processing the borehole seismic data. Much of the work relates to building data management tools for handling the large amounts of data generated by the large borehole seismic arrays. P/GSI was also working on developing velocity model building tools and plotting tools for displaying borehole seismic data together with well logs and surface seismic data. We continued to upgrade the data pipeline tools to manage the input queue of our borehole seismic data into our cluster.

Initially the data recorded was very good but the quality of the data deteriorated after a couple of surveys.

We found that the first analog cables and geophone pods designed and built only lasted two surveys before the cables deteriorated to the extent that the data quality became unacceptable.

During 2003, the second year of this project, three of the 2nd generation cables completely failed at temperatures and pressures below the temperature and pressure specifications in

P/GSI's purchase orders for the five cables. We also P/ discovered the reason for the deterioration of the data recorded by the first arrays after the first two surveys. We found that the design and the manufacturing of 2nd generation borehole seismic receiver cables were flawed in six different ways; three flaws in the geophone pod design and three material and design flaws in the cable.

It became clear during 2003 that the 2nd generation cables could not be repaired but had to be replaced. Paulsson Geophysical Services, Inc. decided to take on the direct responsibility of designing and building new cables working with new suppliers. The new 3rd generation design of the downhole cables was designed and developed entirely by P/GSI personnel. We have verified that the materials and equipment built by the new vendors can operate at the specified temperature of 200° C (400° F) and pressure of 12.20607 kg/cm2 (25,000 psi) by subjecting prototypes of the new design to extensive tests at these temperatures and pressures simultaneously in a test vessel.

During 2004, the third year of this project, we took delivery of 1,000 new omni-directional 15 Hz geophone elements that were used for the first four 3rd generation arrays that were manufactured to replace the previous analog cable arrays. A prototype of the redesigned geophone cable was tested during this period.

During 2004, we received the first high temperature bulk cable from our new cable manufacturer. This high temperature cable was terminated using the 3rd generation pod design. This cable is able to operate at temperatures up to 200° C (400° F) and pressures up to 12.20607 kg/cm2 (25,000 psi). This 80 level high temperature 3C cable is terminated using 15.24 m (50 ft) pod spacings.

In October 2004 Paulsson Geophysical published a paper on our Massive 3D VSP® technology in a geophysical journal, *The First Break,* published by EAGE. One of our customers, Anadarko, published a monitoring case study recorded and processed by P/GSI. This article was published in The *Leading Edge,* a leading industry journal published by SEG.

During 2005, the fourth year of this project, the new cable manufacturer delivered 3,657.6 m (12,000 ft) of our new medium temperature bulk cable to P/GSI. The cable jacket material for this cable is commercially available polyether based polyurethane with a temperature rating of 105°C (221º F). In early 2005 we completed the first all new redesigned cable by terminating and attaching the 80 connectors, using a P/GSI designed molding process, to the 3,657.6 m (12,000 ft) of new bulk cable.

During 2005 we continued to refine the new manufacturing process for our downhole cables based on the experience of the SAFOD well. During this period we also developed a new testing instrument which would allow us to evaluate our cables faster. It is an instrument built by Seismic Source, Inc.

Towards the end of 2005 we placed purchase orders with our new suppliers for equipment to build four complete all new 3rd generation downhole receiver arrays. This equipment was to be delivered in 2006.

A large number of surveys were recorded with the arrays developed under this project, in various oil and gas fields and with various objectives. The arrays using the 3rd generation cables and pods have been able to record outstanding data. The 3rd generation cables, designed by the P/GSI team, have thus far not failed or deteriorated despite being used for seven surveys. The data quality and quantity is far beyond what any other downhole seismic array has been able to record.

The following surveys were recorded with the 2nd and 3rd generation downhole arrays in the period 2002 – 2006.

The surveys recorded since the project was started are listed below together with a note on the performance of the cables used for the particular survey. The arrays were deployed in 27 wells in 16 different surveys in the report time period.

1. Thums, Long Beach, CA, Feb 2002. 2nd generation cable. A five well offshore Massive 3D VSP® recorded in Feb. 2002 recording a total of 7.5 million traces. This is the largest VSP survey ever recorded (see 41234R20Thums.pdf). The Input/Output cable that was used in three of the five wells failed during the third survey.
2. BP Milne Point, AK, March 2002. 2nd generation cable. A four well 960 channel Massive 3D VSP®, March 2002 recording a total of 3.2 million traces. This is the largest on-shore VSP survey ever recorded (see 41234R20BP.pdf). The survey was very successful.
3. LBL/DOE 9C VSP in NM, July 2002. 2nd generation cable Parts of the Input/Output cables used for this survey failed (see 41234R20LBL_DOE_NM.pdf).
4. Large Major Oil Company, Jan. 2003. 2nd generation cable. Our first 160 level VSP survey – two 80 level cables were deployed simultaneously. Parts of the Input/Output cables used for this survey failed. Note that this was a proprietary survey.
5. Large independent. March 2003. 2nd generation cable. The second survey of a time lapse VSP survey recorded to monitor the injection of CO2 for enhanced an enhanced oil recovery project. The Input/Output array failed and the survey had to be re-shot at Paulsson Geophysical Services, Inc.'s expense. Note that this was a proprietary survey.
6. Large Major Oil Company. March 2003. 2nd generation cable. A Massive 3D VSP® shot concurrent with the surface seismic survey. The Input/Output array failed. Note that this was a proprietary survey.

7. Anadarko, WY. July 2003. 2nd generation cable. Re-shooting the second survey of a time lapse VSP survey recorded to monitor the injection of CO2 for enhanced an enhanced oil recovery project.
8. Anadarko, AK, February 2004. 3rd generation cable. The first survey using the redesigned 3rd generation cable. The objective of the survey was to map and delineate methane hydrate deposits on the North Slope of Alaska. P/GSI presented a joint paper with Anadarko at the SEG 2005 conference in Denver Colorado on this Massive 3D VSP® survey. This paper was selected as one of the best 20 papers presented at the 2004 SEG meeting. The survey was an outstanding success.
9. Large Major Oil Company. February 2004. 2nd generation cable. A three well Massive 3D VSP® survey. The largest Massive 3D VSP® survey ever to be recorded in the Middle East. The objective was to characterize an oil field with very poor surface seismic data. The Input/Output arrays failed during the survey and the data was judged unacceptable by the client. Note that this was a proprietary survey.
10. LBL/DOE, TX. August 2004. 3rd generation cable. The third survey using the new 3rd generation pod design was completed recording data for Lawrence Berkeley Laboratory for a CO2 sequestration project in Frio, Texas. This survey was a time lapse survey recorded for Department of Energy (DOE), Lawrence Berkeley Laboratory (LBL) and University of Texas, Bureau of Economic Geology (BEG). The outstanding data recorded during this survey showed that the new geophone pods display superior dynamic performance over the pods that were incorporated in the previous cables. The superior vector fidelity of the data recorded with the new 3rd generation cable allow us to perform better and more accurate separation on the P and S wave fields resulting in better P and S wave images. The objective of this survey was to map the injection of CO2 in a saline aquifer for the purpose of demonstrating technology to sequester CO2.The survey was an outstanding success. LBL has published several papers on this survey.
11. LBL/DOE, TX. October 2004. 3rd generation cable. The second survey of a time lapse VSP to monitor the effect of injecting CO2 in a saline aquifer to sequester CO2. The survey was an outstanding success. LBL has published several papers on the two time lapse surveys.
12. Large Major Oil Company. March 2005. 3rd generation cable. A two well walkaway survey recorded in Canada. The survey was an outstanding success. The recorded data from this survey is outstanding. Note that this was a proprietary survey.
13. Earthscope, USGS. May 2005. 3rd generation cable. We recorded a VSP survey and a passive seismic monitoring survey for Earthscope, USGS and Stanford. We recorded this survey by deploying our newly built 80 level cable array in a well next to the San Andreas Fault (The SAFOD well) for about two weeks. The maximum deployment depth was a drilled depth of 2,743.2 m (9,000 ft) and the maximum temperature was about 110º C (232 º F). At the time of the survey the well was drilled to a depth of 3,048 m (10,000 ft). The well was deviated about

50° from the vertical. When the well was logged the logging tools had to be deployed using tubing. Since the P/GSI downhole receiver array uses tubing as an integral part of its deployment system, P/GSI was able to deploy the 80 level receiver array without any problems. In the two week period we recorded about 1,000 large and small earthquakes. We correlated about 100 of the larger earthquakes recorded by P/GSI with the earthquakes recorded on the extensive seismic network deployed by USGS on the surface around the SAFOD research site. However, 90% of the earthquakes recorded on the downhole array were too small to be recorded on the surface receivers. One of the small earthquakes, (M0.0) recorded by the P/GSI array was used by USGS and SAFOD project to guide the borehole towards an active part of the San Andreas Fault. The well penetrated the San Andreas Fault on August 2, 2005. This survey has generated a number of publications at the AGU, SEG and other geophysical meetings. The survey was an outstanding success.

14. Large Major Oil Company. November 2005. 3rd generation cable. Recorded a large walk away survey in a San Joaquin Valley Oil Field. The survey was a success. We recorded data in excess of 100 Hz in an area where surface seismic only records 15 – 20 Hz. We saw clear reflections from a depth of 1,828.8 m (6,000 ft) undershooting the near surface heavy oil zone that had been extensively steamed. In this survey we successfully operated the first new cable to a maximum temperature of 111.11° C (232° F) without any damage. This survey was our first commercial survey with our all new 3rd generation downhole receiver array. The data was processed with the resulting image delivered in early 2006. Note that this was a proprietary survey.
15. Large Major Oil Company. March 2006. 3rd generation cable. A two well Massive 3D VSP® survey recorded in Canada. This survey was the largest Massive 3D VSP® ever to be recorded in Canada. The survey was an outstanding success recording 400 Hz data. This was the seventh survey using this cable and there were no signs of deterioration or aging of the cable after these seven surveys. These results demonstrate the viability of the new 3rd generation array design and manufacturing. Note that this was a proprietary survey.
16. Large Major Oil Company. September 2006. 3rd generation cable. The largest single well Massive 3D VSP® survey ever recorded – about 2.8 million traces. The survey was an outstanding success recording 160 Hz data. Note that this was a proprietary survey.

RESULTS OF NON-PROPRIETARY SURVEYS

Thums, Long Beach, CA. 2nd generation cable.

Shot Point Coverage and the five wells used for the 3D VSP survey

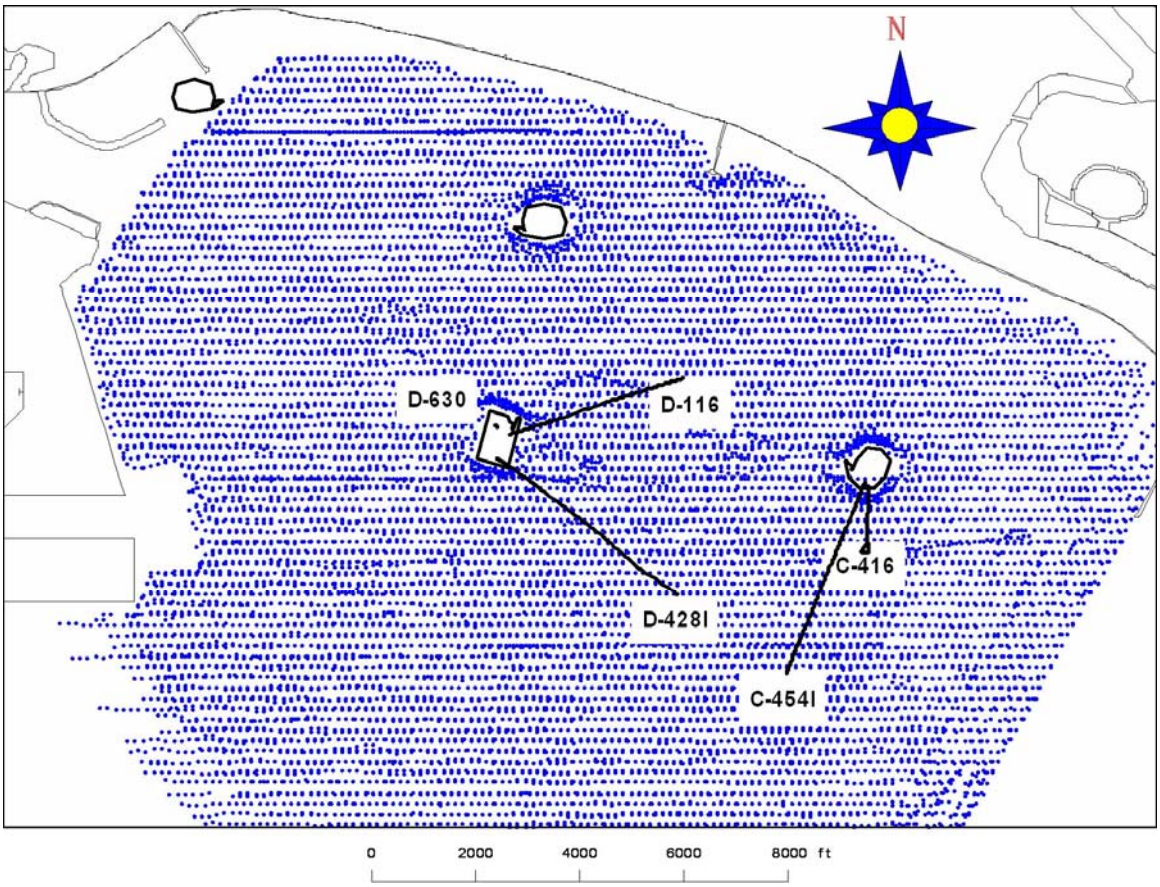

Figure 1. Shotmap from the Thums offshore survey with a total of 35,000 shots (Paulsson et al., AGU).

This survey was a five well offshore Massive 3D VSP® in Feb. 2002. With its 7.5 million traces recorded using 35,000 shot points this is the largest VSP ever recorded. Results were published at the Annual Meeting of the AAPG in 2003.

Discovered in 1932, Wilmington Oil field is the third largest oil field in the Lower 48 States. It is in an advanced state of depletion and currently undergoing water flooding over large parts of the field. To prolong the economic life of the field, it became critical to more thoroughly understand details of the complex faulting and distribution of the basinal turbidite reservoirs. Existing ocean-bottom seismic data are characterized by 15 - 20 Hz frequency and are insufficient to resolve any but the largest-scale features.

The field operator, Thums, a unit of Oxy, is operating this field on behalf of the City of Long Beach and State of California, engaged the services of Paulsson Geophysical Services, Inc. (P/GSI) to acquire a multi-well Massive 3D VSP®. Combining multi-well acquisition techniques with high-resolution, in-well technology offered the potential to very efficiently acquire seismic data of sufficient resolution to unravel the structural and stratigraphic complexities. The Massive 3D VSP® survey generated an image that had 120 Hz data multi-component data, dramatically better than the existing 15 - 20 Hz ocean-bottom seismic data.

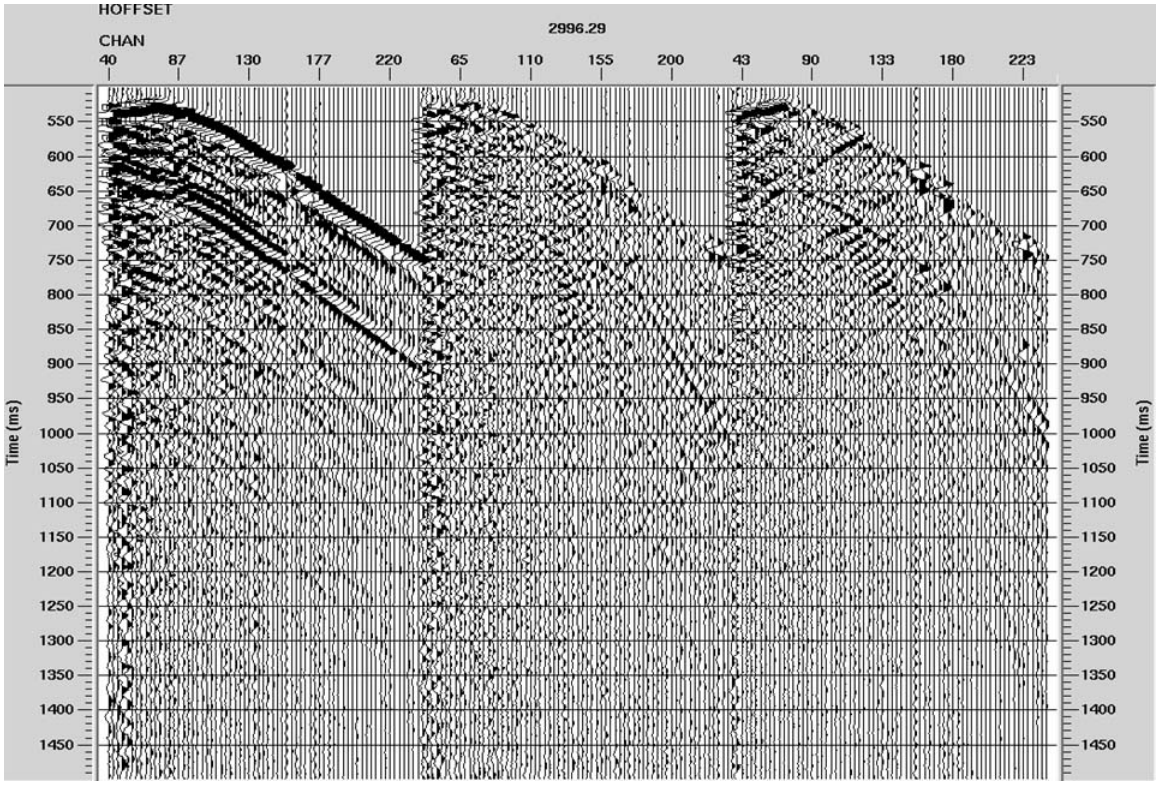

Figure 2. From the Thums offshore survey. A single shot record using an 812.8 c/cm (320 cubic inch) airgun recorded by P/GSI downhole array. The source offset is about 914.4 m (3,000 ft). Note the high signal to noise ratio. The three components have been rotated. The first component is pointing towards the source and one of the radial components is horizontal and the second radial component is perpendicular to the two first components. (Paulsson et al., AGU 2003).

Full Bandwidth Images in the same cross section of the oil field

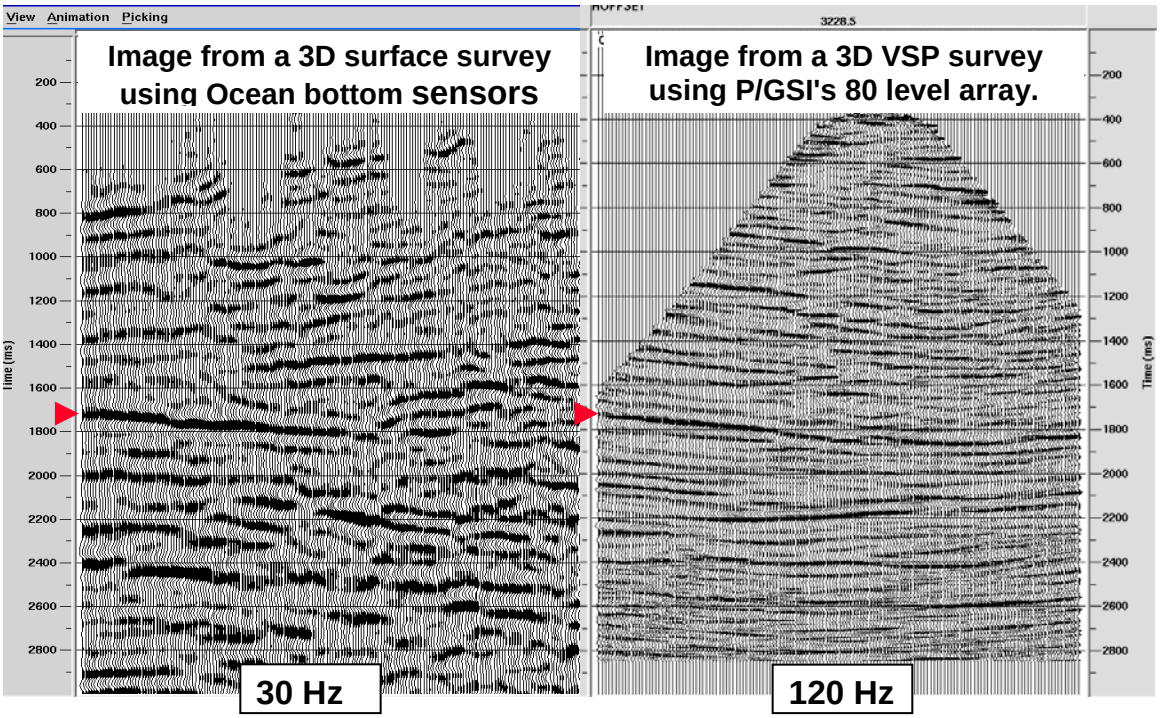

Figure 3. From the Thums offshore survey. Two images from the same cross section. The left image is from a 1995 OBS survey and the right image is from P/GSI's Massive 3D VSP® survey recorded in 2002. (Paulsson et al., AGU 2003).

BP Milne Point, AK. 2nd generation cable.

A four well Massive 3D VSP® was recorded in March 2002 to aid drilling at BP's Milne Point S Pad project, a development of the Schrader Bluff formation. Field development is dependant upon multilateral completions in a thin and highly faulted reservoir zone. Successful drilling of the multilaterals requires prediction of numerous small throw faults not seen in conventional surface seismic. A simultaneous 3D VSP was acquired in 4 wells to provide high resolution seismic data in order to detect small faults within a 9.144 m (30 ft) thick sand. Results published at the SEG 2002.

The 3D VSP resulted in stacked data with frequencies up to 120 Hz and a central peak frequency of 50-60 Hz near the edge of the survey. The 15.24 m (50 ft) receiver spacing interval allowed a close match of the velocities at the vertical well location. The 3D VSP provided a high frequency, high fold image over the Schrader Bluff development area. Drilling in the summer of 2002 confirmed the accuracy of this survey. Clair et al. 2002.

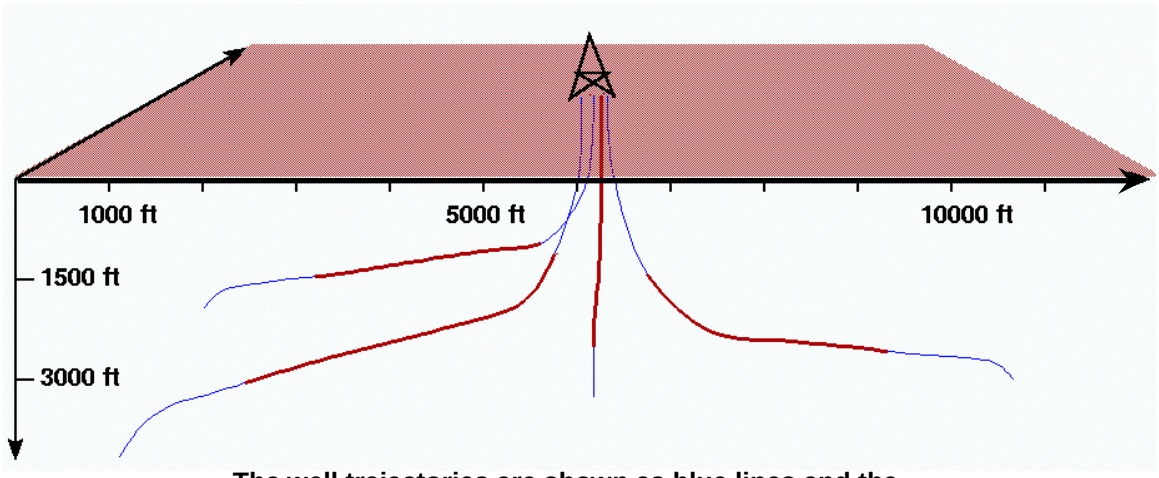

The well trajectories are shown as blue lines and the position of the four arrays is indicated by the red lines.

Figure 4. From the BP onshore Milne Point survey. Four 80 level arrays were deployed in four different wells. Three of the wells were highly deviated. We recorded a record breaking total of 960 downhole channels in this survey was 960 channels. The total number of source points was about 3200 producing a 3 million trace Massive 3D VSP® (Clair et al. 2002).

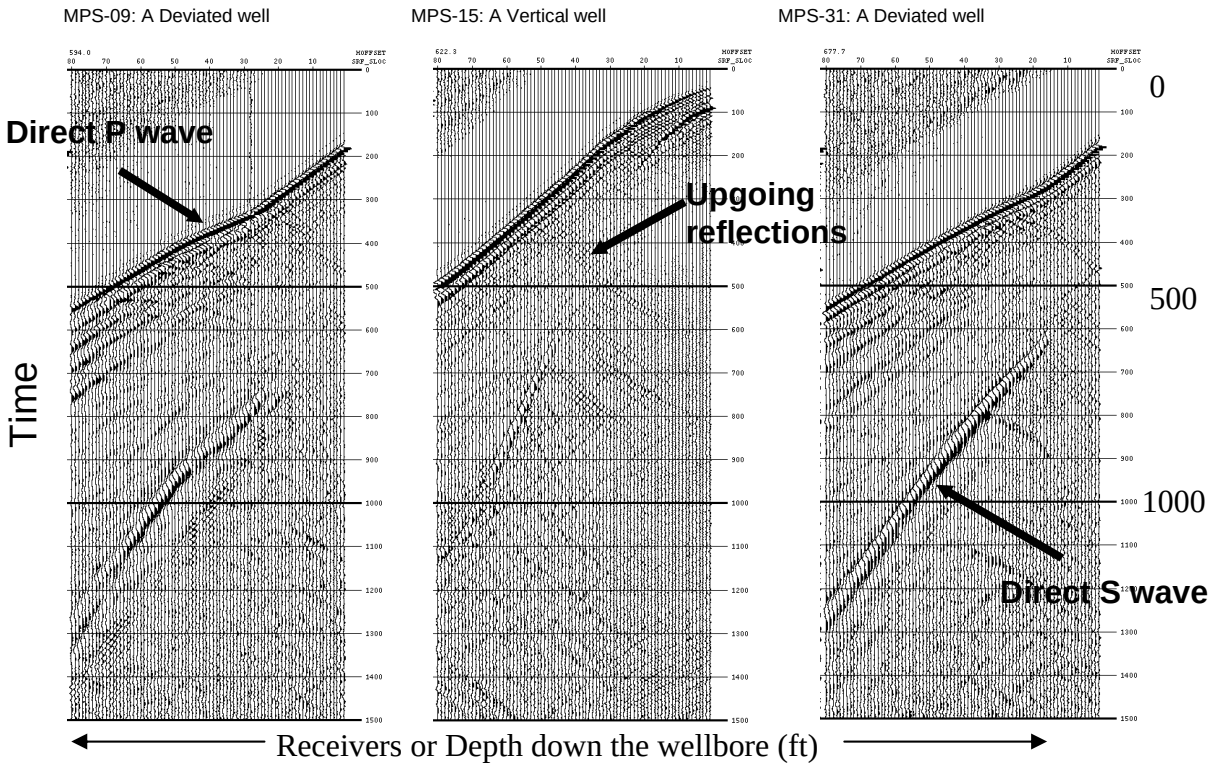

Figure 5. From the BP onshore Milne Point survey. A single sweep, 8 – 200 Hz, recorded by P/GSI's downhole array. The source offset is about 152.4 m (500 ft). This figure shows raw data from three of the four wells. Note that two of the wells are highly deviated. (Clair et al. 2002).

LBL/DOE 9C VSP in NM, July 2002. 2nd generation cable.

This survey was recorded for Dr. Ernie Majer at LBL recording 9C 3D data to study fractured reservoir imaging using back scattered seismic energy. The system recorded data with outstanding quality. The results from this survey were published at the 2002 SEG meeting in Salt Lake City, Utah.

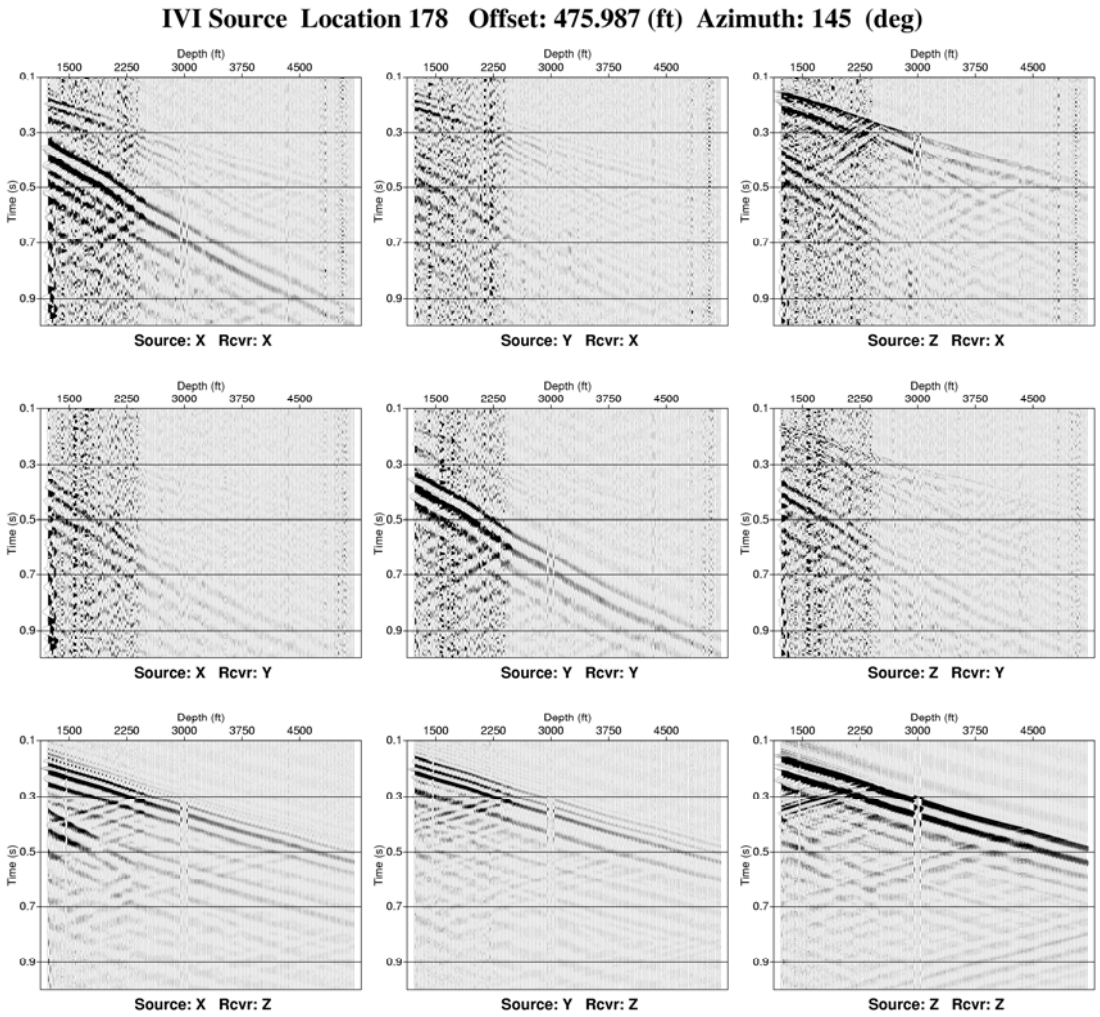

Figure 6. From the LBL onshore New Mexico survey. A single sweep, recorded by P/GSI downhole 80 level 3C array. The source offset is about 152.4 m (500 ft). This figure shows the 9C data recorded using a 3C source and a 3C receiver array. (Majer et al. 2002).

Anadarko, WY. 2nd generation cable. Two time lapse surveys recorded in 2002 and 2003

The second survey of a time lapse VSP survey recorded to monitor the injection of CO2 for enhanced an enhanced oil recovery project. Results published at the SEG and in The Leading Edge in 2004 (O'Brien et al.).

The time lapse survey for Anadarko in Wyoming is the second time lapse 3D VSP P/GSI has recorded and the first with the new arrays co funded by DOE. We have found that much less cross equalization is needed with borehole seismic data as compared with surface seismic due to less seasonal changes in the data. In a paper published by O'Brien et al. in 2004 they are showing how the VSP successfully imaged the in injection of CO2 for the purpose of enhancing the oil production using P/GSI massive 3D VSP technology.

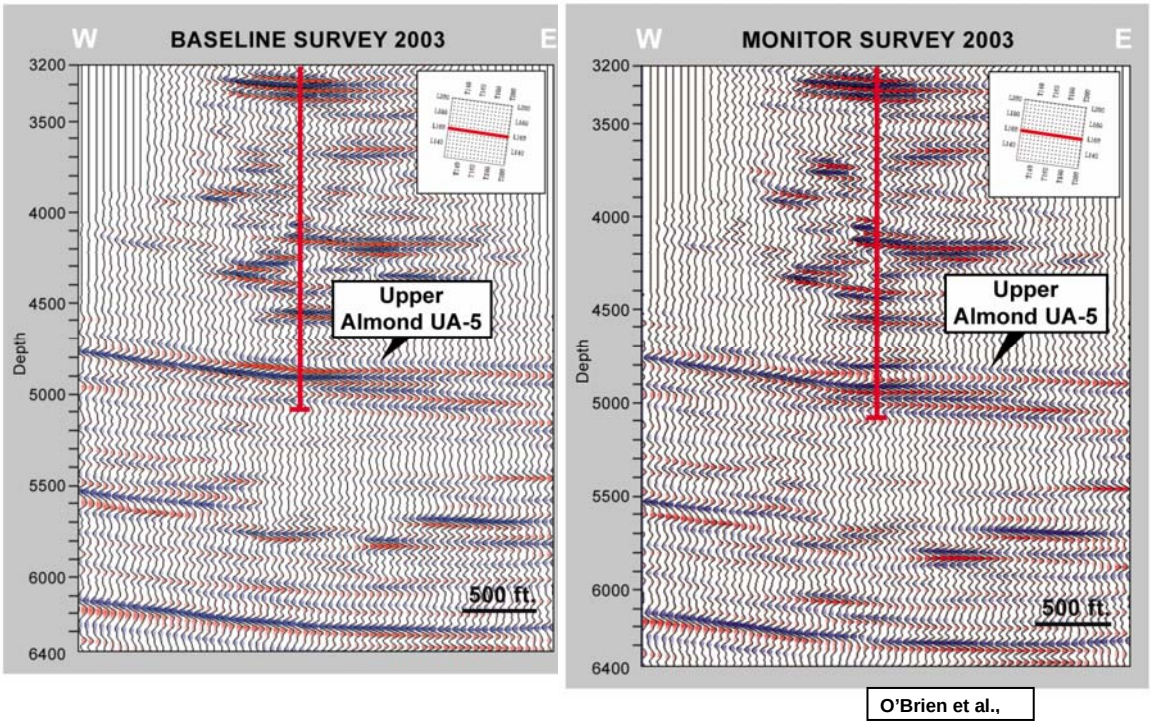

Figure 7. From the Anadarko onshore Wyoming survey. Time lapse image recorded and processed 18 month apart. The main difference between the two surveys is 18 months of injection of CO2. The result clearly shows the result of the CO2 injection. (O'Brien et al. 2004).

The images generated by the Massive 3D VSP® allowed the engineers to shorten the pilot flood and to go to the full field flood lowering the cost for the pilot flood.

Anadarko and DOE, WY. 3rd generation cable.

This was the first survey using the Paulsson Geophysical Services, Inc. designed 3rd generation cable. The objective of the survey was to map and delineate methane hydrate

deposits on the North Slope of Alaska. This survey was recorded in February 2004 in Alaska near Kuparik River. We utilized surface vibrators as seismic sources using 10 – 220 Hz sweeps. The data recorded was of outstanding quality proving that the 3rd generation array is a viable and successful design. The results from this survey were published at the SEG in 2004. The abstract and the slides are shown in the appendices.

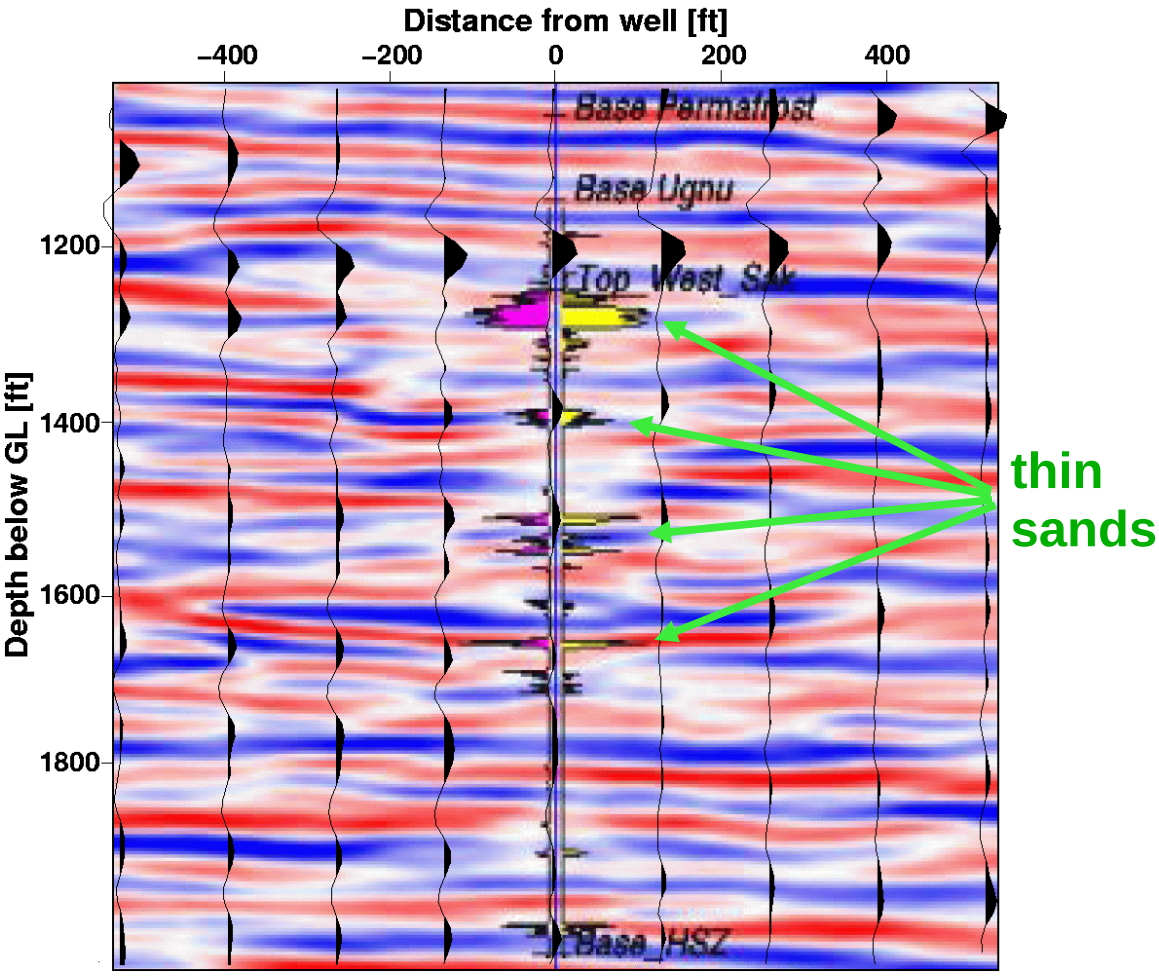

Figure 8. From the Anadarko/DOE onshore Alaska survey. The objective with this survey was to image thin sands of Methane Hydrates. This image show the quality of the Massive 3D VSP® images, in red, white and blue colors, as compared with the surface seismic images shown in black traces. The VSP was processed with a 4572 m (15 ft) bin size while the surface seismic was processed with a 35.052 m (115 ft) bin size. The VSP images have a center frequency of 135 Hz while the center frequency of the surface seismic data was only 35 Hz. (McGuire et al. 2004).

LBL/DOE, TX. 3rd generation cable. Two time lapse surveys recorded in 2004

In 2004 we recorded two time lapse VSP and Cross well surveys for Lawrence Berkeley Laboratory for the purpose of monitoring the injection of CO2 in a geologic medium to demonstrate the viability of permanently sequester CO2 thus removing it from the

atmosphere. The data was outstanding and LBL has shown that the data was able to clearly outline the area in the reservoir that had been injected with the CO2. The data from the VSP recorded with the P/GSI array has furthermore demonstrated that the CO2 injection can be monitored with a seismic technique. The results shown by the P/GSI array has encouraged BEG and LBL to propose a new phase in the continued research to develop safe and effective methods to sequester CO2.

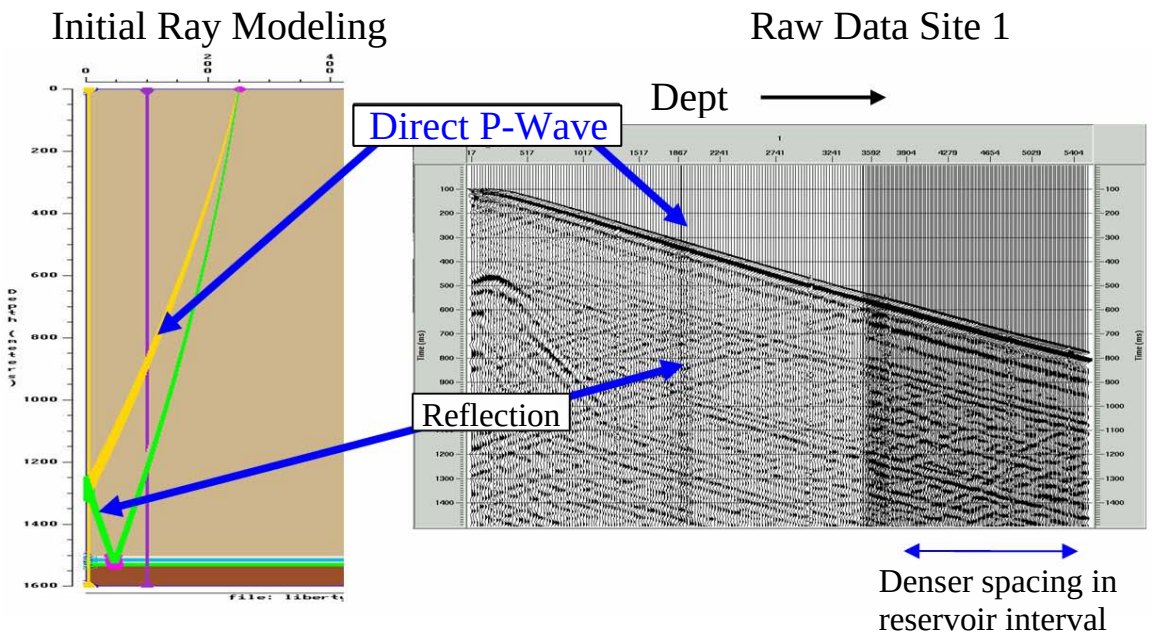

Figure 9. From the LBL onshore Frio Texas survey. The objective with this survey was to monitor the injection of CO2 for the purpose of demonstrating that sequestering of CO2 can be monitored with a borehole seismic technique. This figure shows the outstanding quality of the data that was recorded. (Daley et al. 2005).

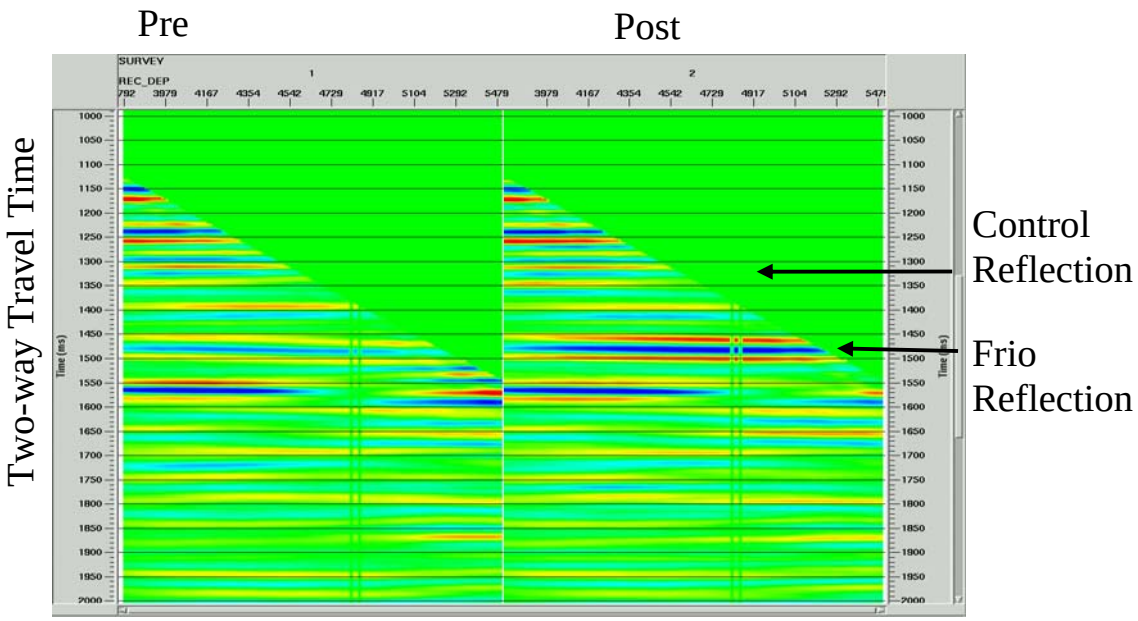

Figure 10. From the LBL onshore Frio Texas survey. The objective with this survey was to monitor the injection of CO2 for the purpose of demonstrating that sequestering of CO2 can be monitored with a borehole seismic technique. This figure show the outstanding quality of the images generated from the time lapsed data. (Daley et al. 2005).

Earthscope, USGS. 3rd generation cable.

Paulsson Geophysical Services, Inc. recorded a zero offset VSP next to the San Andreas Fault, a sparse 3D VSP and monitor the seismic events from the San Andreas Fault. Several papers published at the AGU in 2005 and at the SEG 2006

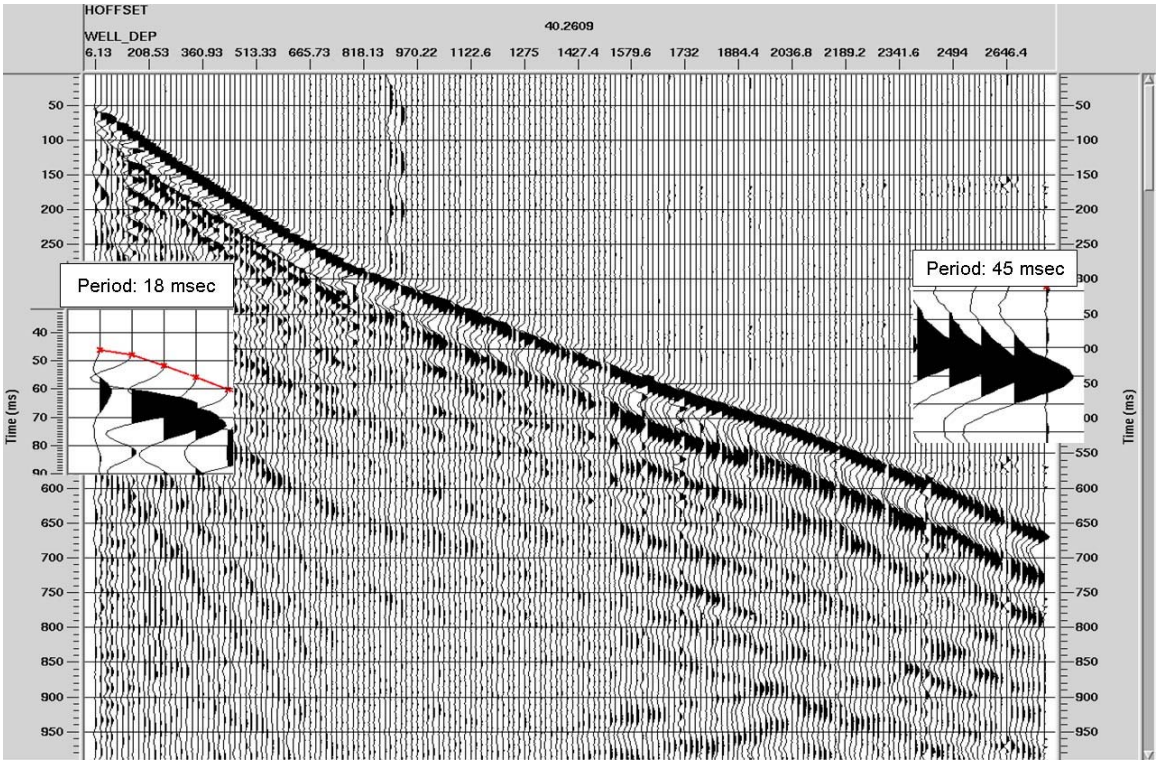

Figure 11. From the SAFOD onshore California survey. A data sample of the zero offset VSP next to the San Andrea Fault. The source used was a 2.268 kg (5 lb) dynamite charge placed at a depth of 6096 m (20 ft). The objective with this survey was to image the area around the San Andreas Fault. (J. Andres Chavarria et al. 2005).

Paulsson Geophysical Services, Inc. completed a successful experiment to image the geologic structure and monitor earthquakes along the San Andreas Fault. The survey site is near Parkfield in central California. Paulsson deployed one 80-level, 3-component 1,219.2 m (4,000 ft) long receiver array from ground level to a depth of about 2743.2 meters (9000 feet), using three settings, below ground in the fully-cased San Andreas Fault Observatory at Depth (SAFOD) well.

The receiver string occupied the well from April 24th-May 10th 2005, during which time about 1,000 of earthquakes of magnitudes ranging from M-2 to M2.7 were recorded, including events too small to detect on conventional seismographs positioned above ground. Many of the earthquakes had very clear, high resolution and high frequency p-wave and s-wave arrivals that will be used by geoscientists studying the mechanism of faulting. In addition to the microseismic monitoring, the downhole receivers were used in a successful active source experiment that imaged the location and geometry of the San Andreas Fault itself. The high-quality data obtained in this experiment was used to steer the remaining drilling of the SAFOD well and to constrain geophysical models for San Andreas Fault rupture. The SAFOD well successfully penetrated the San Andreas Fault in August 2005. Improved geological and mechanical models of faults will ultimately lead to improved public safety plans for communities located along the fault.

Micro earthquake M0.0 recorded May 5, 2005 at 18:41 UTC – Rotation to source

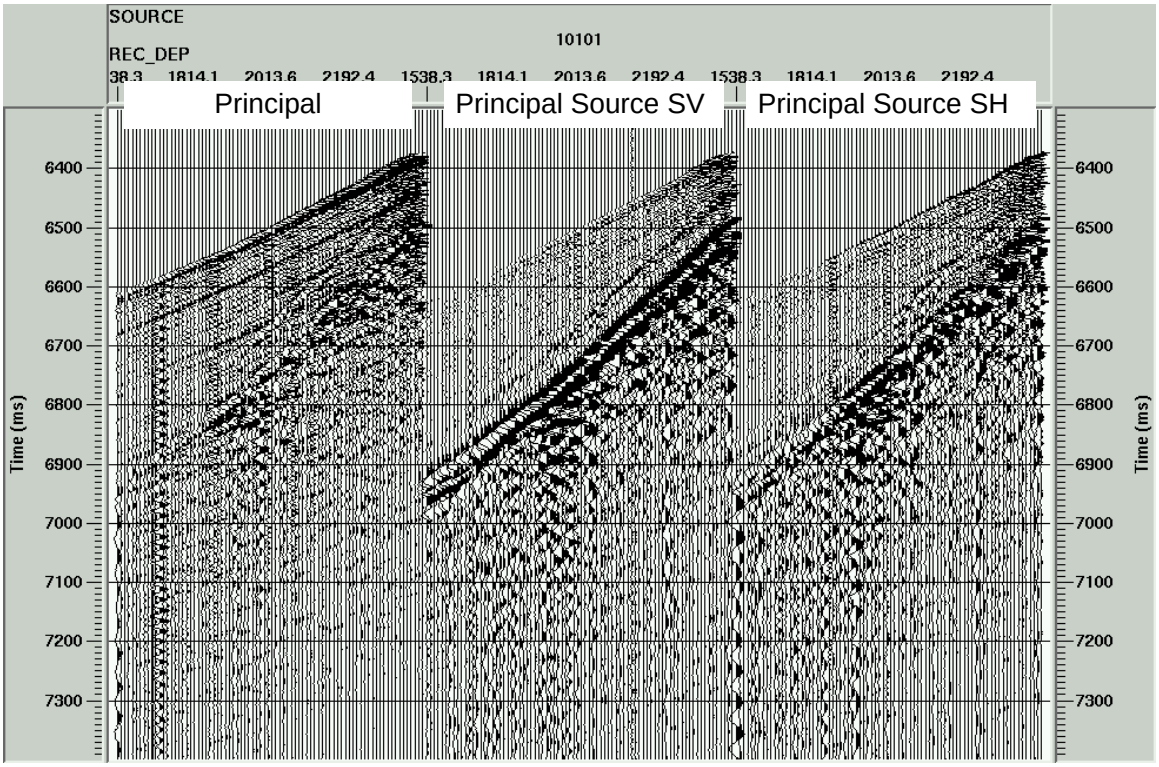

Figure 12. From the SAFOD onshore California survey. This is a sample from one of the 1000 earthquakes recorded by the array while deployed next to the San Andrea Fault. The source of the energy was a M0.0 earth quake. The objective with this earthquake monitoring was to map the area that actively slipping. This zone was the primary drilling target for the hole that was to penetrate the San Andreas Fault. (J. Andres Chavarria et al. 2005).

The SAFOD VSP experiment is an example of technology that was developed under the oil and gas program but has benefits and impacts outside the energy sector of the U.S. economy. A technology that was developed to find and develop oil and gas resources proved to be extremely useful in this scientific study aimed at earthquake hazard reduction. The SAFOD well is funded by the National Science Foundation and is being drilled in partnership with the U.S. Geological Survey. After the SAFOD well reached its total depth, long-term microseismic monitoring is being conducted with a similar downhole seismic recording system.

3D Massive VSP's Recorded by P/GSI 1998 - 2006: Updated September 26, 2006

Survey Well #	Date	Customer	Survey type	Array size	Depth (ft)	Max Press. (psi)	Max Temp (deg F)	Comments
1	January 1, 2002	Thums/Oxy	3D VSP	80	4200	1819	125˚F(e)	Offshore survey
2	February 7, 2002	Thums/Oxy	3D VSP	80	3900	1689	125°F(e)	Offshore survey
3	February 11, 2002	Thums/Oxy	3D VSP	80	4100	1775	125°F(e)	Offshore survey
4	February 20, 2002	Thums/Oxy	3D VSP	80	4300	1862	125°F(e)	Offshore survey
5	February 24, 2002	Thums/Oxy	3D VSP	80	4400	1905	125°F(e)	Offshore survey
6	March 1, 2002	BP	3D VSP	80	4200	1819	100°F(e)	Four arrays deployed in four wells
7	March 1, 2002	BP	3D VSP	80	4200	1819	100°F(e)	Four arrays deployed in four wells
8	March 1, 2002	BP	3D VSP	80	4200	1819	100°F(e)	Four arrays deployed in four wells
9	March 1, 2002	BP	3D VSP	80	4200	1819	100°F(e)	Four arrays deployed in four wells
10	July 1, 2002	Lawrence Berkeley Lab	9C 3D VSP	80	5200	2252	150°F(e)	
11	January 1, 2003	Chevron	3D VSP	160	12600	5456	239°F	
12	March 1, 2003	Anadarko	4D VSP	80	4400	1905	128°F	Time lapse survey to monitor CO2
13	March 1, 2003	ExxonMobil	3D VSP	80	7600	3291	183°F	
14	February 1, 2004	Anadarko and DOE	3D VSP	80	2600	1126	40°F	New pod and cable design
15	March 1, 2004	PDO, Oman	3D VSP	40	4593	1989	145°F	
16	March 1, 2004	PDO, Oman	3D VSP	40	4593	1989	145°F	
17	March 1, 2004	PDO, Oman	3D VSP	40	4593	1989	145°F	
18	June 1, 2004	Lake Tahoe Pub. Utility Dist.	VSP	20	1000	433	100°F (e)	
19	July 1, 2004	Lawrence Berkeley Lab	Time lapse VSP	80	5200	2252	160°F (e)	
20	October 1, 2004	Lawrence Berkeley Lab	Time lapse VSP	80	5200	2252	160°F (e)	
21	March 1, 2005	Shell	2D VSP	80	1800	779	100°F	
22	May 15, 2005	Earthscope and NSF	VSP and Microseismic	80	9600	4157	221°F	
23	November 1, 2005	Chevron	2D VSP	80	5200	2252	232°F	
24	March 1, 2006	Shell	3D VSP	80	2000	866	190°F	
25	March 1, 2006	Shell	3D VSP	80	2000	866	190°F	
26	September 10, 2006	BP	3D VSP	160	10500	4547	220°F	

Table 1. Above is a summary of the surveys recorded with the 80 – 400 level receiver array co-funded by DOE and Paulsson Geophysical Services, Inc.

The surveys recorded by the receiver arrays developed under this project, shown in Table 1, represent the largest onshore and offshore VSP surveys ever recorded. Without the long tubing deployed arrays developed in this project, VSP surveys would still be confined to use short wireline based arrays.

CONCLUSIONS

The objective of this project was to develop and test a downhole receiver array and advanced elements of a companion seismic data processing package for high resolution imaging of gas reservoirs. This project has met all the objectives. The resulting hardware and software have been applied in a large number of wells – a total of 27 at the time of this report.

Repeat clients have applied the technology in areas as diverse as the North Slope of Alaska, offshore California, and Texas. High quality, high frequency data have been recorded and high resolution depth images have been generated. The images have been shown to match the well logs in the survey wells as well as available surface seismic images.

The images generated are consistently much higher frequency, typically more than twice the frequency, compared to data recorded using surface seismic techniques. All the images have been generated using a Kirchoff Prestack Depth Migration technique, so that all the images are presented in depth – not time, as is common in surface seismic imaging.

We have also been able to generate images in areas where surface seismic has failed to generate any data. Several clients have drilled successful wells on the images generated by Paulsson Geophysical Services, Inc. That is the ultimate proof of the value of the technology generated under this project.

PUBLICATIONS

The following surveys have been published and the papers are shown in the following appendices. We also include PowerPoint presentations for these surveys in the Topical Reports section of the report.

1. Thums, Long Beach, CA. A five well offshore Massive 3D VSP® in Feb. 2002. Results published at the AAPG 2003.
2. BP Milne Point, AK. A four well 960 channel Massive 3D VSP®, March 2002. Results published at the SEG 2002.
3. LBL/DOE, NM. A 9C VSP recorded in July 2002. Results published at the SEG 2005 and in The Leading Edge November 2006.
4. Anadarko, WY. The second survey of a time lapse VSP survey recorded to monitor the injection of CO2 for enhanced an enhanced oil recovery project. Results published in The Leading Edge 2004.
5. Anadarko and DOE, AK. Survey to map a methane hydrate deposit. Published at the SEG 2005.
6. LBL/DOE, TX. A set of time lapse (2) VSP surveys to monitor the effect of injecting CO2 in a saline aquifer to sequester CO2. Published at the SEG 2005 and in The Leading Edge November 2006.
7. A. Earthscope, USGS. Record a zero offset VSP next to the San Andreas Fault, a sparse 3D VSP, and monitor the seismic events from the San Andreas Fault. One of several papers published at the AGU in 2005 and at the SEG 2006.
8. B. Interferometric imaging of the San Andreas Fault at Parkfield Using a Massive 3D VSP®. One of several papers published at the AGU in 2005 and at the SEG 2006.
9. C. High-Resolution Fault Zone Monitoring and Imaging Using Long Borehole Arrays. One of several papers published at the AGU in 2005 and at the SEG 2006

8. Massive 3D VSP® Technology Development by Paulsson Geophysical Services, Inc. Published in the First Break Volume 23, October 2004

AAPG Annual Convention
Salt Lake City, Utah
May 11-14, 2003

Björn Paulsson[1], Martin Karrenbach[2], Karen Blake[2] (1) Paulsson Geophysical Services, Inc, Brea, CA
(2) Paulsson Geophysical Services, Inc,

3-D Massive VSP at Wilmington Oil Field, Long Beach Unit

A new high-resolution seismic imaging technology has been used to image part of the Wilmington Oil Field, which is the third largest oil field in the continental United States. The field is located on a 13 mile long and 3 mile wide anticline that extends from onshore San Pedro to offshore Seal Beach. Vertical faults divide the field and production stems mainly from five major turbidite sandstone intervals ranging from 2,000 feet to 11,000 feet in depth.

The Long Beach Unit (LBU) of the Wilmington field is being produced from four islands constructed in the harbor area. Since 1965, 800 million barrels of oil have been produced from the LBU, an estimated one billion barrels is still in place and remains to be recovered. Recovery efforts include water flooding, fracturing and horizontal drilling.

In February 2002 Paulsson/Geophysical Services, Inc. completed a high-resolution 3-D Massive VSP seismic survey of the producing reservoirs and deeper exploration prospects. An 80 level three-component borehole array was used to acquire a total of 30,000 shots from two islands. A total of 5 wells (vertical and deviated) were instrumented. An initial velocity model was constructed and refined using direct arrival and reflection tomographic methods. Finally, the processed up-going wave field was pre-stack depth migrated providing images of the LBU directly in depth. Converting the 3-D VSP image back into the time domain shows frequencies up to 120 Hz, which is a great improvement in resolution over traditional surface seismic data in that area.

DE-FC26-01NT41234

A Massive 3D VSP® Survey at Milne Point, Alaska

Claire Sullivan, Allan Ross, James Lemaux, Dennis Urban, Brian Hornby, Chris West, and John Garing, BP Exploration Alaska, Björn Paulsson, Martin Karrenbach, and Paul Milligan, Paulsson Geophysical Services, Inc.

Summary

A Massie 3D VSP® was collected to aid drilling at BP's Milne Point S Pad project, a development of the Schrader Bluff formation. Field development is dependant upon multilateral completions in a thin and highly faulted reservoir zone. Successful drilling of the multilaterals requires prediction of numerous small throw faults not seen in conventional surface seismic. A simultaneous 3D VSP was acquired in 4 wells to provide high resolution seismic data in order to detect small faults within a 30 ft thick sand.

Introduction

The Schrader Bluff formation is a Tertiary marginal marine sandstone located on the North Slope of Alaska. The sands range from unconsolidated to weakly consolidated, with biodegraded oil ranging from 14-22 API gravity. At Schrader Bluff, the current focus is on deeper OA and OB reservoirs, with future development moving into the upper N sands and Ugnu formations. The reservoir depth is approximately 4000 ft (Figure 1).

The vintage surface seismic 3D over the area was acquired to image the deeper Ivishak formation and subsequently has very low fold (4-6) at the shallower Schrader Bluff interval. Statics problems are considerable due to the highly variable permafrost zone and degrade the image quality. The asset team was unable to predict the location of small 20-30 ft faults or local structural dip in the OA and OB sands with the surface seismic. This resulted in several sidetracks while attempting to maintain long multilaterals in the 30 ft thick sands in wells drilled from adjacent pads. The development plan for S pad requires 19 miles of slotted liner from 14 multilateral wells to be set in two 30 ft sands.

In order to avoid expensive sidetracks, high resolution data is required. The VSP method was chosen because it provides extremely high fold data. Significantly higher frequency was expected due to quiet borehole conditions, good elastic coupling to the formation, and minimized attenuation due to shorter raypaths. Placement of geophones below the permafrost reduced the static and velocity problems.

3D VSP design and acquisition

Typically VSPs suffer from inadequate lateral coverage. To improve the areal coverage beyond what a single well would provide, four injectors were pre-drilled and fitted with 80 three-component geophone pods at 50 foot spacing, the tool length totaling 4000 feet. This arrangement provided 320 receiver positions without having to move arrays or repeat any source positions and thus is referred to as a massive VSP.

Since the field is developed from a single pad, location of the VSP wells was not ideal, but was optimized for lateral coverage and increased frequency content. The central vertical well had geophone locations from near surface to several hundred feet above the reservoir. The other 3 wells were deviated up to 75 degrees from vertical and projected out from the pad. The geophone arrays in the deviated wells were placed below the permafrost zone at 2000 feet tvdss.

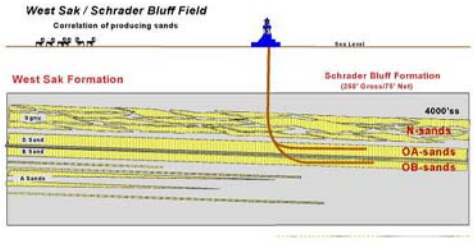

.

Figure 1. Schematic of multilateral in the Schrader Bluff OA and OB sands.

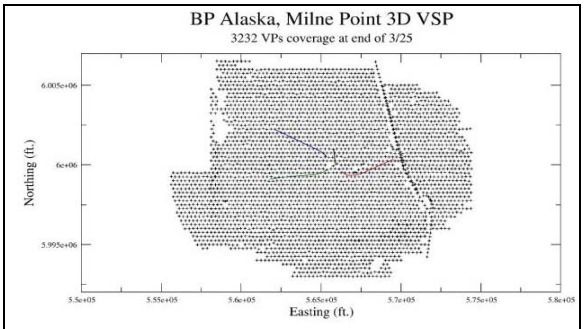

Figure 2. Map of shot coverage and geophone array placement.

DE-FC26-01NT41234

A Massive 3D VSP® Survey at Milne Point, Alaska

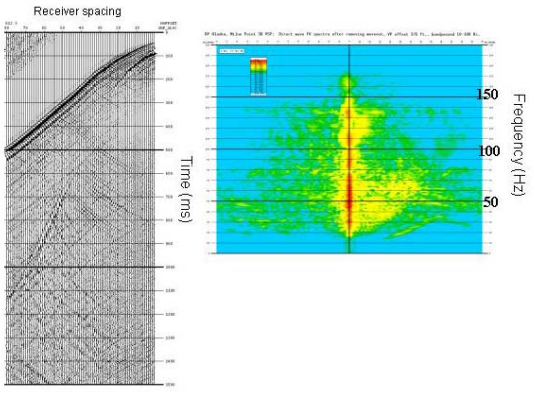

Figure 3. Raw shot record (left) at 600 ft offset. Direct P-wave, direct S-wave and reflections are seen in record. Spectral image (right) shows frequencies up to 170 Hz at –30 dB.

The placement of the geophone arrays and the source positions were determined by pre-survey modeling of the of the fold coverage.

The survey was shot in 5 days with 3232 vibration points into 320 three-component geophones totaling over 3 million traces (Figure 2).

Results

The 3D VSP resulted in stacked data with frequencies up to 120 Hz and a central peak frequency of 50-60 Hz near the edge of the survey. Figure 3 shows a raw shot record and associated spectral image. Reflections at reservoir level were recorded at offsets up to 7000 ft from the vertical well.

The 50 ft receiver spacing interval allowed a close match of the velocities at the vertical well location. Comprehensive wireline logs were obtained at this well only. The match between the sonic log velocity and the zero-offset VSP can be seen in Figure 4.

Conclusions

The 3D VSP provided a high frequency, high fold image over the Schrader Bluff development area. Drilling in the summer of 2002 will test the accuracy of this survey.

Acknowledgments

We wish to thank BP Exploration Alaska for allowing us to present this work. Special thanks to WesternGeco and Trace Energy for their contributions. Equipment used for this survey was funded under a DOE grant, # DE-FC26-01NT41234.

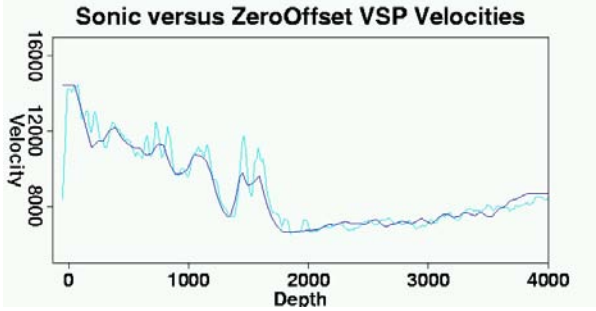

Figure 4. Comparison of velocities from sonic log and zero-offset VSP. The light blue line is the log velocity sampled at 10 feet. The dark blue line is the VSP velocity measured from first break analysis.

Acquisition of time-lapse, 6-component, P- and S-wave, crosswell seismic survey with orbital vibrator and of time-lapse VSP for CO2 injection monitoring

T. M. Daley, L.R. Myer and E.L. Majer all at Lawrence Berkeley National Laboratory*

Summary

Using an orbital vibrator source (2-components), and a 40 level 3-component geophone string, a 6-component crosswell survey was acquired before and after a CO2 injection in a saline aquifer. Decomposition of the two source components and component rotation of both source and sensors created good separation of P- and S-wave energy allowing independent analysis of travel time and reflectivity. A time-lapse VSP was also acquired.

Introduction

As part of a Department of Energy (DOE) funded project on geologic sequestration of CO2, a time-lapse crosswell seismic survey was acquired before and after injection of CO2 into a saline aquifer. The aquifer is in the on shore Gulf of Mexico Frio formation sandstone, near Houston, Tx. Among the goals of this pilot sequestration test are the following:

1) Demonstrate that CO2 can be injected into a brine formation without adverse health, safety, or environmental effects.
2) Determine the subsurface distribution of injected CO2.
3) Demonstrate validity of conceptual models.
4) Develop experience necessary for the success of large-scale CO2 injection

The Crosswell and VSP experiments are part of an integrated suite of scientific studies with many contributing institutions including the Texas Bureau of Economic Geology.

Data Acquisition

An 80-level 3-component geophone string, supplied by Paulsson Geophysical was used for the crosswell acquisition and a time-lapse vertical seismic profile (VSP) which was acquired simultaneously. For the Crosswell survey, source and receiver spacing was 1.5 m, with the sources spanning 75 m and the sensors spanning 300 m. Five source 'fans' were acquired to give 1.5 m sensor spacing from the 7.5 m fixed sensor spacing. The crosswell survey was conducted using the injection well (for sensors) and a nearby monitoring well (for source) which is about 30 m offset. Crosswell source locations were centered on the injection interval. The crosswell sensors were also centered on the injection interval, which is the 6-7 m thick, upper C sand in the Frio formation which is at a depth of about 1500 m. Initial analysis of the crosswell data shows good quality P- and S-wave direct arrivals. Time-lapse tomographic imaging is planned for both P- and S-waves.

The orbital vibrator source is an eccentric mass rotated by an electric motor. The source is fluid coupled to the surrounding formation. The rate of rotation is linearly varied up to 350 Hz and back to stop. Useable energy is acquired above about 70 Hz, giving a 70 to 350 Hz bandwidth. At each source location a clockwise and counter clockwise sweep is recorded. Decomposition of these two sweeps provides two equivalent sources with orthogonal horizontal oscillations (Daley and Cox, 2001). Component rotation using P-wave particle motion rotates these two sources into in-line and cross-line equivalents, with in-line being horizontal and in the plane of the two boreholes (Gritto, et al, 2004). Figure 1 shows a 6-component receiver gather (all source depths for one receiver depth) with in-line and cross-line sources for the vertical and two horizontal receiver components.

The VSP used an 80 level, 3-component geophone string and explosive source. Eight source shot points were acquired. The sensors were interleaved to give spacings of 1.5 to 7.5 m. The shotpoints were offset 100 to 1500 m from the sensor well. The location of the shotpoints was designed to monitor the estimated CO2 plume location and to provide structural information at the injection site. VSP data have good quality direct and reflected events. Comparison of variable sensor spacing shows advantage of increasing spatial sampling.

Data Analysis

After the two acquired orbital vibrator sweeps (clockwise and counter-clockwise rotation) are decomposed into orthogonal 'x' and 'y' data traces, these traces are numerically rotated into in-line and crossline orientations. The rotation angles were calculated using the P-wave particle motion recorded on one of the sensor components. The angles from each sensor were combined in a weighted average with the weights determined by the particle motion linearity.

For tomography, the travel times were picked using the in-line source for P-wave and the crossline source for S-wave (see Figure 1). Initial results indicate a reduction in velocity, as expected from CO2 injection.

The initial processing of the VSP has focused on time lapse change in reflection amplitude of the reservoir horizon. An amplitude equalization was applied using a reflection above the reservoir. An initial result from one source location is shown in Figure 2.

DE-FC26-01NT41234

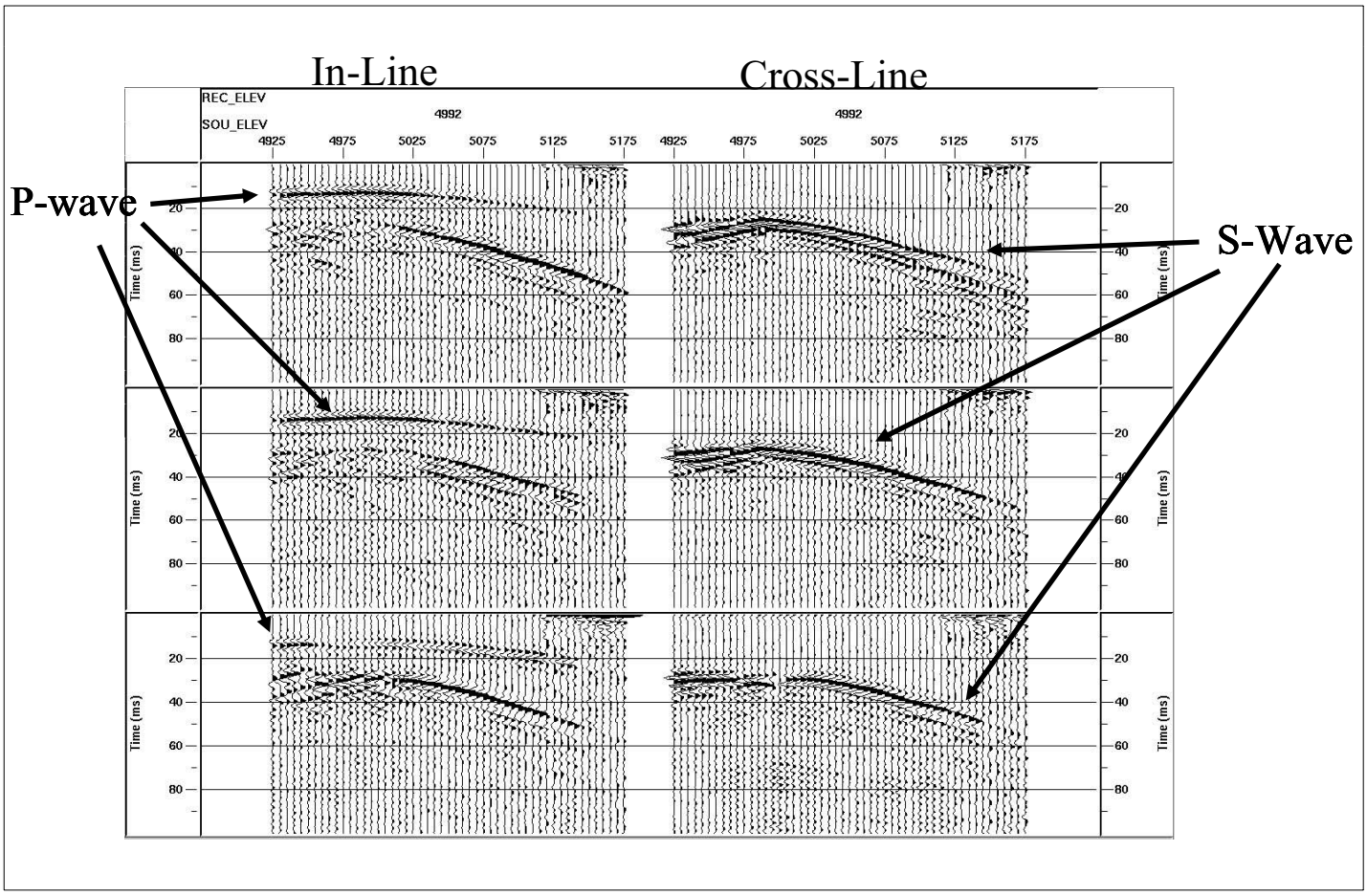

Figure 1: 6-component crosswell receiver gather. The two columns are in-line and cross-line source components. The rows are vertical and two horizontal receiver components (top to bottom). Each trace amplitude is normalized to its own maximum. The cross-line source component shows good separation of S-wave energy (i.e. minimization of P-wave).

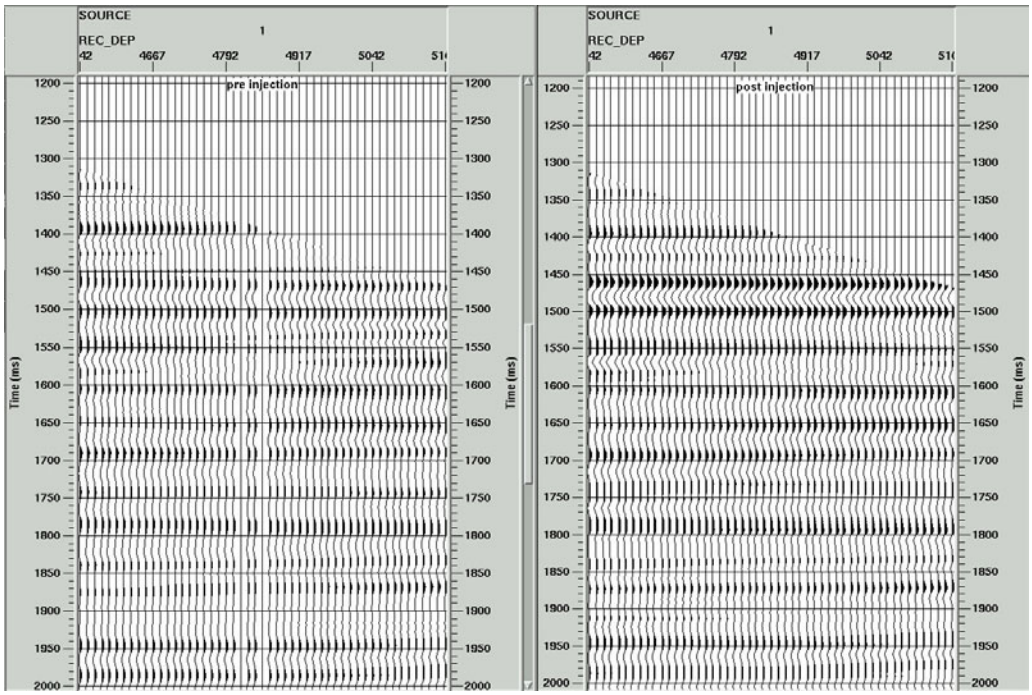

Figure 2 VSP reflection section before (left) and after (right) CO2 injection. An increase in amplitude is seen in the reservoir reflection between 1450 and 1500 ms.

DE-FC26-01NT41234

Time Lapse Crosswell and VSP for CO2 Monitoring

Conclusions

Seismic monitoring data has been collected as an integral part of a CO2 injection experiment. Both VSP and crosswell data were acquired. A massive 80 level 3-component sensor string allowed high spatial sampling over a large depth interval. The use of an orbital vibrator borehole source allowed both P- and S-wave data to be colleted. The pre and post injection data is good quality, both for VSP and Crosswell.

Initial analysis of time-lapse crosswell P-wave tomography changes indicate velocity reduction in the reservoir. Initial analysis of VSP time-lapse change indicates an increase in reflection strength.

References

Daley, T. M. and Cox, D., 2001, Orbital vibrator seismic source for simultaneous P- and S-wave crosswell acquisition, Geophysics, 66, 1471-1480.

Gritto, R., Daley, T. M. and Myer, L.R., 2004, Joint cross-well and single-well seismic studies of CO2 injection in an oil reservoir, Geophysical Prospecting, 52, 323-339.

Acknowledgments

This work was supported by the Assistant Secretary for Fossil Energy, Office of Coal and Power Systems; Office of Oil, Gas and Shale Technologies, and the National Energy Technology Laboratory under U.S. Department of Energy contract DE-AC03-76SF00098.

Thanks to P/GSI for supporting the use of 80-level sensor string. Thanks to Texas Bureau of Economic Geology (TBEG) and Sue Hovorka for management of the CO2 injection. Thanks to Don Lippert, Rob Trautz, (of LBNL), Spud Miller and David Freeman (of Sandia Technology).

EDITED REFERENCES

Note: This reference list is a copy-edited version of the reference list submitted by the author. Reference lists for the 2005 SEG Technical Program Expanded Abstracts have been copy edited so that references provided with the online metadata for each paper will achieve a high degree of linking to cited sources that appear on the Web.

Acquisition of time-lapse, 6-component, P- and S-wave, crosswell seismic survey with orbital vibrator and of time-lapse VSP for CO2 injection monitoring

References

Daley, T. M., and D. Cox, 2001, Orbital vibrator seismic source for simultaneous P- and S-wave crosswell acquisition: Geophysics, **66**, 1471–1480.

Gritto, R., T. M. Daley, and L. R. Myer, 2004, Joint cross-well and single-well seismic studies of CO2 injection in an oil reservoir: Geophysical Prospecting, **52**, 323–339.

Time-Lapse VSP Reservoir Monitoring

John O'Brien, Fiona Kilbride, and Frank Lim, Anadarko Petroleum Corporation

Introduction

While 3-D seismic imaging has been the primary tool used for geophysical reservoir monitoring to date, vertical seismic profiling (VSP) has characteristics that make this technique particularly suitable for time-lapse surveying. In particular, the use of downhole receivers provides the following advantages:

- Increased frequency content which improves vertical and lateral resolution, allowing us to examine the reservoir in greater detail, both statically and dynamically, and
- Improved signal/noise ratio which permits us to measure and quantify time-lapse changes in the reservoir with a high degree of confidence.

With the recent development of multilevel downhole arrays having fifty or more three-component geophones, we now have the capability of recording large 3-D VSP surveys in a time-efficient manner. Such surveys generate high quality and high fidelity 3-D images of the subsurface in the vicinity of the wellbore and provide a powerful tool for time-lapse imaging.

In this paper we present the results of a 3-D VSP time-lapse imaging project performed in the Monell Unit of Patrick Draw Field, Wyoming. In 2001 Anadarko Petroleum Corporation initiated a miscible CO_2 enhanced oil recovery (EOR) pilot project in the Monell Unit. The objectives of the project were to test the injection process and the response of the reservoir to CO_2 injection prior to start-up of a full-field CO_2 flood. As part of that project, movement of the CO_2 front in the reservoir was monitored by time-lapse 3-D VSP; these results are presented in this paper. To the best of our knowledge, this is the first such 3-D VSP reservoir monitoring application reported in the literature.

Monell Unit. The Monell Unit constitutes the southern portion of the Patrick Draw Field located in south-central Wyoming (Figure 1). The reservoir interval is comprised of the Upper Almond UA-5 sandstone, the youngest sandstone member of the Upper Cretaceous Mesaverde group. The Upper Almond was deposited in a barrier island/tidal inlet channel setting, with predominantly north-south trending elongate barrier bars. The field is a stratigraphic trap: the reservoir pinches out updip into swamp and lagoonal shales and is overlain by the Lewis Shale.

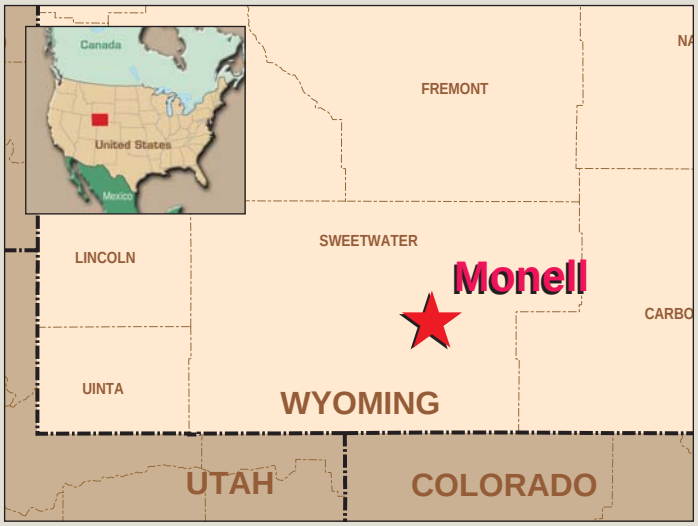

Figure 1. Map showing the location of the pilot project.

The general dip of the reservoir is to the south east at 4° to 5°. Due to the depositional environment the reservoir is quite homogeneous, with little variation in thickness, porosity, or permeability. Little significant faulting has been identified from 3-D seismic or from borehole correlations. Reservoir characteristics are summarized in Table 1.

Average net thickness	25 ft.
Porosity	20 %
Permeability	30 mD
Depth	4,800 ft.
Oil Gravity	43° API
Gas/Oil Ratio	500 scf/bbl
Original Sw	46%
Present Sw (before CO_2 flood)	67%
Reservoir Pressure	2,000 psi
Reservoir Temperature	120° F

Table 1 Reservoir characteristics of the Monell Unit, Patrick Draw Field, Wyoming.

The Monell Unit, which had an original-oil-in-place of 110 MMBO, was initially produced under solution gas drive that yielded 24 MMBO. The field was subsequently waterflooded and yielded an additional 16 MMBO, leaving 70 MMBO as a remaining target for enhanced oil recovery. Given the remaining oil-in-place, the homogeneous nature of the reservoir and its shallow depth, this field was identified as a strong candidate for EOR.

CO_2 Pilot Project. The Monell EOR program was initiated with a pilot project that consisted of a single five-spot pattern with a CO_2 injector at the center, two producing wells

DE-FC26-01NT41234

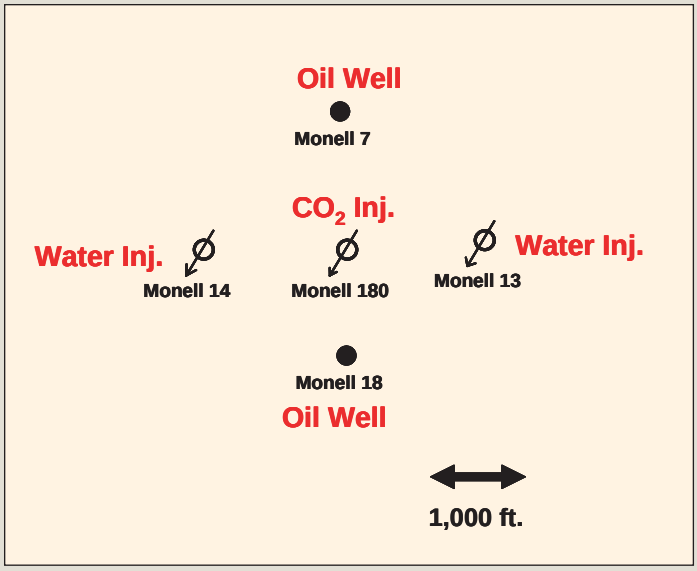

Figure 2. Monell CO2 EOR Pilot Project.

located ¼ mile north and south of the injection well, and two water injectors ¼ mile to the east and west (Figure 2). The water injectors were utilized to maintain reservoir pressure and to confine the CO_2 flood.

The CO_2 injector well, Monell 180 ST 1, is a nominally vertical well drilled specifically for the pilot project. A full suite of wireline logs was recorded in this well, including dipole sonic and density logs for geophysical analysis. This is the well in which VSP data were recorded.

The pilot project was launched in July 2001 with installation and testing of the oilfield equipment and of the injection processes. Continuous CO_2 injection commenced in Jan. 2002, at which time the baseline 3-D VSP survey was recorded. This provided a high quality baseline image of the reservoir. Only minor amounts of CO_2 had been injected prior to the baseline survey, insufficient to affect the seismic response.

The pilot project continued in operation for an additional 18 months during which time a total of 430 MMcf of gas was injected at an average daily rate of 0.8 MMcf/d. The pilot project was completed in June 2003 and the time-lapse monitor 3-D VSP was then recorded.

Rock Properties and Seismic Response. Prior to start-up of the pilot project a study of the rock and fluid properties was performed to determine the time-lapse seismic response of the reservoir and to assess the feasibility of geophysical monitoring. Figure 3 shows the wireline log data for the Monell 180 ST 1 well, including the gamma ray, P-wave sonic and density logs, and the computed acoustic impedance. The reservoir interval occurs at a depth of 4633 ft. in the well and is 42 ft. thick, which is thicker than the field average of 25 ft., and includes a thin (5 ft.) tight streak.

The Upper Almond UA-5 is overlain by the relatively homogenous Lewis Shale. Log data recorded before CO_2 flooding show that the Upper Almond UA-5 sand has a higher velocity than the Lewis Shale but a lower density. The density contrast is greater than the velocity contrast and so the reservoir has lower acoustic impedance than the overlying shale. This interface is predicted to generate a trough on the seismic section according to the sign convention used throughout this paper, which is the reverse of the SEG polarity convention.

The Upper Almond UA-5 reservoir overlies a complex of sands, shales, and coals. The coals, although quite thin, have anomalously low acoustic impedance and so produce a strong seismic response. This is accentuated by the influence of the sands within this complex which are cemented and have relatively high acoustic impedance. The resulting effect is a significant degree of interference whereby the peak event corresponding to the base of the Upper Almond UA-5 is superimposed on the leading energy of the underlying reflections, thus masking the base of the reservoir.

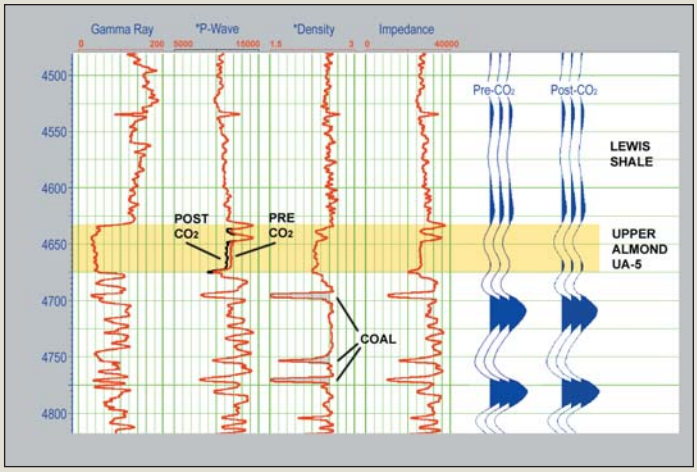

Figure 3. Monell 180 ST 1 wireline log data. The Upper Almond UA-5 interval is the reservoir. The red curve on the P-velocity track shows the velocity before CO_2 injection and the black curve shows the computed velocity after injection, a difference of 700 ft./s. The seismic traces show 1-D synthetic seismograms for both the pre-injection and post-injection cases.

The effect of CO_2 flooding on the rock properties has been estimated by application of the Biot-Gassmann Equations for pore fluid substitution in the Upper Almond UA-5 (Table 2). These computations are based on an oil saturation of 33% before CO_2 flood and an estimated CO_2 sweep efficiency of 50%. Under these conditions we predict a decrease in P-wave velocity of 700 ft./s. (6%) in the sandstone due to CO_2 flooding and a negligible change in density.

Pore Fluid Saturations

	Brine	Oil	CO_2
Before CO_2 flood	67%	33%	-
After CO_2 flood	67%	16.5%	16.5%

Formation Rock Properties

	P Velocity (ft./s.)	Density (gm/cc)	Acoustic Impedance
Lewis Shale	11,000	2.55	28,000
UA-5 Pre-flood	11,700	2.30	26,900
UA-5 Post-flood	11,000	2.30	25,300

Table 2. (Top): Pore fluid saturation for Upper Almond UA-5 sand before CO_2 flood as well as the predicted saturations after flooding. (Bottom): Average rock properties for Lewis Shale and Upper Almond UA-5 sand. Rock properties for interval underlying the UA-5 reservoir are more complex, as discussed in the text.

Figure 3 includes 1-D synthetic seismograms for both cases, before and after CO_2 flooding:

- Before CO_2 flooding the reservoir seismic response consists of a trough doublet which overlies a strong peak; the upper trough corresponds to the top of the reservoir (Top UA-5) while the lower trough results from superposition of the base-of-reservoir (Base UA-5) and leading energy from the underlying reflections.
- After CO_2 flooding the upper trough increases in amplitude by 30%. The interference pattern underlying this is modified due to the increase in amplitude of the reflection from the base of the UA-5 sand.

These differences should be detectable using time-lapse 3-D VSP acquired and processed properly, particularly the brightening of the trough event at the top of the reservoir. With this encouragement, a time-lapse 3-D VSP program was designed and executed to monitor CO_2 movement in the reservoir during the pilot project.

3-D VSP Acquisition. For VSP data acquisition the reservoir interval in the Monell 180 ST 1 well was isolated using a bridge plug. The borehole overlying the plug was then instrumented with an array of eighty 3-C geophones deployed over a depth of 4,000 ft. up to the near-surface. Geophones were deployed on production tubing, within casing.

A vibroseis source with a peak force of 62,000 lbs. was used as the seismic source. Two vibroseis units were employed, shooting in ping-pong fashion. Based on in-field testing, a sweep frequency of 8-180 Hz was used for VSP acquisition.

Source locations were placed on a rectangular grid with 500 ft. spacing between shot lines and 200 ft. spacing between shots along each line. Source locations extended 5,000 ft. from the geophone array in both inline and crossline directions, yielding a survey with full azimuthal coverage and with full offset coverage out to offsets equivalent to the depth of the target. A total of 1,007 shots were recorded yielding a dataset in excess of 240,000 traces. Total recording time was less than 30 hours per survey. This provided a comprehensive measurement of the seismic wavefield, recorded efficiently in an operationally attractive short time.

Source Locations

Source line interval	500 ft.
Source point interval	200 ft.
Maximum offset (Inline/Xline)	5,000 ft.
Number of VP's	1,007

Seismic source

Source type	Vibroseis
Sweep	8-180 Hz, linear sweep
Sweeps/VP	4
Sweep Length	12 sec.

Receiver Well

Reservoir depth	4680 ft. (MD)

Receiver array

Number of levels	80
Geophone depths	405 ft - 4,355 ft.
Level spacing	50 ft.
Geophones	15 Hz SM45, 3C pods

Table 3 Acquisition parameters for the Monell baseline and monitor 3-D VSP surveys.

As the goal of the project was to monitor changes in the reservoir, the baseline and monitor surveys were designed, acquired and processed as consistently as feasible:

- Source points were reoccupied with an accuracy of +/- 2 ft. for 1000 of the 1007 shots.
- Receiver locations were reoccupied with an accuracy of +/- 1/4 ft.
- Vibrator sweep parameters were repeated.
- Similar vibrator units were employed.
- An 80-level 3-C geophone array was used for both surveys.

Both surveys used geophones of the same design and specifications; however the baseline survey used a first-generation geophone array while the monitor survey used a re-engineered second generation array which proved to have better signal/noise characteristics. This was the largest difference in field acquisition between the two surveys.

3-D VSP Processing. To maintain consistency between the baseline and monitor surveys, the two were co-processed through a common sequence with the same parameters, as summarized below:

1. Edit shots and assign geometry.
2. Hodogram analysis.
3. Determine geophone orientations.
4. Rotate data into uniform coordinate system.
5. Pick first breaks.
6. Compute shot statics separately for each survey. Statics solutions for the two surveys agree to within +/- 1 msec.
7. Determine (X,Y) locations of receivers based on first break traveltimes from a ring of shots around the well. This shows a maximum difference of 42 ft. relative to the conventional well deviation survey. The VSP derived (X,Y) locations were used in VSP processing.
8. Shot ensemble deterministic source signature - deconvolution.
9. Separate upgoing P-wavefield.
10. Radon filter to suppress downgoing Shear-wave energy.
11. Trace amplitude balance based on the amplitude of the P-wave direct arrival, followed by time-variant gain.
12. Test AGC to improve signal/noise ratio. Baseline and monitor surveys were processed from this point forward both with and without AGC. Time-lapse differences were judged to be equivalent in both processing flows. As application of AGC results in a higher quality migrated image, the VSP sections shown in this paper include this AGC step in the processing flow.
13. Generate a 1-D velocity model by inverting first break times from near-offset shot records. The 1-D profile was extended below the well using a constant velocity gradient.
14. Extend the velocity model to 3-D using the structural interpretation derived from well formation tops.
15. P-wave Kirchhoff PreStack Depth Migration using source offsets 0-5,000 ft. and dip aperture 0°-6°. This was deemed appropriate as structural dips in the image area are 4°-5° with no significant faulting in the VSP image zone. The incidence angle aperture was limited to 0°-25° to minimize anisotropy effects. The 3-D VSP provides a high quality image of radius 1,500 ft. around the borehole at the Upper Almond level.
16. Cross-Equalization Analysis. The baseline and monitor migration volumes were analyzed for systematic differences in depth, phase and amplitude gain. Only minor differences in depth and phase were observed. To compensate for these, a bulk static shift of 3 ft. and a small spatially varying residual static and phase shift were applied. No gain adjustment was required.
17. Spectral balance and amplitude envelope balance.
18. Generate time-lapse difference volumes.

The excellent match achieved between the baseline and monitor surveys, as indicated by the cross-equalization analysis, is attributed to the consistency in field acquisition and data processing.

VSP Results. Figure 4 shows a comparison of a set of co-located shots from the baseline and monitor surveys. The Upper Almond UA-5 reflection is clearly seen over the full geophone array. This comparison demonstrates the high quality and reproducibility of the survey. Figure 4 also shows amplitude spectra for a data window that includes the Upper Almond reflection, showing that the reflection data includes frequencies exceeding 130 Hz.

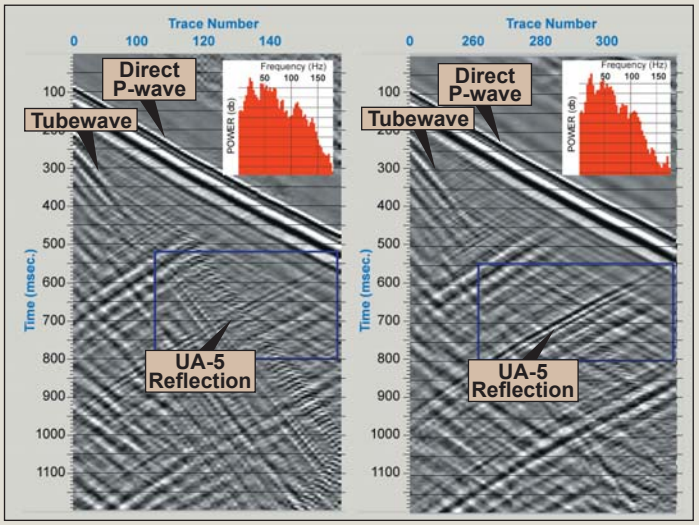

Figure 4. Comparison of co-located shots from the baseline survey (left) and monitor survey (right). Source offset = 406 ft. Figure shows vertical component data with AGC applied for display purposes. Inserts show the amplitude spectra of a data window including the Upper Almond UA-5 reflection. At near offsets the tube wave is stronger on the baseline survey than on the monitor but diminishes on both at larger source offsets.

Figure 5 shows an east-west line from the fully processed baseline VSP survey that ties the Monell 180 ST 1 well. This provides an excellent image of the Upper Almond UA-5 reservoir, and also images the stratigraphic thickness variations in the Upper Almond underlying the UA-5. The survey has a dominant wavelength of 80 ft. in the zone of interest, measured directly from the depth section, showing the excellent vertical resolution achieved with this survey.

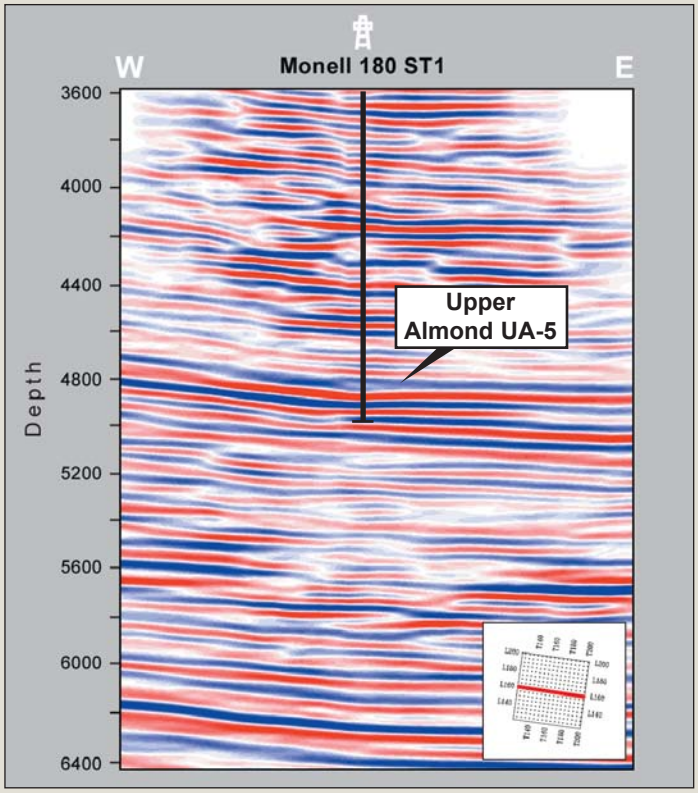

Figure 5. East-west line from prestack depth migrated baseline 3-D VSP survey tying the Monell 180 ST 1 well. The Upper Almond UA-5 is the blue trough doublet above the 4800 ft. marker at the well location.

Figure 6 shows a profile from the VSP volume spliced into a coincident line from an overlying 3-D seismic survey. The correlation between the two is excellent. While the surface seismic data has good bandwidth up to 60 Hz at these shallow depths, the VSP data has significantly higher frequency content and vertical resolution that provides more detailed imaging.

To assess the amplitude fidelity of the 3-D VSP in the zone of interest, the Upper Almond Top UA-5 trough event was mapped. Figure 7 shows the corresponding amplitude map, based on an rms amplitude extraction over a 40 ft. window encompassing the Top UA-5 event. Figure 7 also includes a UA-5 net sand thickness map based on well control.

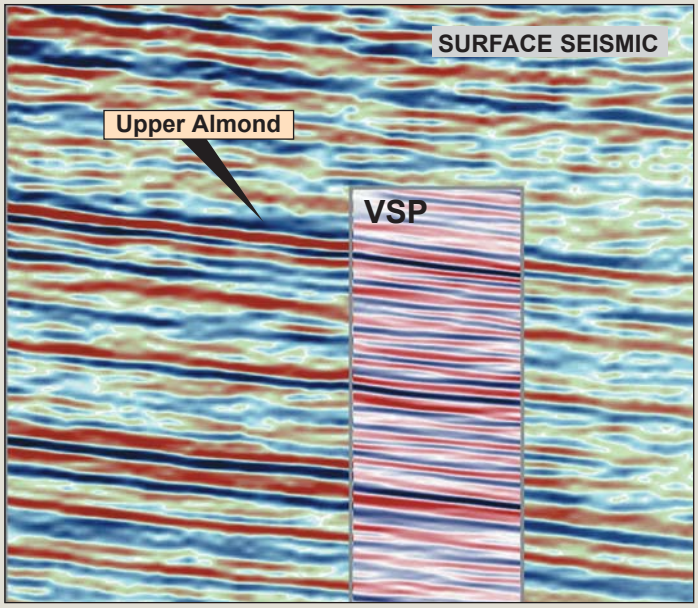

Figure 6 Comparison of segment of Monell 3-D VSP baseline survey (insert) and 3-D surface seismic.

The amplitude map shows a significant degree of character, even over this limited spatial area. Relative to the "background" amplitudes observed on the east and west

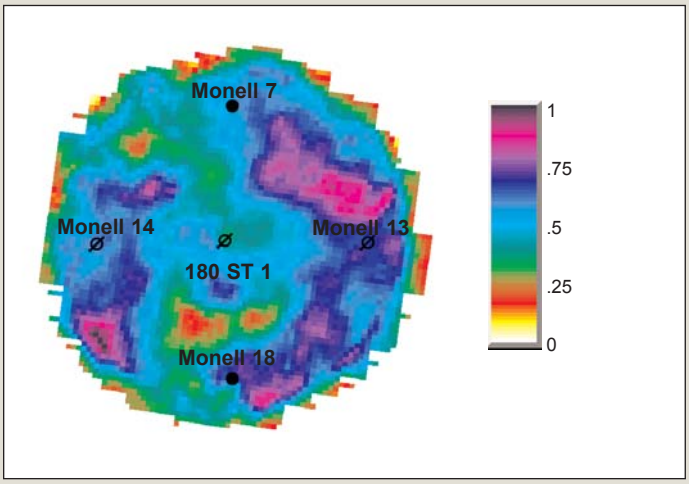

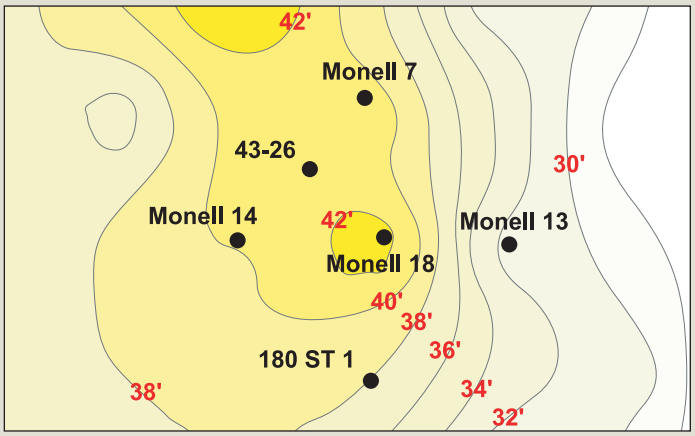

Figure 7. (Top): Map of Upper Almond Top UA-5 rms amplitude for baseline 3-D VSP survey. Low amplitudes on the periphery are edge effects. (Bottom): Map of UA-5 net sand thickness based on well data, plotted with 2 ft. contour interval. Higher amplitudes appear to correlate with thinner net sand thickness.

DE-FC26-01NT41234

sides of the survey, a ridge of lower amplitudes extends north-northwest from the Monell 180 ST 1 well while another area of lower amplitude is seen 600 ft. south of the well. These appear to correlate with net sand thickness, higher amplitudes being associated with thinner net sand thickness.

This relationship can be evaluated further by comparing the measured VSP amplitudes with those predicted by seismic forward modeling. Figure 8 shows a normal incidence wedge model based on log data from the Monell 180 ST 1 well, where the thickness of the UA-5 sand has been modified in 2 ft. increments per trace. The wavelet in this model has a frequency content that corresponds to the final migrated VSP survey. The lower display in Figure 8 compares the model amplitude response with the measured amplitudes at the six well locations within the image area where sand thickness has been determined by the drill bit.

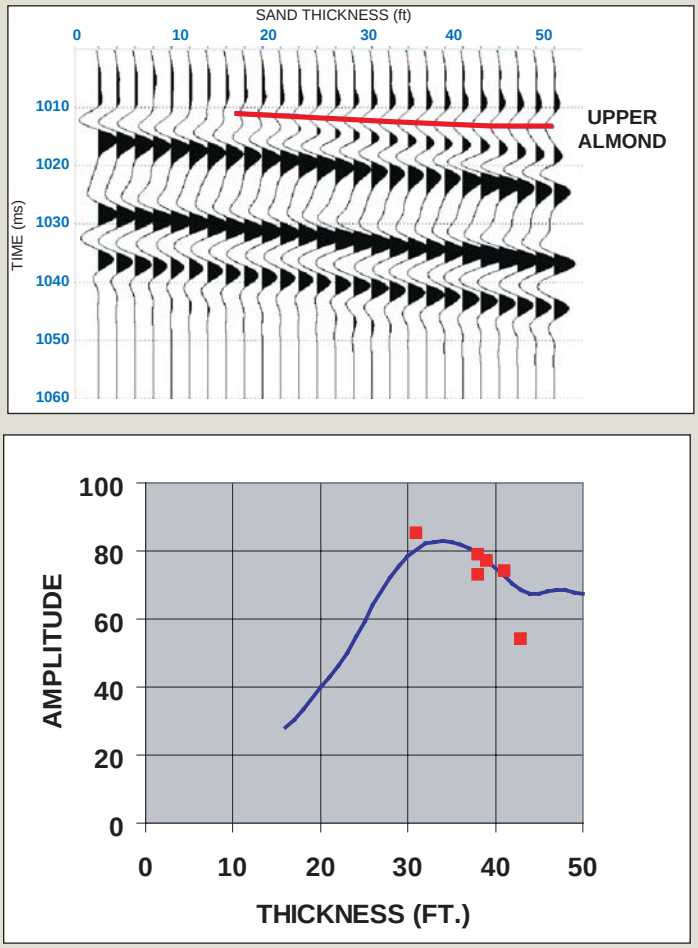

Figure 8. (Top) Normal incidence wedge model for Upper Almond UA-5 sand saturated with brine/oil. (Bottom) Plot of Upper Almond UA-5 trough amplitude versus gross sand thickness for wedge model (blue curve) and for the baseline VSP survey (red squares).

This comparison is based on the five wells used in the pilot project as well as Monell 43-26 which has been drilled subsequently as part of the full field EOR program. Comparing measured data and model results indicates that the UA-5 sand is at or above tuning thickness in the image area, and that reflection amplitude does indeed decrease with increasing sand thickness.

While sand thickness is identified as a major controlling factor in the amplitude response, the influence of variations in the underlying sand/shale/coal sequence cannot be ruled out. However as these factors should be common to both baseline and monitor surveys, they are not expected to impact the time-lapse analysis.

To examine the time-lapse effects Figure 9 shows a comparison of an east/west vertical section on both the baseline and monitor surveys that ties the Monell 180 ST 1 well :

- The two surveys show a high degree of similarity outside the reservoir interval that demonstrates the repeatability of the method.
- On the baseline survey, the Upper Almond UA-5 shows a singlet trough which develops into a trough doublet in the vicinity of Monell 180 ST 1 well due to increased sand thickness. The base of the UA-5 is not resolved from reflections from the underlying coal-bearing section. This agrees closely with the synthetic seismogram shown in Figure 3.
- On the monitor survey the upper trough of the doublet brightens significantly in the vicinity of the CO_2 injection well. This proves to be the most robust and most diagnostic time-lapse indicator. A change in character is also seen on the lower segment of the trough doublet; this is due to a change in the interference effects between reflections from the base of the UA-5 sand and the underlying coal-bearing section. The reflection from the base of the UA-5 sand has increased in amplitude due to the presence of CO_2 and the superposition pattern has been modified accordingly.

Differences between the two surveys can be evaluated more fully by subtracting the monitor depth migrated volume from the baseline volume (Figure 10). Away from the injection well the differences between the two surveys are incoherent and have low amplitude. In the vicinity of the well the difference volume shows a strong trough response reflecting the brightening in amplitude of the Top UA-5 trough event. This overlies a strong peak of comparable spatial extent which is associated with brightening of the Base UA-5 reflection due to CO_2 presence in the reservoir. It is interesting to note that the Base UA-5 event cannot be resolved on either the baseline or monitor surveys due to interference from the underlying coal-bearing sequence; however these interference effects cancel out when we difference the two surveys and the Base UA-5 reflection can now be identified by its increase in amplitude due to CO_2 flooding.

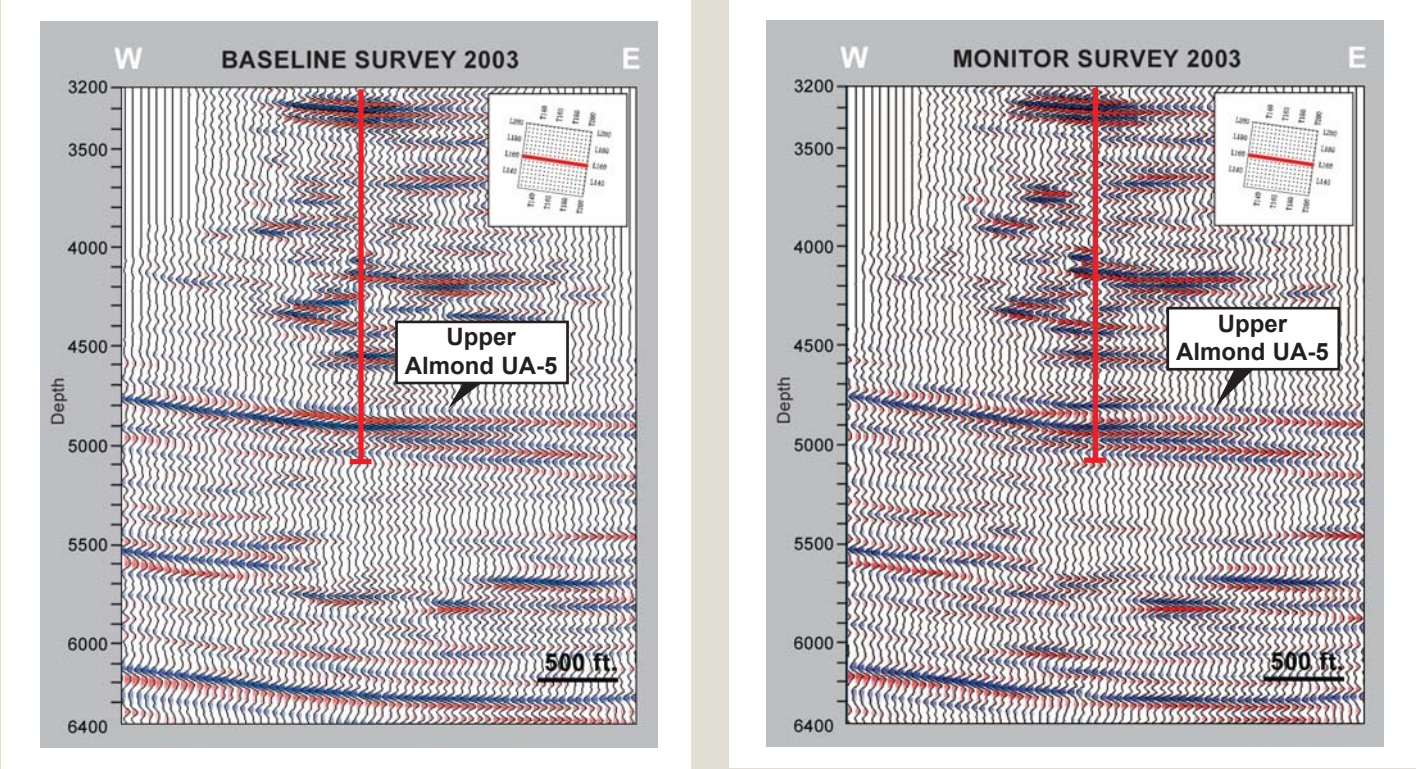

Figure 9 Time-lapse comparison of east/west vertical section through Monell 180 ST 1 well for baseline (left) and monitor (right) 3-D VSP surveys.

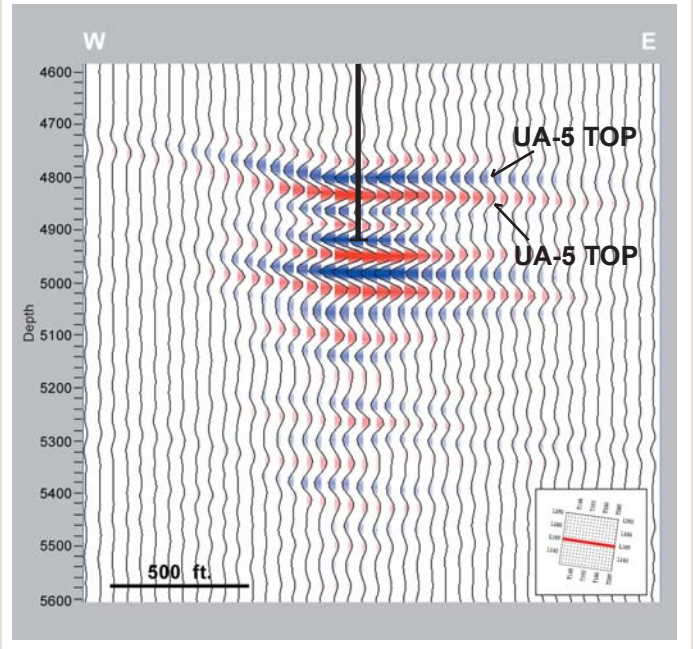

Figure 10. Time-lapse 3-D VSP east-west profile through the Monell 180 ST 1 well (monitor survey - baseline survey). Trace gain and vertical scale are twice that of Figure 9.

The presence of CO_2 in the reservoir also causes a velocity pull-down in the underlying reflections. This affects reflections immediately underlying the CO_2 flooded reservoir; deeper events are less affected by CO_2 in the reservoir and do not experience the same velocity pull-down.

The velocity pull-down causes a misalignment of events on the baseline and monitor surveys which gives rise to a set of events underlying the Base UA-5 peak on the difference volume. These are strictly velocity pull-down effects as amplitudes of the corresponding events on the baseline and monitor surveys are comparable and also no CO_2 was injected at these deeper levels. Comparing the baseline and monitor surveys, the magnitude of the velocity pull-down is measured as 6 - 8 ft. which implies a decrease in P-wave velocity within the reservoir of 14% - 19% due to the CO_2 flood. This is greater than the change of 6% predicted by Biot-Gassmann Equations; the difference may be due to uncertainties in pore fluid properties under reservoir conditions or inadequacies in the theory for multiphase fluids.

Figure 11 shows rms amplitude maps for the Upper Almond Top UA-5 trough event on the baseline and monitor surveys, based on a 40 ft. window encompassing this event. Away from the Monell 180 ST 1 well we see a close similarity in the amplitude distributions. The striking feature of this comparison is the increase in amplitude on the monitor survey in the vicinity of the Monell 180 ST 1 well, the CO_2 injection well, relative to the baseline survey.

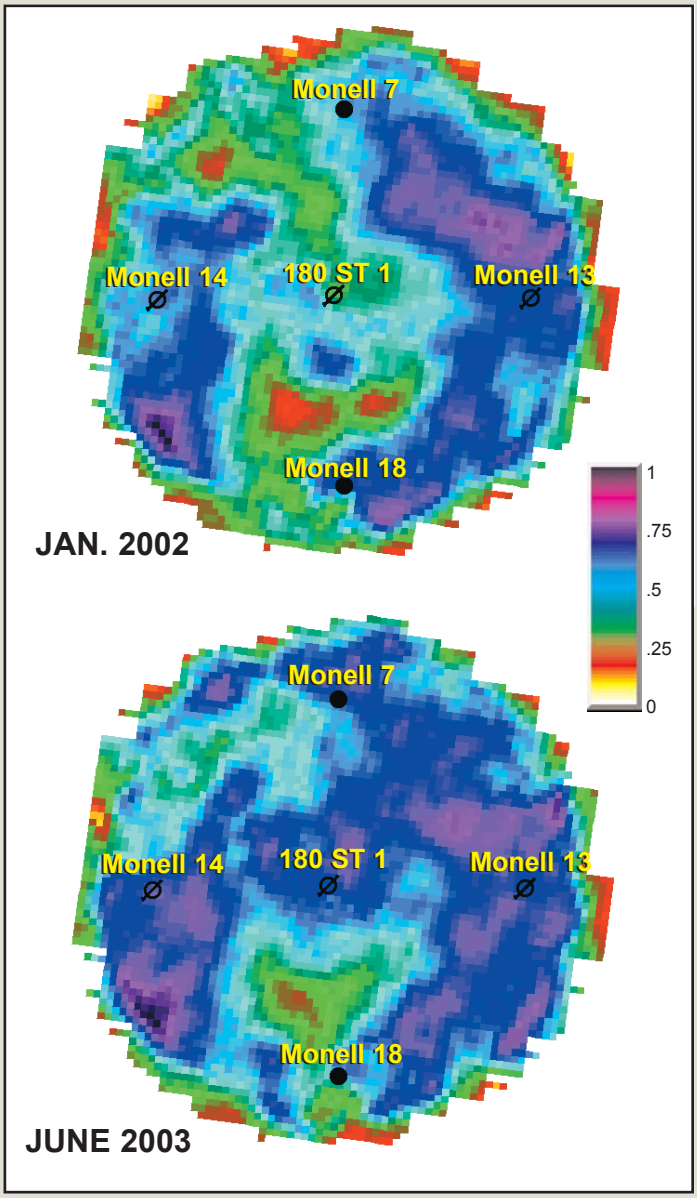

Figure 11 RMS amplitude maps for the Upper Almond Top UA-5 reflection (trough) for the baseline survey (top) and monitor survey (bottom).

Figure 12 shows the Upper Almond UA-5 time-lapse rms amplitude difference, picked on the volume which is the difference between the two cross-equalized surveys (monitor - baseline). This amplitude extraction is based on the equivalent interval that is mapped in Figure 11 for the baseline and monitor surveys. The time-lapse 3-D VSP data clearly map the advance of the CO_2 front.

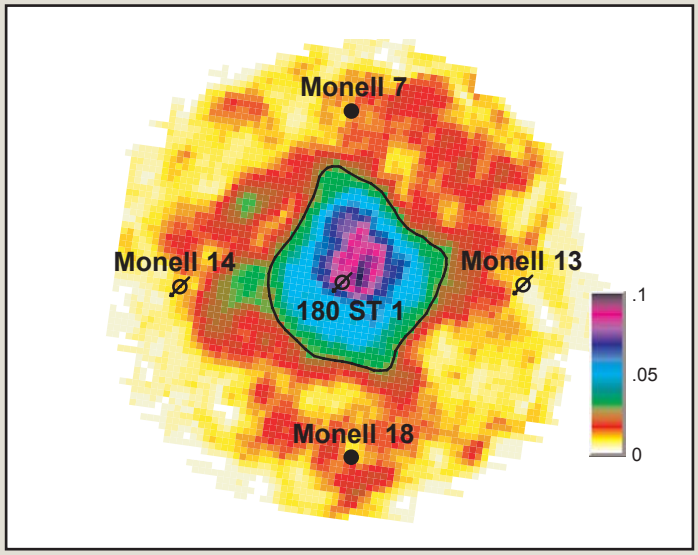

Figure 12. Upper Almond UA-5 time-lapse amplitude map extracted from the difference of the cross-equalized volumes (monitor survey - baseline survey). Solid curve shows the interpreted CO_2 front. Monell 180 ST 1 is the CO_2 injection well and the well in which the 3-D VSP surveys were acquired.

Time-lapse VSP data indicate that the CO_2 flood advanced 700-900 ft. from the injector well, generally in a radial direction. There is some preference for CO_2 movement towards the north-northwest which is the updip direction. VSP data show good areal sweep efficiency with no indications of CO_2 channeling nor any areas that remain unswept behind the flood. The VSP results agree with production data recorded during the course of the pilot project (Table 4). During this time the two producing wells recorded increased oil production, with Monell Unit 7 (north) showing greater enhancement than Monell Unit 18 (south). No CO_2 breakthrough is observed in either well.

	Pre CO_2 flood	Production after 18 months CO_2 flood
Monell 7	10 bbl/d	80 bbl/d
Monell 18	10 bbl/d	25 bbl/d

Table 4 Production data for Monell CO_2 pilot project.

As production data provides information only at a few discrete locations, these data cannot tell us how far the CO_2 flood has advanced between wells or determine the shape of the CO_2 front. This is information that time-lapse VSP monitoring can provide; it can identify the spatial location of the CO_2 front, the configuration of the front and the areal sweep of the flood. These results can then be used for improved history-matching of the reservoir simulation model to improve the accuracy of predicting ultimate oil recovery and for better full field CO_2 flood performance predictions.

We can also obtain an estimate of the potential oil recovery of the pilot flood from the time-lapse data. Knowing the areal extent of the CO_2 front and the volume

injected, we can estimate the CO_2 saturation within the reservoir. Assuming the flood extends over the full height of the reservoir and that saturation is uniform behind the flood front, mass balance calculations yield a CO_2 saturation of 15%. For a miscible flood, we can assume that CO_2 displaces an equal volume of oil in the reservoir. This indicates that an additional 28% of the original-oil-in-place is being displaced by the CO_2 flood in the pilot area, beyond that produced through primary or secondary recovery. Actual oil production will, of course, depend upon the flood continuing at the same efficiencies and the extent to which displaced or mobilized oil is recovered in producing wells.

Conclusions. 3-D VSP imaging offers distinctive advantages that make it a powerful technique for time-lapse reservoir imaging. The high frequency content of VSP data provide imaging detail with superior vertical and lateral resolution. The high signal/noise quality of the data yields images whose fidelity is sufficiently good that we can identify time-lapse effects with confidence and monitor changes in the reservoir. While the area imaged is small compared to that covered by a surface seismic survey, this may be sufficient for certain projects such as the Monell pilot project. Alternatively the technique may be expanded to a multiwell configuration.

In this paper we have presented a case study where time-lapse 3-D VSP successfully imaged the Monell CO_2 pilot project with a level of detail which would not be available from surface seismic. Specific findings of this study are:

- 3-D VSP imaged the Upper Almond reservoir with high vertical and lateral resolution and frequency content in excess of 130 Hz, and with high signal/noise ratio.
- Survey repeatability is excellent.
- The time lapse survey successfully monitored the CO_2 flood, showing that the CO_2 front moved a radial distance of 700 - 900 ft. from the injector.
- The CO_2 flood is quite homogeneous, with a slight preference towards north-northwest (updip), in agreement with production data.

Time-lapse VSP aided significantly in evaluating the response of the reservoir to CO_2 injection, which was the primary goal of the pilot project. The impact of time-lapse monitoring can be summarized as follows:

- Provided direct and conclusive evidence of favorable CO_2 flood sweep efficiency.
- Shortened the evaluation time of the CO_2 pilot test.
- Provided input to reservoir simulations to predict tertiary oil recovery.
- Provided cost effective justification for proceeding with full field CO_2 flood, which requires large capital investment for new wells and facilities.

The full field CO_2 flood has now been launched and is being developed in a staged approach. Since the pilot is located within the full-flood area, a second monitor VSP survey is under consideration to ensure the expansion flood is behaving favorably within the pilot area.

Acknowledgement

We wish to thank Anadarko Petroleum Corporation for permission to present this paper. We also thank the many geoscientists at Anadarko and at P/GSI who contributed to the success of this project.

The 3-D VSP surveys were acquired and processed by P/GSI. Seismic data are from PGS data library and are shown courtesy of PGS Onshore, Inc.

Gas hydrate exploration with 3D VSP technology, North Slope, Alaska

Donn McGuire, Anadarko Petroleum Corp, Steve Runyon and Tom Williams, Maurer Technology, Inc., and Bjorn Paulsson, Alex Goertz and Martin Karrenbach, Paulsson Geophysical Services, Inc.*

Summary

A 3D VSP survey was recorded in February 2004 in conjunction with a continuously cored hydrate exploratory well on the North Slope of Alaska. The purpose of the VSP was to identify and delineate lateral variations in the subsurface within the hydrate stability zone (HSZ) by using high frequency seismic sources arrayed in a 3D surface pattern and high-density 3 component geophones in the wellbore. The VSP data will be correlated with on-site core measurements in order to calibrate seismic properties measured from the rock samples with those recorded by the VSP survey.

Introduction

Methane hydrates are naturally occurring substances in which molecules of methane are trapped within a lattice of ice. These substances are stable within a domain of temperature and pressure in both permafrost and deep ocean environments. Each volume of gas hydrate is typically equivalent to 160 volumes of methane gas (Sloan, 1998). Naturally occurring gas hydrates have been detected in wells drilled on the North Slope of Alaska for many years (Collett, 1988). Studies of well log data suggest the zone in which hydrates are stable can be 800 to 1000 meters thick and extend for thousands of square kilometers (Figure 1).

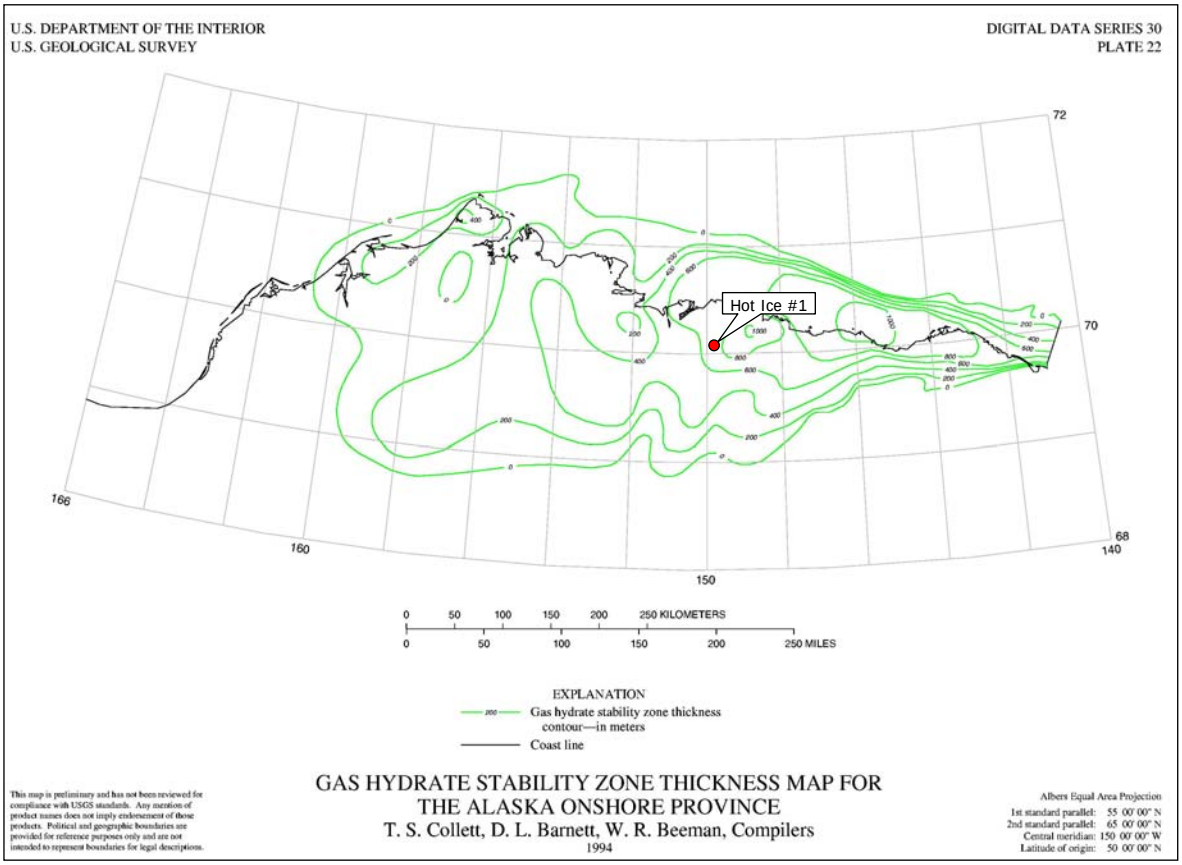

Figure 1. Map of Hydrate Stability Zone thickness on the Alaska North Slope.

DE-FC26-01NT41234

Gas Hydrate Exploration with 3D VSP

The occurrence of methane hydrates can be estimated in well log data but only by analyzing a suite of logs that includes gamma ray, resistivity, acoustic and mud logs. A type log with gamma ray, resistivity and sonic curves from Kuparuk River Field is shown in Figure 2.

Hydrates occurring within the permafrost are difficult to identify because many of the gas hydrate mechanical properties resemble those of ice (Collett & Kuuskraa, 1998). The primary indicator is an increase in gas shows on mud logs, but these occurrences are dependent on the mud system (mud weight, temperature and viscosity) being used.

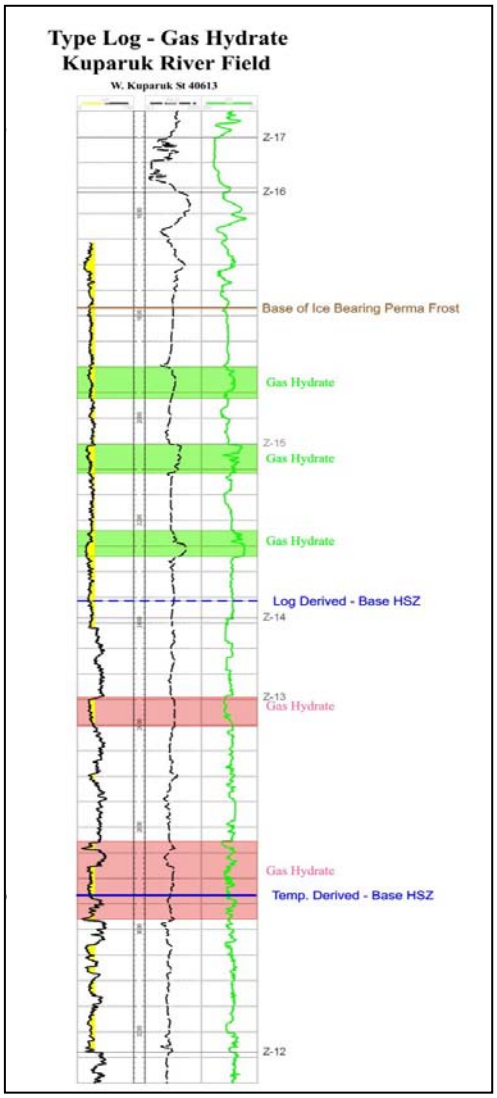

Figure 2. Type log of permafrost and hydrate-bearing reservoirs with electric log responses

Correlation of well log and core data indicated that, within the HSZ of the Alaska North Slope, hydrates would most likely occur in the Ugnu and West Sak sequences of the Sagavanirktok Formation. These are the lowermost sandstone units of the fluvial-deltaic, coal bearing sandstone, conglomerate and shale formation. The conglomerates, sands, and gravels are unconsolidated to moderately indurated at depth, and porosity is a function of compaction since no significant cements or diagenesis are evidenced.

Methods

In 2001, Anadarko Petroleum, Maurer Technology and Noble Drilling proposed to drill an exploratory well on the Alaska North Slope to investigate the occurrence, subsurface distribution and produceability of methane hydrates. Later that year, the U.S. Department of Energy's Office of Fossil Energy approved a cost-sharing proposal for the project (contract DE-FC26-01NT41331). Investigation and analysis of geological, geophysical and drilling data resulted in the spudding of the Hot Ice #1 well in March 2003 in section 30 of T9N, R8E. The well was suspended due to warm weather in April, 2003. Operations were resumed in January 2004 and drilled to TD in February. The well was continuously cored from surface to total depth in order to sample the entire thickness of the permafrost and hydrate stability zone. An on-site mobile core laboratory was designed and fabricated to measure rock properties at the well site in nearly in-situ conditions. Geophysical measurements of the core included compressional and shear velocities and density.

The velocity and density properties of methane hydrates are such that there is a weak impedance contrast between the hydrate-bearing sandstones and their surrounding shales. Analysis of 2D and 3D seismic data around area wells with log indications of hydrates showed little direct evidence of hydrate occurrence, primarily due to low fold coverage and surface ice-lake effects in the shallow seismic section. Seismic imaging of gas hydrates require better signal to noise, higher frequencies and denser sampling than found in traditional surface seismic data.

Synthetic seismograms were constructed with the well logs from the nearby Arco Cirque #2 well (Sec 17, T9N-R7E) to investigate the frequencies necessary to resolve the individual hydrate zones. The synthetic modeling suggested that a minimum of 160 Hz. would be required to discriminate individual hydrate bearing sands seen in that well.

A 3D VSP, using 3-component receivers, was identified as the best technique for recording seismic data to image the shallow subsurface at the Hot Ice #1 well. Design of the acquisition parameters utilized local well data for modeling subsurface coverage and for estimating the variations in offset and fold distribution for different surface source location grids.

The base of the HSZ at the Hot Ice #1 well was calculated to be at approximately 2000 ft. measured depth, based on temperature and pressure gradient data. The well was drilled to 2300 ft. to sample the full thickness of the HSZ. The depth of the well thus

defined the maximum offset distance for imaging hydrate-bearing sands. Longer offsets were added to image a regional marker horizon below the well for structural calibration.

Pre-survey planning identified the need for 25 foot vertical sampling in the well bore to avoid aliasing at the higher frequencies and to provide the best opportunity for imaging thin hydrate-bearing sands. The final survey design was based on a 2750 foot radius around the well bore to image deeper marker reflectors and had source point intervals increasing from 120 ft. at the well to 175 ft. at the perimeter. The combination of 1185 surface source points and 80 levels of 3 component geophones resulted in a 3D survey of 284,400 traces.

Numerous sweep lengths, frequency ranges and numbers of sweeps per station were tested at the well location. The final production sweep parameters were 2x10 second linear sweeps from 8 to 220 Hz. per surface position.

Data Example

Processing of the VSP data is in progress, and has proceeded through of the stages of trace editing, geometry assignment, 3C orientation, first break picking., deconvolution of the 3C oriented data, and preliminary steps of migration velocity analysis, amplitude correction, filtering and 3D Kirchhoff depth migration. Figure 3 is an example from the most recent processing output. Preliminary processing indicates useable frequencies (less than -30 dB down from maximum) over 200 Hz have been retained, and good quality, laterally consistent reflection events have been imaged. Completion of the data integration and interpretation is expected by July, 2004.

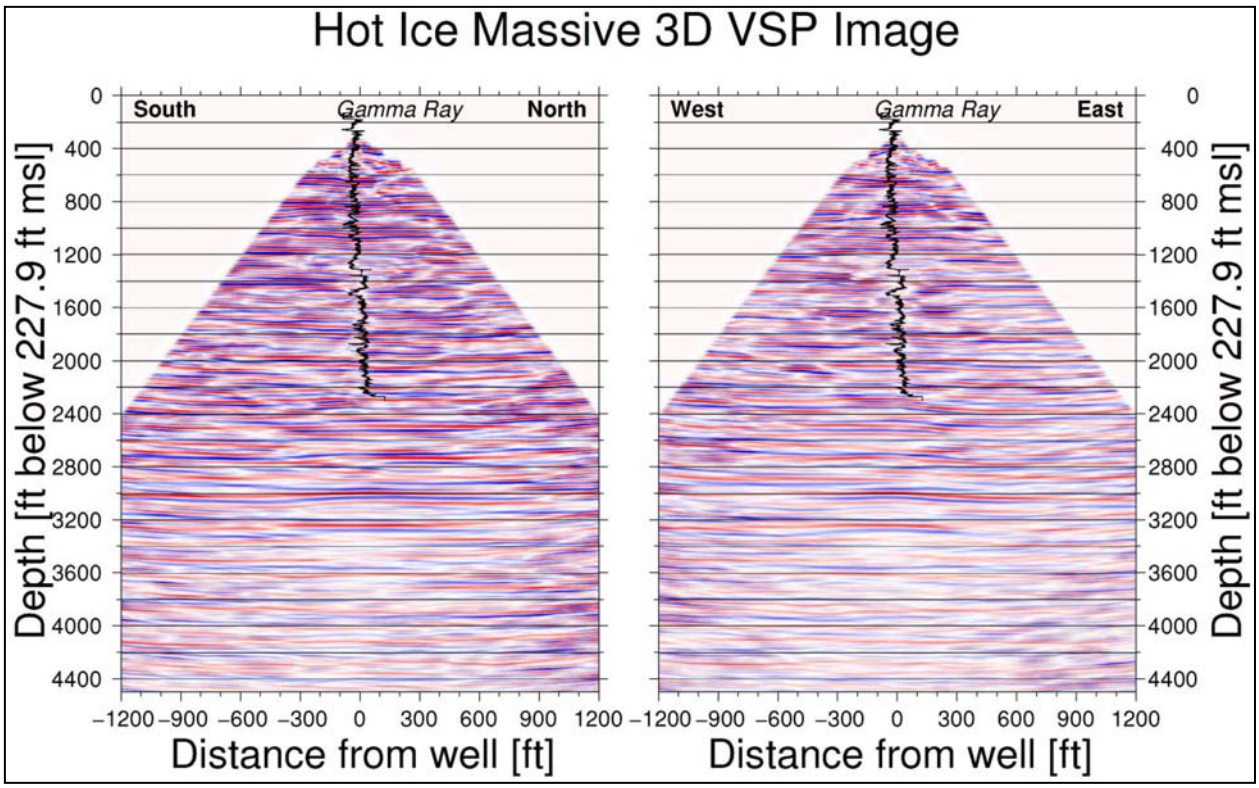

Figure 3. Migrated upgoing P-wave data with Hot Ice #1 Gamma-ray well log.

Gas Hydrate Exploration with 3D VSP

Conclusions

The massive 3D VSP successfully recorded high-frequency multicomponent seismic data at the Hot Ice #1 well. The seismic source signal was composed of 2 10 second linear sweeps from 8-220 Hz. transmitted from each of 1185 surface locations. The seismic data were recorded by 80 3-component geophones spaced at 25 foot intervals over the length of the wellbore resulting in over 283,000 live traces. Upon completion of the data processing, the VSP data will be correlated with well information and core measured rock properties for calibration and interpretation. This will allow zones of interest in the well to be mapped and interpreted throughout the area covered by the VSP. Well results, core measurements and the VSP interpretation will be discussed in the oral presentation.

References

Collett, T.S., Bird, K.J., Kvenvolden, K.A., and Magoon, L.B., 1988, Geologic interrelations relative to gas hydrates within the North Slope of Alaska, USGS Open-File Report 88-389, U.S. Geol. Surv., Menlo Park, CA. 150 p.

Collett, T.S., Barnett, D.L., and Beeman, W.R., compilers, 1994, Gas Hydrate Stability Zone Thickness Map for the Alaska Onshore Province, Plate 32, Digital Data Series 30, U.S. Geol. Surv., Menlo Park, CA.

Collett, T.S. and Kuuskraa, V.A., 1998, Hydrates contain vast store of world gas resources, *Oil & Gas Journal*, 96:19.

Sloan, E. D., 1998, Clathrate hydrates of natural gases (2nd ed.): New York, Marcel Dekker Inc. 705 p.

Acknowledgements

We wish to thank all of the personnel from Anadarko Petroleum, Paulsson Geophysical , Inc. and PGS Onshore who participated in the VSP survey.

This project was funded through a cost-share cooperative with the U.S. Department of Energy National Energy Technology Laboratory, contract DE-FC26-01NT41331

Equipment used for this survey was funded under DOE grant DE-FC26-01NT41234

Cost-effective imaging of CO_2 injection with borehole seismic methods

ERNEST L. MAJER, THOMAS M. DALEY, VALERIE KORNEEV, DALE COX, and JOHN E. PETERSON, Lawrence Berkeley National Laboratory, USA
JOHN H. QUEEN, Hi-Q Geophysical, Ponca City, Oklahoma, USA

Currently there is a critical need to increase oil and gas recovery from existing and new reservoirs. In addition, the ever-increasing need to sequester CO_2 in the subsurface places further emphasis on accurate imaging methods to validate CO_2 injection strategies. Two obstacles to increased efficiency are (1) a thorough understanding of the geologic complexity and fluid distribution and (2) the scaling relationships between fine scale/point measurements and larger scale/volumetric measurements. Although initially expensive, borehole methods may offer a cost-effective solution when integrated into a drilling and development program. New technology such as fiber-optic sensors emplaced during drilling and completion, microhole drilling, and other advances in sensors will make borehole technology much more cost effective when used over the long run. If deployed in a multicomponent and time-lapse fashion, seismic methods also offer the ability to define contrasts in properties, detecting subtle changes in properties associated with fluid content, and/or density and elastic properties changes.

Presented here are several case histories of using crosswell and vertical seismic profiling (VSP) methods in a time-lapse as well as static application to image the efficiency of CO_2 injection. Furthermore, the use of microholes for the emplacement of sensors to be used for borehole seismic imaging and its cost effectiveness are presented. One of the main obstacles preventing wider use of high-resolution seismic methods is the availability of holes. If small-diameter, relatively shallow, low-cost holes can be used as effectively as larger deeper holes, VSP and other borehole methods would become much cheaper.

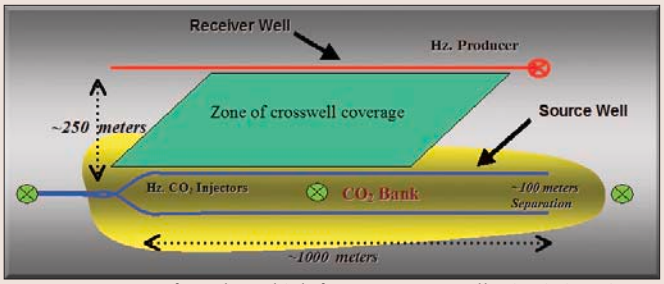

Figure 1. Layout of Weyburn high frequency crosswell seismic imaging experiment.

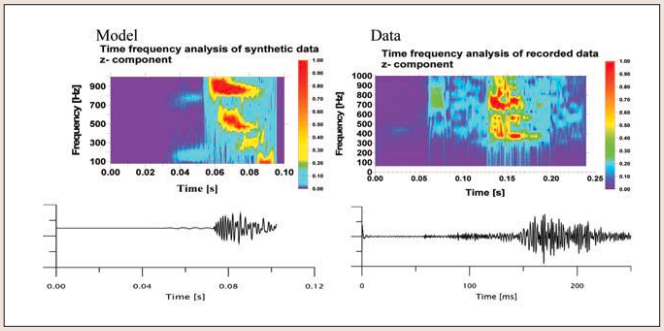

Figure 2. Finite difference modeling of crosswell seismic data compared to the actual data.

Weyburn Field, Saskatchewan, Canada. In order to determine the applicability as well as refine the borehole methods, a comprehensive plan for using seismic methods for mapping fluid migration was carried out at Pan Canadian's (now EnCana's) Weyburn Field in the Williston Basin in southern Canada from 2000 to 2003. The Weyburn oil field is located southeast of Weyburn, Saskatchewan, within the north-central Williston Basin which contains shallow marine sediments of Cambrian to Tertiary age. The Weyburn Field was discovered in 1954 and hosted an estimated 1.4 billion barrels of oil. Primary production within the field continued until 1964. Shortly after the initiation of waterflood in 1964, oil production peaked at 46 000 b/d in 1965. A waterflood has continued since then, with horizontal infill drilling commencing in 1991. Approximately 24% of the original oil in place had been recovered by 2000 when CO_2 injection began. The oil reserves reside within a thin zone (maximum thickness of 30 m) of fractured carbonates, which were deposited in a shallow carbonate shelf environment sealed by an evaporitic dolomite and shale sequence (Bunge, 2000). The oil resides in two units. Midale Marly unit has relatively high porosity (16–38%) and low permeability (1 to >100 md), and a relatively lower porosity (8–20%) and higher permeability (10 to > 500 md) Midale Vuggy unit. The CO_2-based enhanced oil recovery scheme was initiated in September of 2000 in 19 patterns of the EnCana Weyburn unit at an initial injection rate of 95 million ft^3 per day (mmcfd) (5000 tons/day). In 2003, the rate of CO_2 injection increased to 120 mmcfd, of which 25 mmcfd was CO_2 recycled from oil production. The CO_2-enhanced oil recovery (EOR) is contributing more than 5030 b/d to the total daily production of 20 560 b/d for the entire Weyburn unit. The CO_2 flood will be expanded gradually over the next 15 years into an additional 75 patterns with ~20 million tons of injected CO_2 anticipated over the lifetime of the project. The source of CO_2 is the Dakota Gasification Company's synthetic fuel plant, which is located in Beulah, North Dakota. The CO_2 is transported 320 km via pipeline to the Weyburn Field.

The seismic work consisted of a time-lapse (two) 3D VSP (P/GSI), a nine-component VSP (OYO Geospace), time-lapse (three) 3D, 9-C surface seismic surveys (Colorado School of Mines), time-lapse (three) 3D P-wave surface seismic (EnCana), a crosswell seismic survey in two horizontal wells in the reservoir (Lawrence Berkeley National Laboratory (LBNL/OYO), four offset single-component VSPs (Zseis/LBNL), and two vertical crosswell seismic surveys (Zseis/LBNL).

Horizontal crosswell: Two reasonably parallel horizontal wells separated by 250 m were used for the crosswell survey (Figure 1). The source well is a sidetrack from a nearby horizontal well, and the receiver well is a producer; both are open hole. The upper reservoir layer, ~ 1500 m in depth in which the wells resided, has a velocity of 3500 m/s that is much lower than layers above and below (5000–6000 m/s). The effect of being in a thin low-velocity layer obviously controls the first-arrival data. The main issue considered was the volume sampled with the first arrival (which travels in the lay-

DE-FC26-01NT41234

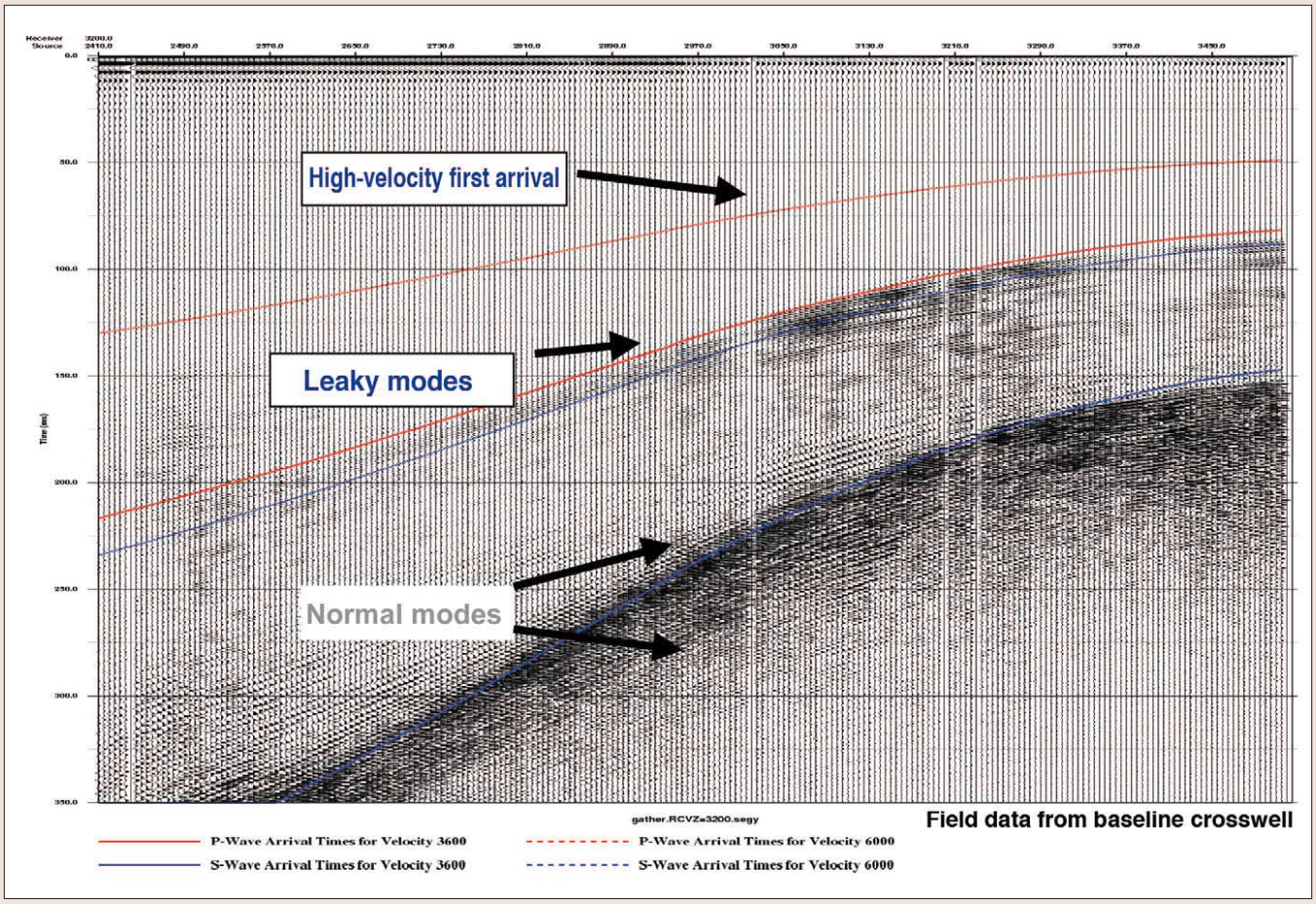

Figure 3. *Example of the crosswell seismic data showing the leaky and normal modes; as can be seen the "first arrival" data from the high-velocity layers bounding the reservoir (red line at top of figure) are not usable.*

ers above and below the reservoir layer) compared to the direct arrival traveling in the layer in which the wells are located. To determine the frequency content, arrival time, and amplitude of the different arrivals, a 2D finite-difference elastic modeling was performed. From this modeling it was determined that the direct arrival in the low-velocity zone was very weak as were the refracted arrivals in the bounding layers. However, a strong arrival was the guided wave in the low-velocity layer with definite dispersive characteristics (Figure 2).

Another prime concern was the position control. In vertical wells, the crosswell technology is well developed to place the sensors using wireline technology. In long horizontal wells such as the subject case, there was no established deployment technology that was available for crosswell tools in such wells. For this work, it was critical that not only absolute position be maintained, but that repeatability to within 0.5 m be achieved to ensure that errors in positioning are less than those produced by CO_2 saturation. Other factors controlling the acquisition were the time allowed to do the survey, the overall cost, the size and length of instruments that could be placed in the wells, and the safety issues (this is an H_2S site).

After considering the above issues it was determined that this project needed in general a wide-band (up to several kilohertz) signal recorded at a few meters spacing using as many recording levels as possible simultaneously. Coiled tubing deployment was chosen to protect the integrity of the hole. To achieve the high frequency necessary to resolve the thin layer as well as provide a wide bandwidth for dispersion studies, a commercial piezoelectric source was selected and modified to fit on the end of coiled tubing. Furthermore, protective spacers and the power cable run through the center of the tubing were required. This all had to be sealed, which created issues if the tool could not be pushed far enough; i.e., in most coiled tubing jobs fluid can be injected out of the end if obstructions are encountered. Factors on wellbore safety and unknown limits on pushing the string limited us to a coiled tubing filled with oil that had 48 levels of hydrophones spaced 15 m apart.

The piezoelectric source was pushed into the injection well as far as possible (more than 700 m). Several repeat runs were done to ensure that we had confidence in the placement. The final location was nearly 2200 m from the surface. The source was then pulled back a few meters to take the "coil" out of the line. The receiver coil tubing was then pushed as far down the production well as possible. The 48-level hydrophones were at 15-m spacing in the coiled tubing. The source was activated with a sweep of 200 to 2000 Hz every 3 m. After the source was dragged along the horizontal section of the hole, it was pushed back to its starting position for another run. The receiver string was then pulled three meters, and the source sweep was repeated. This was done five times in total so that a complete crosswell survey at 3-m spacing was acquired. To check source repeatability on the last run, the source sweep was repeated while the hydrophones were kept in place.

A weak first arrival and a large dispersive guided wave were recorded as expected (Figure 3). Conventional data processing could not be applied; hence we performed an amplitude analysis to produce an attenuation tomogram of different center frequencies of the guided waves. This was

DE-FC26-01NT41234

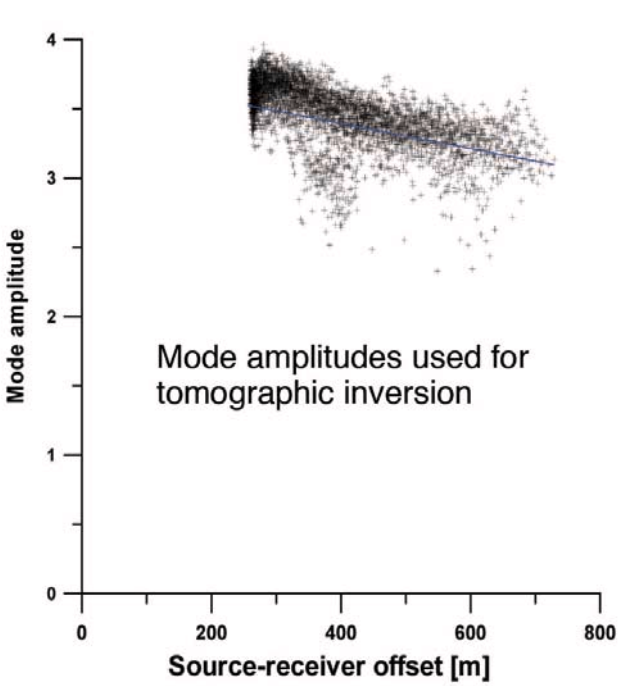

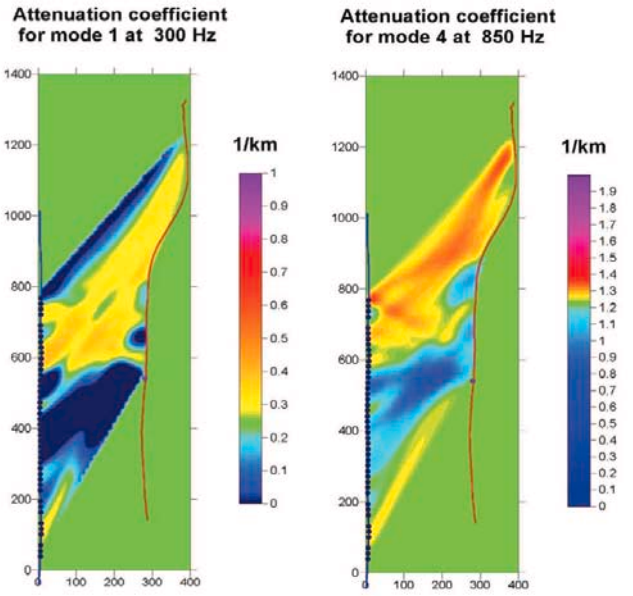

Figure 4. The 300- and 850-Hz mode results of the amplitude tomography.

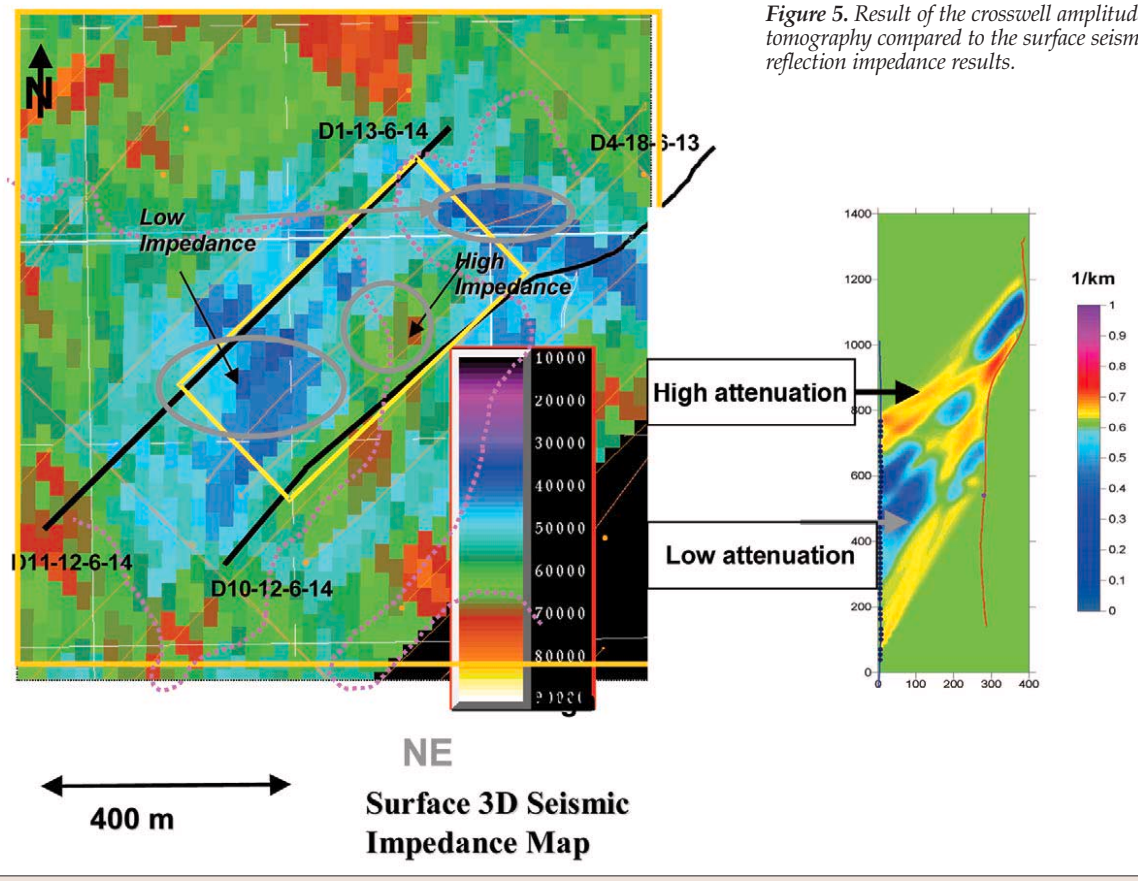

Figure 5. Result of the crosswell amplitude tomography compared to the surface seismic reflection impedance results.

done by examining the amplitude as a function of frequency and performing a modal decomposition of the data for each wave path (Figure 4). If one compares the crosswell and surface results in this region, the amplitude results correlate well with the impedance results. That is if the low-amplitude tomographic results due to denser fracture patterns are zones of higher reflectivity in the surface seismic (Figure 5). The tomograms for different frequencies (Figure 6) have been converted from an attenuation image to permeability within the depth slice by using porosity and fluid viscosity from the reservoir model, and using Biot relationships to calculate the permeability. The resulting permeability values clearly depend on the parameters from the reservoir model and the assumed attenuation mechanisms, but the observed trends should be robust. The calculated permeability values range from 50 to 150 md, which is compara-

DE-FC26-01NT41234

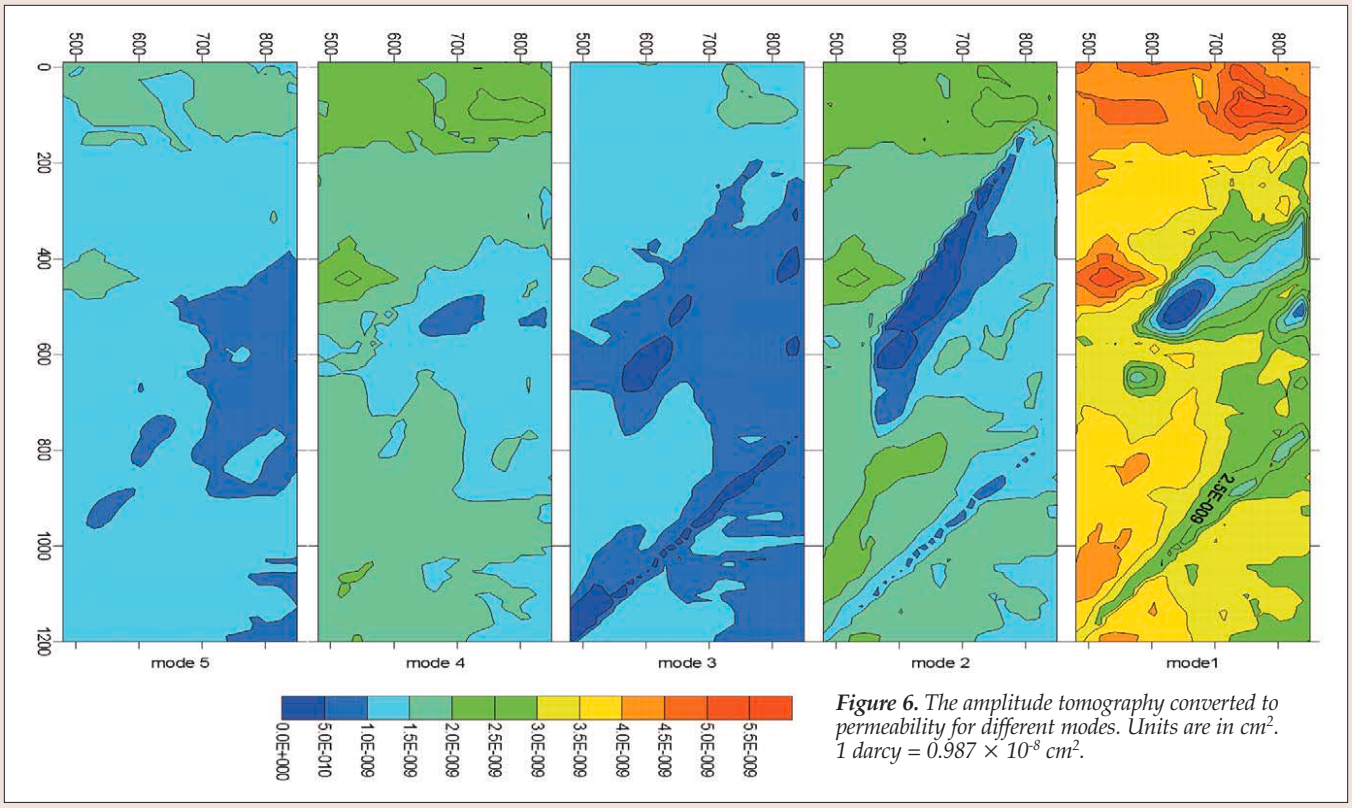

Figure 6. *The amplitude tomography converted to permeability for different modes. Units are in cm^2. 1 darcy = 0.987 × 10^{-8} cm^2.*

ble to the range of permeabilities measured within this unit (10–500 md). Of note, the spatial trends in the calculated permeability are at an angle to the horizontal injection wells (oriented along-trend) and are also oblique to the local seismic impedance and porosity trends suggesting the presence of off-trend zones of enhanced permeability. Due to the acquisition geometry, the tomographic image cannot resolve permeable zones which are oriented parallel the horizontal wells.

VSP and vertical crosswell: As part of the seismic imaging program at Weyburn, two perpendicular crosswell seismic surveys and four VSP offsets were acquired in November 2002. The purpose was to obtain detailed structural information above, in, and below the CO_2 injection horizon in the vicinity of an injection pattern which had low oil recovery but relatively high CO_2 injection rates. This zone had been identified as an area that had one of the largest volumes of CO_2 injected, a significant surface seismic anomaly, yet very little CO_2 had reached the nearby production wells. In addition to this work, a 3D vertical seismic profile (80-level 3-C VSP) time-lapse survey was acquired by EnCana in the same area prior to this work. The vertical crosswell was intended to provide reflection and tomographic images of reservoir properties at the meter resolution scale, exploring for structural reasons why the CO_2 had not migrated to the production wells.

In November 2002, following the third CSM 9-C surface seismic, EnCana and LBNL carried out the vertical crosswell and VSP experiment. A commercial company was contracted to carry out the crosswell survey with its piezoelectric source and 10-level hydrophone recording system. Two crosswell seismic profiles in three vertical wells located in one of the injection patterns were obtained. This provided crosswell data perpendicular (Profile 1) to the injection wells (390 m between wells) and parallel (Profile 2) to the horizontal injection wells (580 m between wells) (Figure 7). The vertical coverage was 380–1337 m deep at 3-m spacing. The

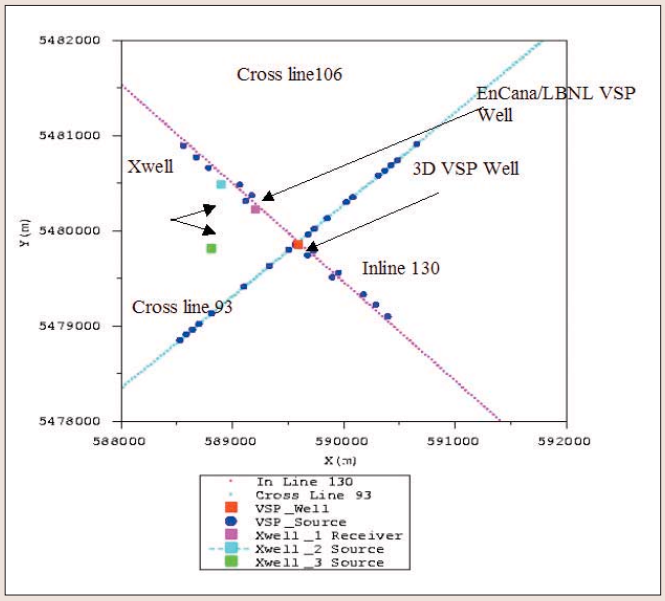

Figure 7. *Relative location of the VSP and vertical crosswell surveys. This entire area was also covered by the surface seismic as indicated by the inline and crosslines that cut through the 3D VSP.*

source sweep was 200–2000 Hz with peak energy around 500 Hz, and thus provided resolution about 10 times the surface seismic peak frequency.

In addition to the crosswell survey, we performed four offset VSP surveys, after the crosswell completion. A near offset at about 24 m from the receiver well (shotpoint 3) and three distant VSP points (at 580 m, shotpoint 4; 800 m, shotpoint 1; and 1200 m, shotpoint 2). The vertical coverage of the VSP was also from 380 m to 1337 m. Both vertical and horizontal component sources were used to generate P-wave and S-wave data, but the best data were obtained using the vertical component (i.e., P-wave) source. The P-

DE-FC26-01NT41234

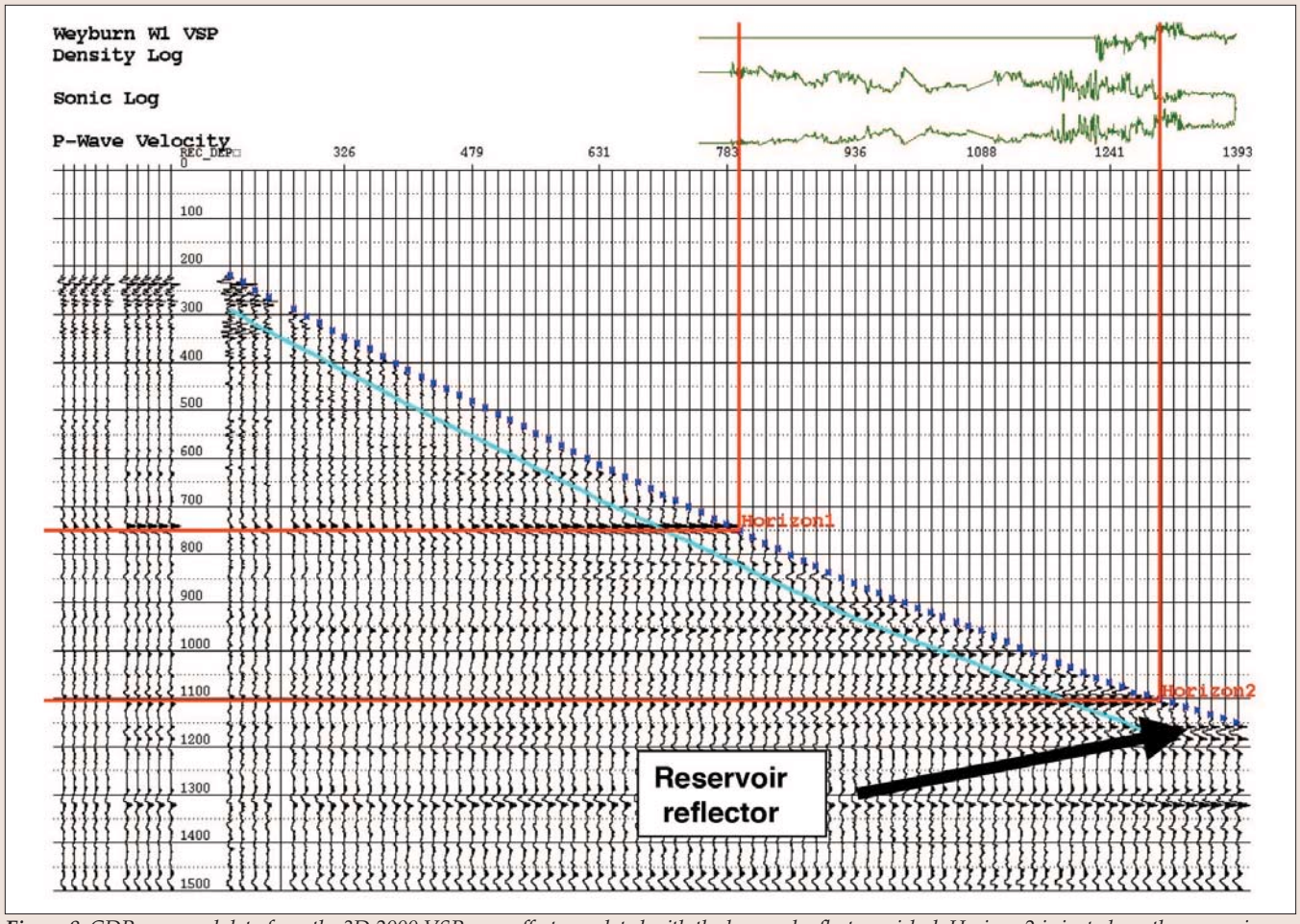

Figure 8. *CDP processed data from the 3D 2000 VSP near offset correlated with the logs and reflectors picked. Horizon 2 is just above the reservoir. The reflector at approximately 1150 ms is the reflector picked for the surface seismic as the top of the reservoir in this region.*

wave source sweep was 8–150 Hz with a 10-s sweep length. The S-wave (oriented perpendicular to the well) was from 10 to 90 Hz, 10-s sweep length. A stack of eight sweeps was acquired at each level for each source. The S-wave was abandoned after six levels due to poor signal-to-noise ratio.

The P-wave VSP data were of fair quality. Tube wave interference was the primary problem due to the low signal levels. A velocity model to process the CDP data was obtained from three different sources, well logs in the area, and the near-offset VSP and the 3D VSP from EnCana, which was collected in 2000. To interpret the results it was necessary to correlate the reflectors to the lithology. After removing the tube waves from the hydrophone VSP, there was some difficulty trying to interpret the zero-offset VSP, (offset 3) and the VSP CDP transforms of the mid- and far-southwest offsets (2 and 4). Because there was a zero-offset VSP that was collected with the first Weyburn 3D/3-C seismic acquisition, it was decided to process this VSP, called W1, to see how well it matched the LBNL/EnCana VSP. The W1 VSP was not acquired in the same well as the hydrophone VSP, but it turned out it was possible to project to the hydrophone VSP. We also used the surface seismic "1150" ms reflector as the top of the reservoir to correlate with in these data (Figure 8). Correlating the hydrophone VSP with the 3D/3-C VSP gave us confidence that we were looking at real reflectors in the hydrophone VSP.

The crosswell data were also of fair signal-to-noise quality. The long distance between the wells was of concern for the particular technology used (piezoelectric source and hydrophones). It should be noted that the same technology was used in the horizontal crosswell survey with success, but those distances were on the order of 250 m between the wells. Commercial processing was used. The velocity profile used to process the data was the one derived from the LBNL/VSP data. Some success was achieved in the short cross section but not in the long cross section. It shows a hint of a through-going feature above the reservoir (Figure 9). Of note are the Marly and Vuggy formations. The crosswell data do resolve the formations quite well but no significant features that would suggest a pathway for the CO_2.

The crosswell data were examined for velocity, amplitude, and tomographic processing. We were able to overcome tube wave interference mainly by simple *f-k* processing and data filtering. We also noticed the good resolution of the velocity structure in both data sets (profile 1 and 2). The beds are quite well resolved, and one sees the overall velocity structure above the reservoir. There are some areas that are less resolved due to high attenuation, however. To determine if this was of particular significance we looked at the amplitude and traveltimes for each of the offsets. A significant velocity difference between the two profiles was observed (Figure 10). The first thought was that we had the wrong information on the wells or that the data had been switched between the two profiles. After obtaining the deviation logs we saw that this was not the case. The large (25–20%) velocity anisotropy appears to be real. There is also an amplitude difference (other than geometrical spreading) between the two data sets.

Both EnCana's and CSM's 4D results have shown strong seismic anomalies that effectively correlate with the performance in the CO_2 flood front movements and confor-

DE-FC26-01NT41234

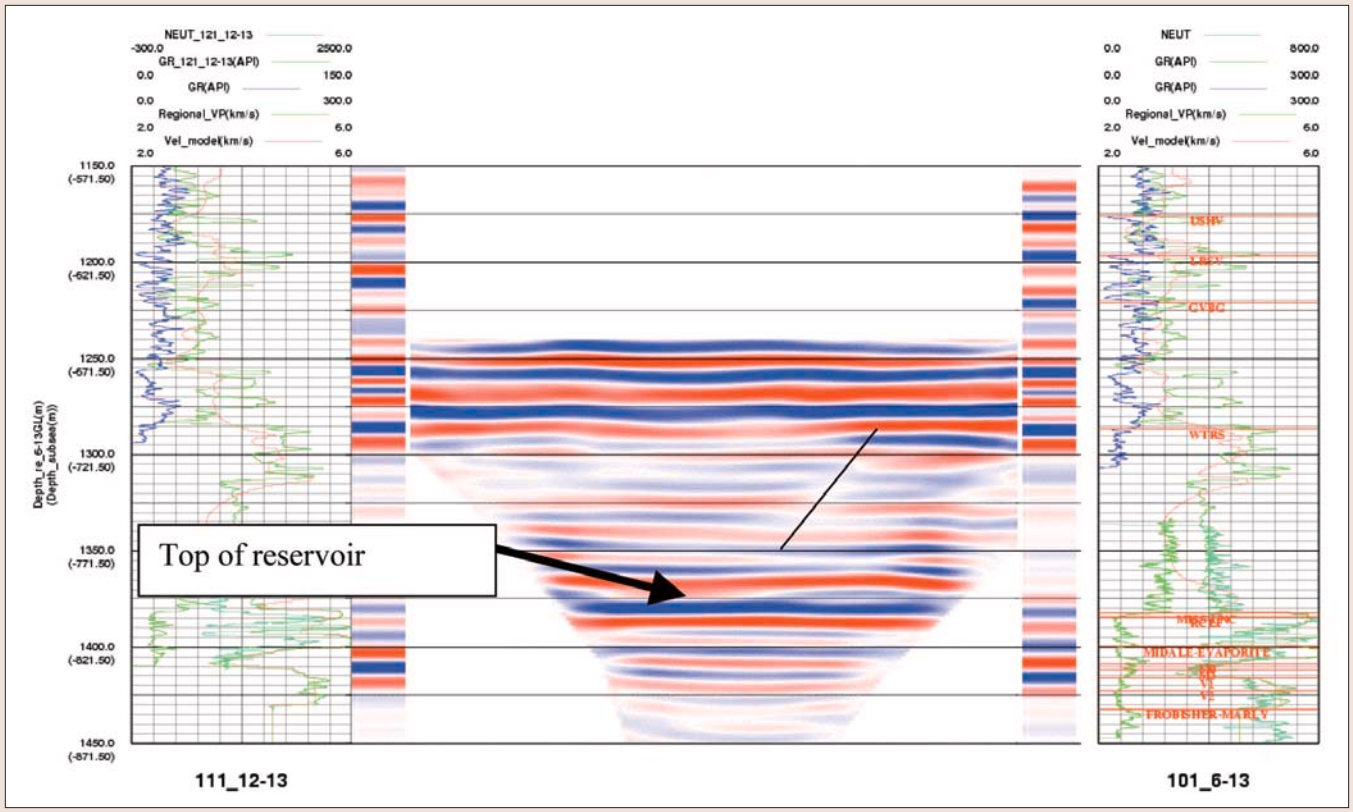

Figure 9. Profile #1 result for entire interval. The dark line is the top of the reservoir. There do not appear to be any obvious faults, although one may see a hint of a fault above the reservoir.

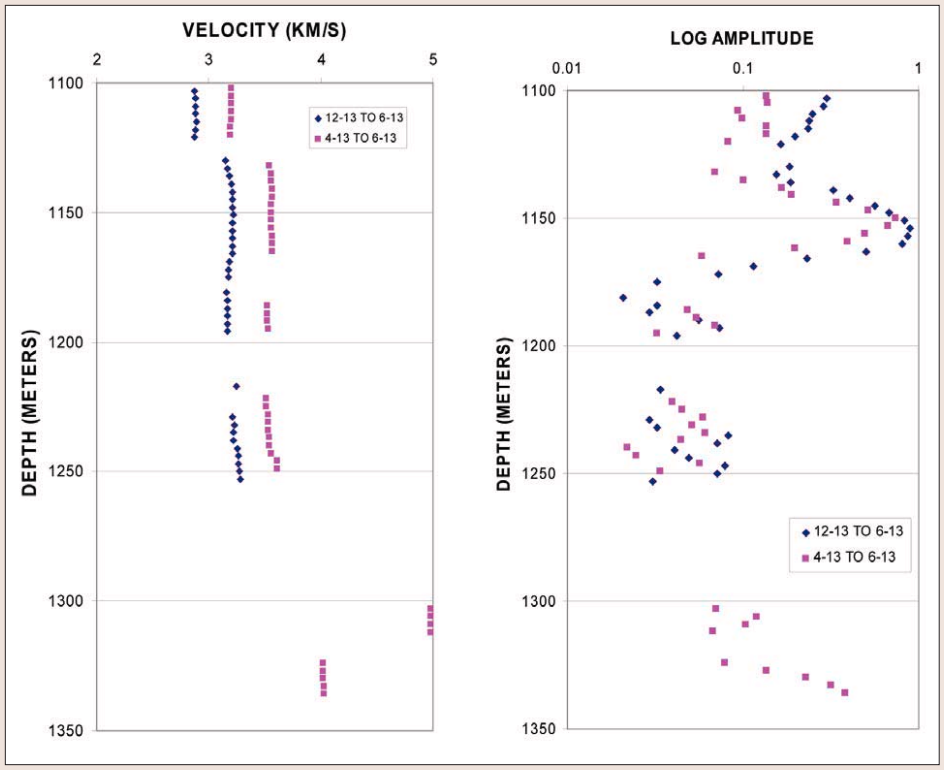

Figure 10. Comparison of the two different velocity and amplitude profiles along the long (pink) and short (blue) profiles. Note the much lower velocity parallel to the assumed fracture direction (SW to NE).

mance efficiency, supported largely by information such as production data and tracer study. However, the 4D surface seismic has also produced some unexpected results. For example, the pattern of the subject VSP and crosswell has so far behaved quite abnormally. It has not yet generated any production response even after it had received a total 3.4 billion ft^3 volume of CO_2 (or equivalently 12.3% HCPV), an amount that would have made a normal pattern yield good production response. Although this pattern is still taking injection, pattern pressure has increased significantly. A horizontal injection logging conducted within one of the two legs reveals that more than 40% of total injected volume moves toward the last 300 m of the lateral distance. The injection well was found drilled mainly within the reservoir with the underlying impermeable layer. Around the injectors, the seismic data consistently shows a very strong 4D seismic anomaly. EnCana's 4D data further show significant time delay at and below the reservoir layers and seismic energy attenuation, both indicating a significant amount of CO_2 gas accumulated near or within the reservoir.

One of the critical questions that needed to be addressed prior to this work was what formation was causing the amplitude changes in the time-lapse surface seismic. There were three possibilities, the bottom of the reservoir, middle, or top. The significance of the VSP data confirm that the reflec-

DE-FC26-01NT41234

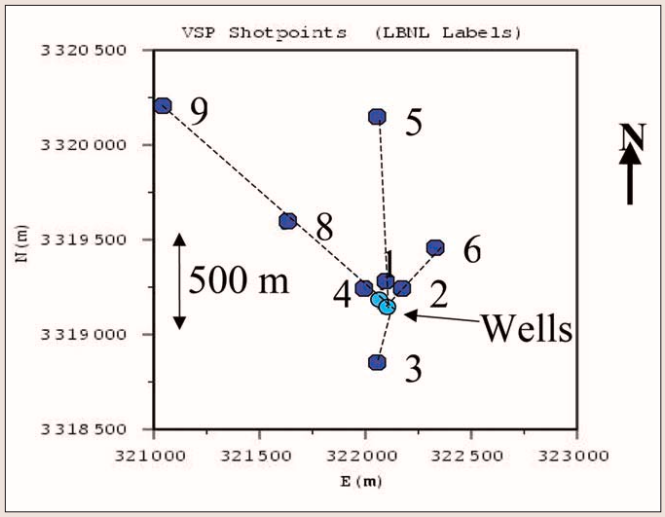

Figure 11. Location of the injection and monitoring wells (blue dots) and the VSP offsets.

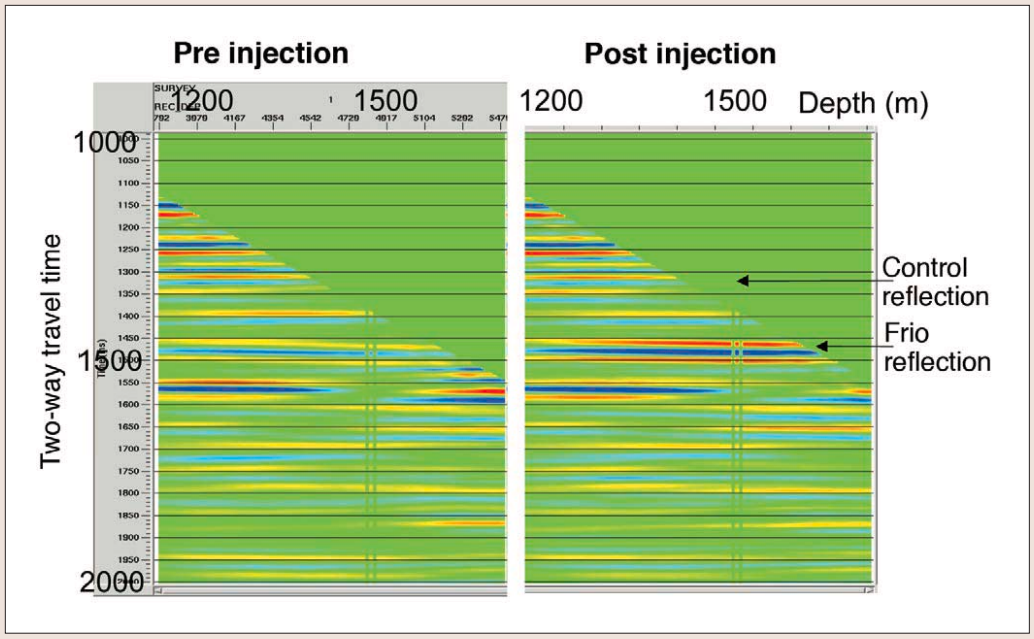

Figure 12. VSP time-lapse results.

tor used as a time lapse in the surface seismic is off the top of the Marly. This is important because it indicates that the anomaly seen in the surface seismic is indeed from the assumed volume of CO_2 injection. The surface seismic clearly indicated that the CO_2 was progressing toward the assumed production wells, but no CO_2 had shown up in these production wells as was the case in other areas where surface seismic did indicate that CO_2 was going in the desired direction. The question must be asked then: Why if we see a surface seismic anomaly do we not see the CO_2 as expected in the nearby production wells? A clue may lie with the crosswell data in the severe velocity anisotropy. The velocity anisotropy may indicate fracturing in the formation, thus causing preferential flow or at least delayed flow. The velocity anisotropy is a maximum just above the reservoir and in other levels above the reservoir. However, if the CO_2 is "leaking" above or below why do we see a surface seismic anomaly? Depending on where the "leaks" are will dictate if the seismic can detect the leakage. If there are leaks close to the injection wells then one would not expect to see a surface seismic anomaly. If they are farther away from the wells then one would not see anomalies close to the well. Thus, as the CO_2 migrated out and encountered a large path then it may migrate up away from the formation and not be directed to the production wells.

Frio CO_2 injection experiment. As part of a U.S. Department of Energy (DOE) funded project on geologic sequestration of CO_2, we acquired borehole (crosswell and VSP) seismic surveys before and after injection of about 1500 tons of CO_2 into a saline aquifer. These experiments were part of an integrated suite of scientific studies with many contributing institutions including the Texas Bureau of Economic Geology. The site is part of the on-shore Gulf of Mexico Frio Formation sandstone, near Houston, Texas, in a historic oil field. A new well was drilled for injection with a 30-m offset from the existing observation well. The CO_2 injection took place over 10 days in October 2004 with about 1600 tons of supercritical CO_2 injected into the upper C-sand of the Frio Formation at a depth of 1528.5–1534.7 m. The Frio "C" sandstone, a 23-m-thick brine-bearing interval above oil production, was selected as the injection target. The upper part of the "C" sandstone has porosities of 30–35% and permeabilities of 2000–2500 md. The top "C" seal is composed of shale, sands, and siltstones that form a minor seal beneath the regional Anahuac Shale and probably serves as a major barrier to vertical flow out of the "C" sandstone. Dips within the injection compartment are steep. Handpicked interpretation of the formation micro-imaging (FMI) log measured dips of 18° to the south at the injection well; interwell correlation measured an average dip of 16° south.

For sensors, both the VSP and crosswell surveys used an 80-level three-component, clamping geophone string, which was deployed on special tubing. Each of the 80 three-component sensors was independently clamped to the borehole wall, allowing measurement of ground motion (velocity). For the VSP, the sensors were spaced every 7.6 m along the string, so the 80 sensors spanned 2000 ft of the borehole. The shotpoints were offset 100–1500 m from the sensor well. The location of the shotpoints (Figure 11) was designed to monitor the estimated CO_2 plume location (mainly VSP sites 1–4) and to provide structural information at the injection site (mainly sites 5–9). Explosive sources were used for the VSP. The three-component sensors allowed optimal measurement of compressional (P) and shear (S) waves, which are orthogonally polarized. For the crosswell survey, the source was an orbital vibrator with a 70–350 Hz bandwidth. Consistent generation of both P- and S-waves is a notable feature of the orbital vibrator. For the crosswell survey the receiver string was moved and interleaved to give 1.5-m spacing with the sources spanning 75 m and the sensors spanning 300 m. Source and sensor locations were centered on the 6–7 m thick injection interval.

The processing of the VSP focused on time-lapse change

DE-FC26-01NT41234

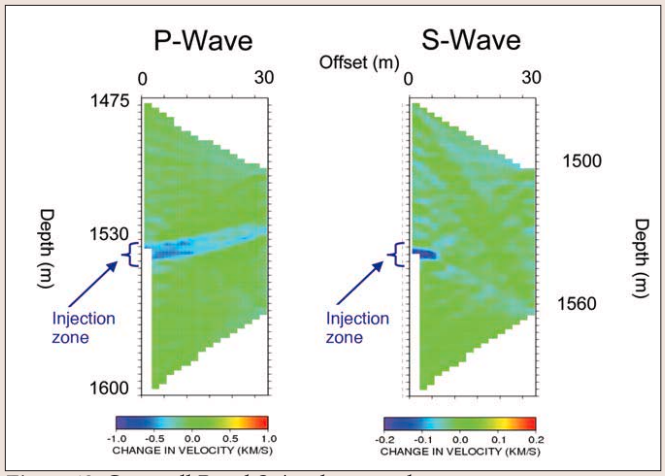

Figure 13. *Crosswell P and S time-lapse results.*

in reflection amplitude of the reservoir horizon. Initial processing included applying time shifts to correct for shot variations (as measured with a surface geophone at each shotpoint), picking of arrival times at each depth, separation of down-going and up-going (reflected) wavefields, converting reflections to two-way traveltime and enhancing the reflected energy signal using frequency-wavenumber filters. Following these processing steps, an amplitude equalization was applied using a reflection above the reservoir, thereby removing the time-lapse changes due to near surface and shallow subsurface variation (such as soil moisture saturation). At this point the time-lapse change reservoir reflection can be analyzed. A clear increase in the reflection strength from the Frio Formation reflection after the CO_2 was injected is seen at source site 1 (Figure 12). Similar results were found from the sites 2, 3, and 4. The crosswell survey processing included source deconvolution and decomposition, picking traveltimes using the inline

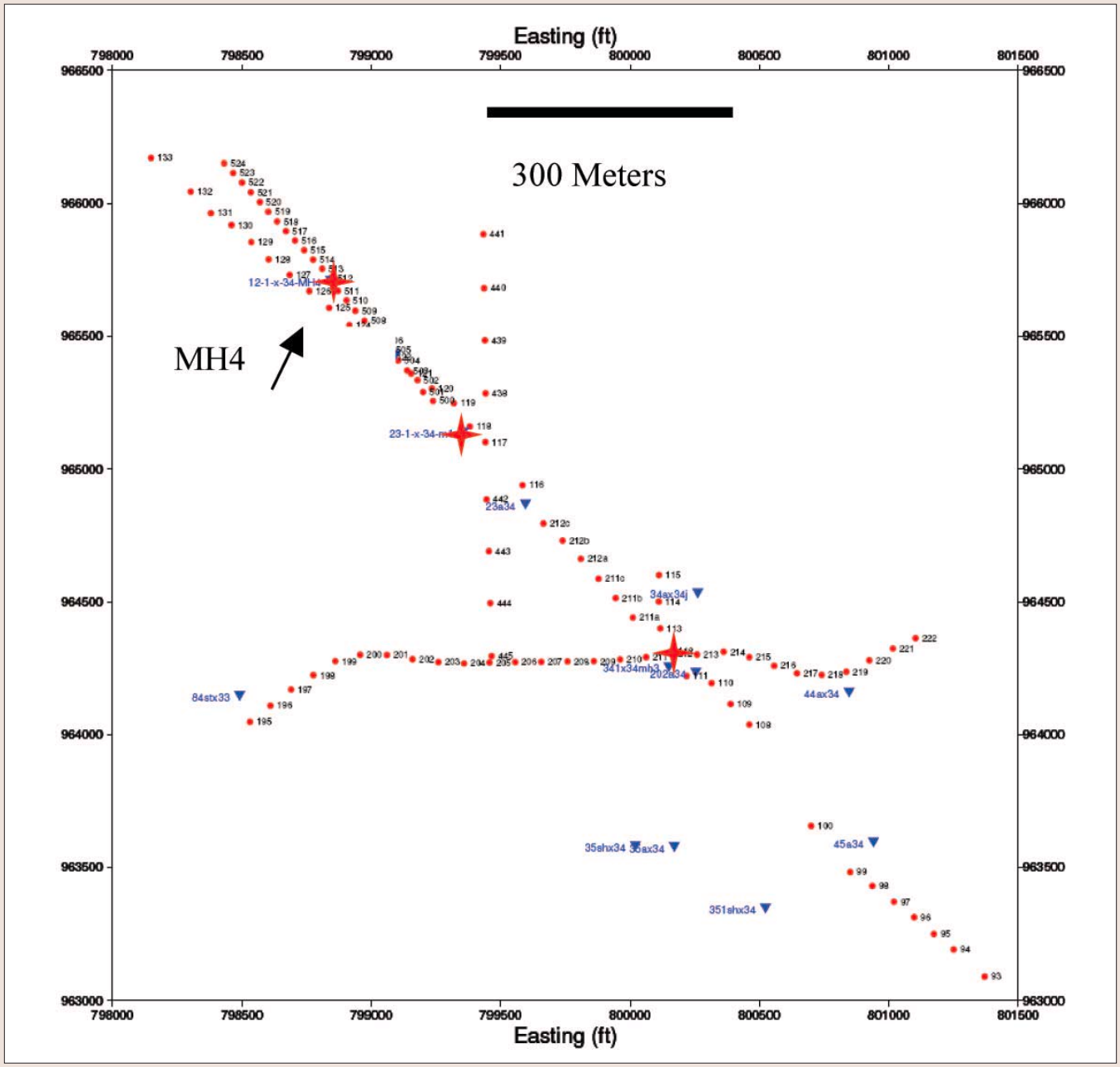

Figure 14. *Geometry of microhole VS. Three full VSP surveys were carried out (150 shots) in three different wells. Total time of deployment including moving and deploying a 48-level string between three different wells was 18 hours.*

DE-FC26-01NT41234

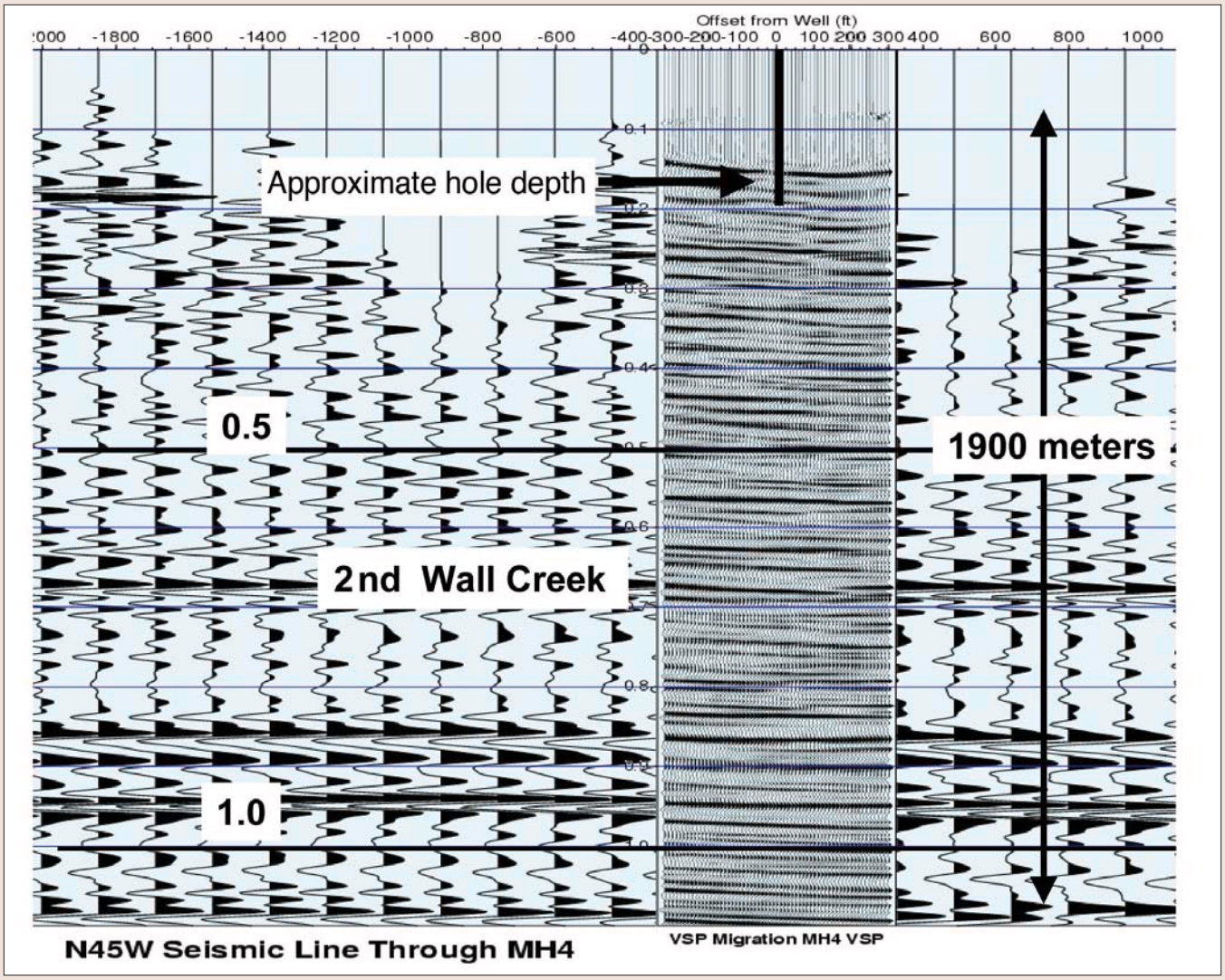

Figure 15. *The zero-offset VSP from the 730-ft PVC hole inserted into the 3D surface seismic data set. Reflections are being seen in the vibroseis data more than five times the hole depth with more than double the frequency content of the surface seismic.*

source and inline sensor for P-wave and the crossline source and crossline sensor for S-wave. Importantly, the data were inverted (2 × 2 m pixel) for the change in velocity, rather than inverting for each velocity field and then differencing. We have found that this improves the resolution of temporal changes. The P-wave tomogram shows a clear zone of change in the injection interval with P-wave velocity decreasing more than 500 m/s in some pixels (Figure 13). The S-wave tomogram shows only small changes except for a small region near the injection zone where the S-wave velocity is reduced by up to 200 m/s (Figure 13). The CO_2 plume is clearly imaged by the velocity change, and the spatial agreement between the well logs and the tomograms provides mutual corroboration to each of these two independent measures of CO_2.

Time-lapse tomographic and VSP imaging did map changes in P-wave velocity and impedance (over 500 m/s) due to the CO_2 plume. The S-wave velocity decrease near the injection well implies that there was some change in rock matrix properties (the shear modulus) in the near well region, which was induced by the CO_2 injection. Overall, the lack of S-wave change confirms that the observed P-wave change is due to fluid substitution of CO_2 for brine. Therefore, we interpret the following observations of velocity change in terms of CO_2 saturation.

1) The velocity change follows the dip of the stratigraphy. This observation is expected for CO_2 with buoyancy causing up-dip migration.
2) The velocity change is not homogeneous between the wells, with a larger change, and therefore a larger residual CO_2 saturation, in the downdip half of the tomogram.
3) The velocity change does not reach the actual top of the C-sand, which is in agreement with observed permeability reduction near the top of the sand.
4) The velocity change on the right half of the tomogram is somewhat layered with a larger change in the lower part (about 3 m thick) of the plume. This observation implies that lower part of the plume has higher saturations, presumably due to the presence of a low permeability zone in the center or upper part of the plume.

The large VSP reflection response was somewhat unexpected because of the thinness of the CO_2 plume (about 5–7 m thick at 1500 m depth), and the uncertainty in the rock physics model. Two "post-injection" VSP data sets were then calculated. The "time-lapse" VSP response was calculated using the same processing as the field data, with the exception of amplitude calibration to a shallower reflection, which is unnecessary for numerical data with no shallow changes. To obtain the post-injection model, we first applied the change

DE-FC26-01NT41234

in velocity, as mapped by the crosswell tomogram, to the 30-m wide zone between wells. This result underestimated the reflection amplitude change measured by the VSP. We then extended the velocity change beyond the wells using a 400 m/s velocity decrease (typical of that seen in the crosswell tomogram) applied to a 4-m thick zone over the horizontal distance predicted to contain CO_2 by the flow modeling. This result overestimated the reflection amplitude change. These two modeled time-lapse VSP responses bound the field measurement. This demonstrates that velocity changes, on the order of those imaged by crosswell tomography, when they are extended beyond the interwell region, are able to generate the large reflection amplitude change observed in the VSP. This result demonstrates that small CO_2 volumes (such as those migrating away from a major injection) are detectable in saline aquifers.

Toward cost-effective seismic imaging. Although VSP and crosswell seismic is being effectively used worldwide it is not being used at the same scale as surface seismic. As subsurface targets become more difficult or the needs become greater due to dwindling supplies of oil and gas there will be a need for higher resolution imaging. The lack of use is often driven by the cost/benefit ratio of the information. The cost is perceived as high due to the cost of access to the subsurface, either in down time of production wells or in direct costs of carrying out the work. In addition to expense being one of the deterrents to VSP, often boreholes are not available to perform VSP. Almost all of the commercial vendors are using instrumentation that is based on "large-scale technology," thus driving up the costs. Although the above case histories show that high-resolution data can be useful, in order to more widely use VSP there is a need to emplace sensors cheaply and reliably in the subsurface. Microdrilling is anticipated to provide the means to do so. Reduced costs for subsurface access will open up a whole new means and industry for reservoir monitoring and characterization. It could have the impact similar to that of 3D seismic, and be the catalyst for the next generation of subsurface imaging.

To achieve this goal it is more than just providing a cheap hole. New drilling technology using coil tubing offers great promise in drilling low cost dedicated holes for characterization and monitoring. Also required is addressing data acquisition and processing using these small holes. Much of the technology exists today to achieve many of these goals. To a large degree it is a matter of tailoring this technology for a particular use rather than starting from scratch. Therefore, over the last several years LBNL has been pursuing an integrated program of modeling, instrumentation evaluation/testing, data acquisition, and processing using microhole technology. This effort is tightly coupled with the microdrilling program at LANL and industry partners with field testing at various sites of opportunity.

Presented here are results of VSP microhole tests at the Rocky Mountain Oil Test Facility (RMOTC) using commercial instrumentation modified for microholes. Tested were such things as how to adapt processing for imaging beneath and ahead of shallow holes. For example can one use shallow (300–500 m) to image effectively to several thousand meters? Also explored were such issues as improvement in signal-to-noise ratio over "big" holes (microholes have a much smaller invasion zone), the bandwidth of signals, pressure versus particle motion sensors, improved tube wave damping, clamping effects, cable noise, ease and speed of equipment deployment, and multidimensional imaging.

A small (15-000 lb force) P-wave vibroseis was used as a source in conjunction with three microholes drilled by LANL. The holes were drilled to approximately 300 m each (red stars in Figure 14). A string of 48 vertical geophones (5-m spacing) were successively put in each well. After the geophones were emplaced, approximately 50 shotpoints were taken for each survey. The data acquisition was standard vibroseis with a sweep of 20–200 Hz. It is important to note, however, the very short deployment time and ease of emplacement of the geophone string. The average time to deploy and be ready for recording was about a half hour. No cranes, rigs, or large winches are needed. All tools are "hand deployed" (total weight of the 48-level, 1500-ft string is 250 lbs). The clamping mechanism is a "vacuum assist" method that shrinks to fit easily down the hole and then expands once the vacuum is removed. This would not be possible in normal size holes. The speed and ease of the deployment with just two people made it easy to move from hole to hole in less than an hour. The time from the last vibroseis shot at one hole to the first shot at the next hole was less than one hour. The VSP data are higher in frequency content and have reflections over five times the hole depth of the microwells (Figure 15). In addition, looking at the target depths of less than 100 m, the reflections in the VSP data are much stronger (better signal-to-noise ratio) than the surface seismic.

Suggested reading. "Integration of Rock Physics and Reservoir Simulation for the Interpretation of Time-Lapse Seismic Data at Weyburn Field, Saskatchewan," by Brown (MSc thesis, Reservoir Characterization Project, Colorado School of Mines, 2002). "Midale reservoir fracture characterization using integrated well and seismic data, Weyburn Field, Saskatchewan," by Bunge (MSc thesis, Reservoir Characterization Project, Colorado School of Mines, 2000). "Orbital vibrator seismic source for simultaneous P- and S-wave crosswell acquisition" by Daley and Cox (GEOPHYSICS, 2001). "Multicomponent seismic characterization and monitoring of the CO_2 flood at Weyburn Field, Saskatchewan" by Davis et al. (*TLE*, 2003). "Pressure and fluid saturation prediction in a multicomponent reservoir, using combined seismic and electromagnetic imaging" by Hoversten et al. (GEOPHYSICS, 2003). "Measuring permanence of CO_2 storage in saline formations: the Frio experiment" by Hovorka et al. (*Environmental Geosciences*, 2006). "Coiled tubing deployment makes crosswell seismic surveying successful in horizontal wells" by Li and Majer (*TLE*, 2003). "High-resolution crosswell seismic imaging between horizontal wells" by Li and Majer (CSEG *Recorder*, 2002). "Weyburn field horizontal-to-horizontal crosshole seismic profiling: Part 3 – Interpretation" by Li et al. (SEG 2001 *Expanded Abstracts*). "Weyburn field horizontal-to-horizontal crosshole seismic profiling: Part 1 – data acquisition" by Majer et al. (SEG 2001 *Expanded Abstracts*). "Weyburn field horizontal-to-horizontal crosshole seismic profiling: Part 2 – Processing" by Washbourne et al. (SEG 2001 *Expanded Abstracts*). "Greenhouse gas sequestration in abandoned oil reservoirs: The International Energy Agency Weyburn pilot project" by White et al. (*GSA Today*, 2004). TLE

Acknowledgments: The work was supported by the U.S. Department of Energy Fossil Energy Oil and Gas program, Coal Program, and by the Petroleum Technology Research Centre of Regina, Saskatchewan, in collaboration with EnCana Resources (the operator of the Weyburn oil field), Natural Resources Canada, Alberta Energy Research Institute, Saskatchewan Industry and Resources, the European Community, and 10 industrial sponsors.

Corresponding author: elmajer@lbl.gov

DE-FC26-01NT41234

Passive seismic monitoring using Gaussian Beams with application to borehole data from the San Andreas Fault at Parkfield, California

Susanne Rentsch, Stefan Buske, Jörn Kummerow and Serge A. Shapiro, Freie Universität Berlin*
J. Andres Chavarria and Alexander Goertz, Paulsson Geophysical Services, Inc. (P/GSI)

Summary

Determining accurate and fast event locations is an important task in earthquake seismology and reservoir characterization. In this paper we present an efficient and robust location method that allows for real time monitoring within large models. The method is based on a recent algorithm we developed that makes use of migration techniques with Gaussian beams that can become expensive for fine grids. Here we present an implementation that makes use of selective ray tracing along principal directions of propagation to decrease computational costs. We applied this enhanced location method to a natural seismicity dataset recorded with a deep borehole array of 80 three-component receivers in the San Andreas Fault Observatory at Depth.

Introduction

In addition to regional earthquake observatories, interest in passive seismic monitoring has increased in the last few years within the oil and gas industry. For analysis of passive seismic data we recently proposed a procedure for the fast location of seismicity using migration of multicomponent data (Rentsch et al., 2004, 2005). This procedure only requires the selection of a time window around a detected event making it less sensitive to picking accuracy than standard location procedures. This in turn allows for the algorithm to be implemented as a highly automatic location procedure. This method has been designed for applications where real time monitoring is important, for example, reservoir characterization (i.e. hydrofrac mapping), and earthquake location in regions with natural tectonic activity. Seismically active areas of this sort, like the San Andreas fault system, are usually on the order of several cubic-kilometers and much larger than the reservoir scale. The use of migration methods for event location may require fine volume discretization that can be computationally expensive if a high resolution is expected. This challenged our migration based location method in terms of real time application. For this reason we implemented a modification to the algorithm by which we increase the runtime efficiency while preserving the spatial resolution. In the next section we describe this procedure and present encouraging results from an earthquake dataset recorded in a deep borehole in the central San Andreas Fault in Parkfield, California.

Location Method

Our approach for the automatic location of seismic sources uses Gaussian-beam migration of multicomponent data. This migration type approach requires a preliminary time window selection around the onset of a detected P-wave instead of precise picking of P- and S-wave arrival times. The length of this window can be in the order of a few dominant periods of the P-wave, it should at least contain the full waveform of the P- wave and if possible not the S-wave. However, since this method is designed for three component data the S-waves can be identified and suppressed automatically by a polarization analysis.

Every time sample within the selected window is treated as part of the direct P-phase, and its polarization information is estimated and used to perform initial-value ray tracing. The energy of the time sample is weighted using Gaussian beams around these rays which restricts the back-propagation to the physically relevant regions only. For details we refer to Rentsch et al. (2004, 2005). Finally, a summation (stacking) of the back-propagated energy of all time samples and receivers leads to regions of maximum energy in the resulting image which represents the event location. This approach however may carry the disadvantage that for densely discretized models the runtime may increase in ways that may make the algorithm not suitable for real time monitoring.

In order to increase the runtime efficiency of the current method we have developed a scheme to decrease the number of rays being backpropagated. Instead of tracing a ray for each time sample of the preselected time window we average the polarization information in order to obtain a single polarization vector. Therefore we make use of auto- and cross-variances of three-component data u_x, u_y and u_z in the preselected time interval containing N time samples as proposed by Jurkevics (1988):

$$C_{ij} = \left[\frac{1}{N} \sum_{s=1}^{N} u_i(s) u_j(s) \right] \tag{1}$$

where i and j represent the component index x, y, z and s is the index variable for a time sample. The 3×3 covariance matrix

$$\mathbf{C} = \begin{pmatrix} C_{xx} & C_{xy} & C_{xz} \\ C_{xy} & C_{yy} & C_{yz} \\ C_{xz} & C_{yz} & C_{zz} \end{pmatrix} \tag{2}$$

is real and symmetric and represents a polarization ellipsoid with best fit to the data. The principal axis of this ellipsoid can be obtained by solving $\mathbf{C}$ for its eigenvalues $\lambda_1 \geq \lambda_2 \geq \lambda_3$ and eigenvectors p_1, p_2, p_3:

DE-FC26-01NT41234

$$(\mathbf{C} - \lambda\mathbf{I})\mathbf{p} = 0 \tag{3}$$

where $\mathbf{I}$ is the identity matrix. When calculating the polarization ellipsoid for a small time window (that includes a few dominant periods) around the P-wave the eigenvector p_1 with the largest eigenvalue λ_1 represents the propagation vector of the P-wave.

As a measure of quality control we use the rectilinearity κ of the calculated eigenvalues:

$$\kappa = 1 - \left(\frac{\lambda_2 + \lambda_3}{2\lambda_1}\right). \tag{4}$$

For an ideal P-wave the rectilinearity is 1.0. To exclude unreliable polarization estimates we remove receivers with low values of rectilinearity, i.e. $\kappa < 0.7$, from the location process.

At receivers that pass the rectilinearity test we use the eigenvector p_1 as the starting direction for raytracing. The eigenvector does not account for the sign of the first motion which means that we get the same vector by reversing the three-component signal. In this way the obtained eigenvector is treated as a bidirectional vector, which results in the tracing of two rays, with opposite directions from each receiver. The energy back-propagation is then performed cumulatively. This means first we are stacking the energy of the time interval for each receiver:

$$E_{Receiver} = \sum_{s=1}^{N} \left(u_x^2(s) + u_y^2(s) + u_z^2(s)\right) \tag{5}$$

where u_x, u_y and u_z are the amplitudes of the three components. Then we propagate this energy backward in space along the two traced rays from each receiver using Gaussian-beam-type weighting factors for each image point as described in Rentsch et al. (2005):

$$E_{Receiver}(x, y, z) = E_{Receiver} \cdot \exp\left(-\frac{r^2}{b^2}\right). \tag{6}$$

The weighting is controlled by the perpendicular distance r of the image point (x, y, z) from the corresponding ray as well as by the width of the Gaussian beam b. The width of the Gaussian beam increases similar to Fresnel zones (Kravtsov and Orlov, 1990; Ishimaru, 1978) with increasing raylength and increasing wavelength to take into account the location uncertainty with increasing travel path. Finally, a summation of all image values over all receivers is done:

$$M(x, y, z) = \sum_{Receiver} E_{Receiver}(x, y, z). \tag{7}$$

This summation yields regions of distinct stacked energy and the region with maximum stacked energy is assumed to represent the hypocenter of the event as mentioned above.

Finally, tracing only two rays per time interval of each receiver instead of one ray per time sample makes the whole location process much more efficient. We have applied the method described above to a recently acquired data set from the San Andreas Fault Observatory at Depth (known as SAFOD) which is described below.

Data

The San Andreas Fault Observatory at Depth consists of a vertical pilot well and a deep deviated well that intersected the fault within the hypocentral region of repeating M∼2 earthquakes (Hickman et al., 2004), which we call target-earthquakes in this paper. From April 28th, 2005 to May 11th, 2005, Paulsson Geophysical Services Inc. (P/GSI) installed an 80 level array of 3C 15Hz seismometers in SAFOD to monitor the seismicity of the active transform fault. During this period of time the array recorded numerous events that included one of the project's target-earthquakes, deep non-volcanic tremors and surface explosions. The 15.24 m spacing array was deployed along the deviated portion of the well using production tubing at depths between 878 m and 1703 m below sea level. The recorded signals were sampled at 0.25 ms rate. Basic preprocessing of the data consisted of geophone orientation using particle motions of far-offset shots. Using the obtained receiver orientation the data was rotated into true vertical-, East- and North-components. The rotated seismograms of one detected event are shown in Figure 1. Both, the P- and the S-wave are clearly visible on most of the receivers.

Due to the deviated borehole pointing towards the hypocentral region of target-earthquakes, the array geometry is unfavorable for our location method in case the event we try to locate is a target-earthquake (see Figure 2 and 3). For target-earthquakes the estimated polarization vectors will have dips and azimuths which are similar to the borehole trajectory. The stacking of beams which are almost parallel to each other does not result in a distinct energy maximum at the hypocenter location, but it rather results in a region of maximum energy that has the shape of a beam (see Figure 2). To overcome this problem we do have to use additional infomation like approximate times of P- and S-wave arrivals to restrict the Gaussian beam stack. In detail, we set the width of the Gaussian beam b to zero for all ray segments where the difference between P- and S-wave arrivals do not approximately match the observed one. If the approximate observed arrival time differences match the calculated (see Figure 2, green box), the beam width is defined in terms of Fresnel zones as described above.

Results

In order to locate the event shown in Figure 1 we applied an automated P-wave and S-wave detection algorithm based on the approach presented in Baer and Kradolfer (1987). Prior to locating the events we transformed the receiver coordinate system into a system perpendicular to the San Andreas fault to match the reference system of the velocity model by Thurber et al. (2004) shown in Figure 3. Once the P-wave was detected we selected a

DE-FC26-01NT41234

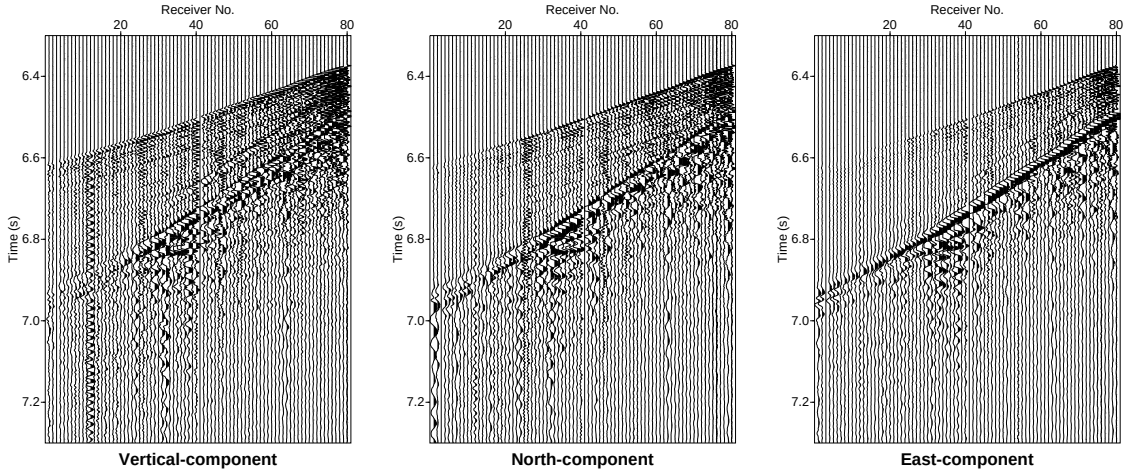

Fig. 1: Traces of one detected event. From left: vertical-, east- and north-component. Receiver No. 1 corresponds to the shallowest receiver and No. 80 to the deepest one, respectively.

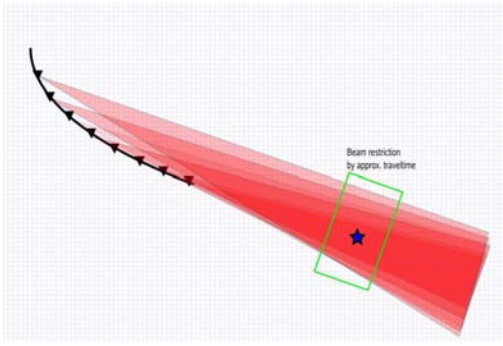

Fig. 2: SAFOD receiver geometry and its relation to our location procedure. A target-earthquake we want to locate is originated somewhere along the elongated borehole trajectory. In order to locate this event we restrict the beams using approximate travel times (green rectangle).

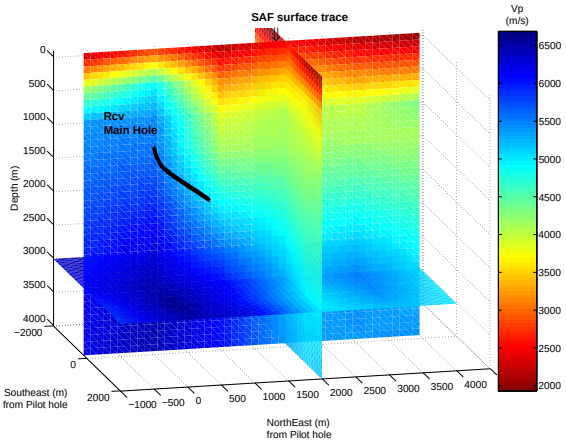

Fig. 3: Velocity model after Thurber et al. (2004).

0.08 s time window around it. The polarization analysis of the selected time interval gave us rectilinearity values close to one for most of the receivers (Figure 4 (top)).

For the event currently analyzed, the estimated dip and azimuth of the polarization vector for almost every receiver follows the dip and azimuth of the borehole (Figure 4 (middle and bottom)). This situation implies that the event shown in Figure 1 lies along the trajectory of the well. It was noted that it constituted one of SAFOD's target-earthquakes, and for locating it, we had to restrict the Gaussian beams with approximate travel time information as described in the previous section. We allowed the deviations between the observed and calculated differences of P-and S-wave arrival times to be in the order of 20 ms.

The image obtained by the Gaussian beam type location using the current velocity model is shown in Figure 5. The back-propagated energy clearly focuses at the hypocenter location at a depth z=2000 m below sea level, x=1400 m Northeast and y=100 m Southeast from the Pilot hole with an uncertainty of 100 m.

Conclusions

We have introduced a computationally efficient and robust earthquake location method based on seismic migration techniques. The method averages the P-wave polarization information over a preselected time window for each receiver and uses it as a starting direction for ray tracing. The location method can be applied in real time to datasets at high resolution irrespective of their spatial scale. The benefit of averaging the polarization is that we do not need to trace a ray for every single sample in the preselected time interval. Stacking of energy along the optimum rays results in small computation times. We applied our migration based location procedure to a recently acquired data set from the San Andreas Fault, near Parkfield. Due to the given acquisition

DE-FC26-01NT41234

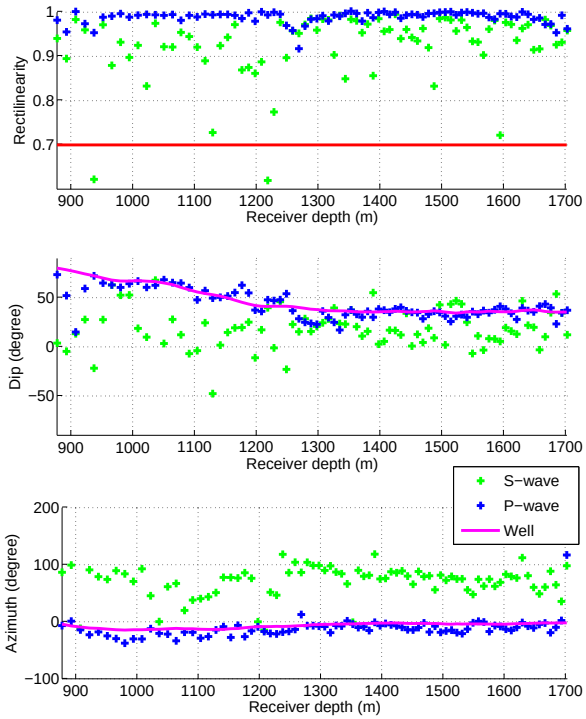

Fig. 4: Polarization analysis of the microearthquake shown in Figure 1: rectilinearity (top), dip (middle) and azimuth (bottom). Blue colors correspond to results obtained from the P-wave and green colors to the S-wave. The red line in the top plot corresponds to the threshold set for quality control. The magenta lines in the middle and bottom plot represent the borehole dip and azimuth at the receiver locations. The azimuths are defined positive clockwise from Northeast.

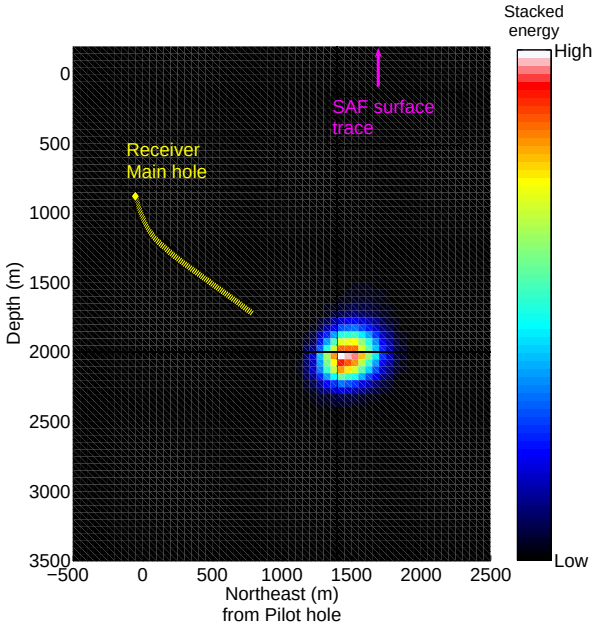

Fig. 5: Resulting image for the target-earthquake. Black and blue colors correspond to small values of stacked energy and red to white colors in the center of this image to large values. The maximum value marks the event location. Yellow diamonds mark the receivers used for location.

geometry we also needed auxiliary information (i.e., approximate travel times) to locate events lying along the trajectory of the SAFOD Main Hole (so called target-earthquakes). The successful location of events, including target-earthquakes, in this segment of the San Andreas Fault, shows the potential of this method for the real time monitoring of fault zones or reservoirs.

Acknowledgments

We thank the sponsors of the *PHASE consortium* for supporting the research presented in this paper. We are also very grateful to Cliff Thurber for providing us with the velocity model. P/GSI thanks the USGS for access to the project and DOE (DE FC26 01NT41234) for funding.

References

Baer, M., and Kradolfer, U., 1987, An automatic phase picker for local and teleseismic events: Bulletin of the Seismological Society of America, **77**, no. 4, 1437–1445.

Hickman, S., Zoback, M., and Ellsworth, W., 2004, Introduction to special section: Preparing for the San Andreas Fault Observatory at Depth: Geophysical Research Letters, **31**, no. L12S01, doi:10.1029/2004GRL020688.

Ishimaru, A., 1978, Wave Propagation and Scattering in Random Media, volume 2: Academic Press, New York, 572 pages.

Jurkevics, A., 1988, Polarization analysis of three-component array data: Bulletin of the Seismological Society of America, **78**, no. 5, 1725–1743.

Kravtsov, Y. A., and Orlov, Y. I., 1990, Geometrical optics of inhomogeneous media: Springer Verlag, Berlin, Heidelberg.

Rentsch, S., Buske, S., Lüth, S., and Shapiro, S., 2004, Location of seismicity using Gaussian beam type migration: 74th Annual International Meeting, SEG, Expanded Abstracts, **23**, no. 1, 354–357.

Rentsch, S., Buske, S., Lüth, S., and Shapiro, S., 2005, Passive seismic monitoring using a migration technique: 67th EAGE meeting, Expanded Abstracts, C023.

Thurber, C., Roecker, S., Zhang, H., Baher, S., and Ellsworth, W., 2004, Fine-scale structure of the san andreas fault zone and location of the safod target earthquakes: Geophysical Research Letters, **31**, no. L12S02, doi:10.1029/2003GL019398.

Interferometric imaging of the San Andreas Fault at Parkfield Using a Massive 3D VSP®

J. Andres Chavarria, Alex Goertz, Martin Karrenbach, Björn Paulsson

The San Andreas Fault Observatory at Depth (SAFOD) has the goal of investigating the physical processes controlling earthquakes in central California at Parkfield. The observatory consists of a deep well that intersected the San Andreas Fault at seismogenic depths of ~3.2 km, where recurring microearthquake activity takes place. Previous to the drilling of Phase II, that intersected the fault at the end of summer 2005, a long array of seismometers was deployed in the deeper part of the well to characterize the fault structure and to aid the monitoring activities of the natural seismicity.

The Massive VSP array consisted of 80 three component seismometers that were deployed during April and May 2005. During this period of time we recorded active data from 13 explosions used to refine the velocity models that improved the locations of target events. In addition to this, we continuously monitored passive data from the natural earthquake activity in the area that was dominated by the Parkfield 2004 event aftershock sequence. During the recording time of this project we were able to record one of the target earthquakes of the SAFOD project as well as recently discovered non-volcanic tremor.

The data recorded by this deep array of seismometers has provided important information to characterize the structure of the fault at scale that is comparable to the scale of the geologic observations. These observations, derived during drilling of the well, consist of cores and cuttings as well as geophysical logs. With the use of the borehole array of seismometers we have been able to directly correlate this lithologic information with seismic phases observed in the VSP data. This has lead to better understanding the nature of the scattering that takes place in this complex fault zone.

Seismic reflections in the dataset were analyzed with Kirchhoff imaging methods to determine a partial image of the San Andreas Fault at depth. Due to the low density distribution of sources in the study area the illumination volume is limited but still shows clear signals originating from sub-vertical structures associated to the strands of the San Andreas Fault inferred from high resolution earthquake location. The existing Kirchhoff imaging methods have been complemented with the use of the use of interferometric imaging by which we extract the Green's function of the data recorded by the array. This takes place with the use of correlation analysis of the data recorded at each level of the array using both active and passive data. This analysis has provided a refined image of the structure of the San Andreas Fault at seismogenic depths with which a better understanding of the system can be achieved.

DE-FC26-01NT41234

High-Resolution Fault Zone Monitoring and Imaging Using Long Borehole Arrays

B. Paulsson, A. Goertz , A. Chavarria, P. Milligan and M. Karrenbach,
Paulsson Geophysical Services Inc., Brea, CA

P/GSI™

Introduction

Large-aperture 3-component borehole seismic receiver arrays are increasingly used in the petroleum industry for high-resolution seismic reservoir characterization. The use of such an array in the San Andreas Fault Observatory at Depth (SAFOD) offers a favorable geometry to image the vertically dipping San Andreas Fault Zone (SAF). In addition, data acquisition within the borehole avoids the highly distorting near-surface weathering layer which leads to a much higher frequency content and vector fidelity of 3-component recordings. On this poster, we will present modeling results and recently acquired seismic data to show how an active-source borehole seismic survey could provide a high enough resolution to localize drilling targets such as rupture patches of repeating micro-earthquakes. Information at this resolution will be necessary to decide on the best location for side-tracks.

Survey Design and Illumination Modeling

We assume a long borehole receiver array with 240 3-component levels placed into the deviated SAFOD main hole. The receiver levels have a spacing of 15.24 m, yielding a total array length of 3.65 km (Figure 1). The survey geometry in Figure 2 is geared towards an ideal illumination of a 4 km by 4 km volume centered between the SAFOD drill site and the SAF. It is optimized by estimating the Fresnel zone at the target depth (the intersection point of the main hole through the SAF). The shot spacing increases with increasing size of the Fresnel zone from 150 m at the wellhead to 350 m on the perimeter.

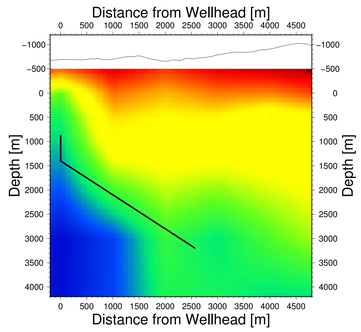

Figure 1: *Approximate location of 240-level receiver array in the SAFOD main hole. Colors denote P-velocities from Thurber et al. (2004)*

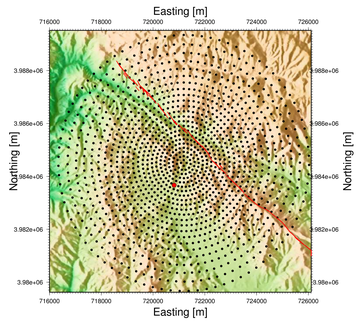

Figure 2: *Optimized shotpoint map of a 3D borehole seismic survey around the SAFOD site.*

We obtain illumination maps by ray tracing in a 3D velocity model (Thurber et al., 2004). The hit-count map on the vertically dipping SAF (Figure 3) denotes the number of reflected rays per bin cell using the survey geometry shown in Figure 1 and Figure 2. The colored area denotes the extent of the image volume. The location of the borehole array is shown as black line. The SAF itself would be imaged down to the penetration depth of the borehole for shots at the surface. Figure 4 depicts the difference between min. and max. incidence angle of reflections off the fault surface. The higher the angular aperture, the better the depth-migrated image of the fault. Furthermore, the angular aperture gives the range over which an Amplitude versus Offset (AVO) analysis is possible.

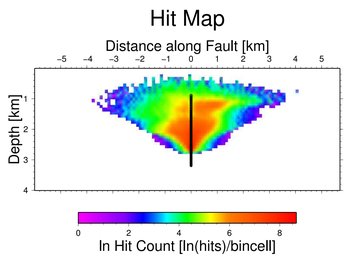

Figure 3: *Hit-count of specular reflections from the vertical SAF. Color scale is logarithmic.*

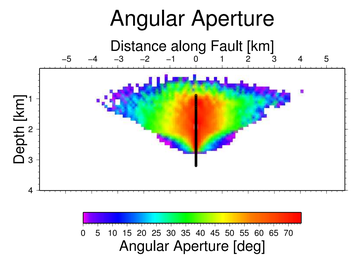

Figure 4: *Difference between min. and max. incidence angle of specular rays on the SAF.*

Real Data Example

In April 2005, an 80-level 3-component (3C) borehole array with 50 ft spacing was deployed in the SAFOD main hole (Figure 5). The 4,000 ft long array was deployed deep within the highly deviated part of the borehole between 5,000 ft and 9,000 ft depth. Aside from recording 13 calibration shots in a 5 km vicinity of the borehole (red squares in Figure 5), the survey also included passively listening to micro-earthquakes from the fault zone over a period of 10 days. The calibration shots consisted of 80 lb of pentolite fired in 100 ft deep shot holes.

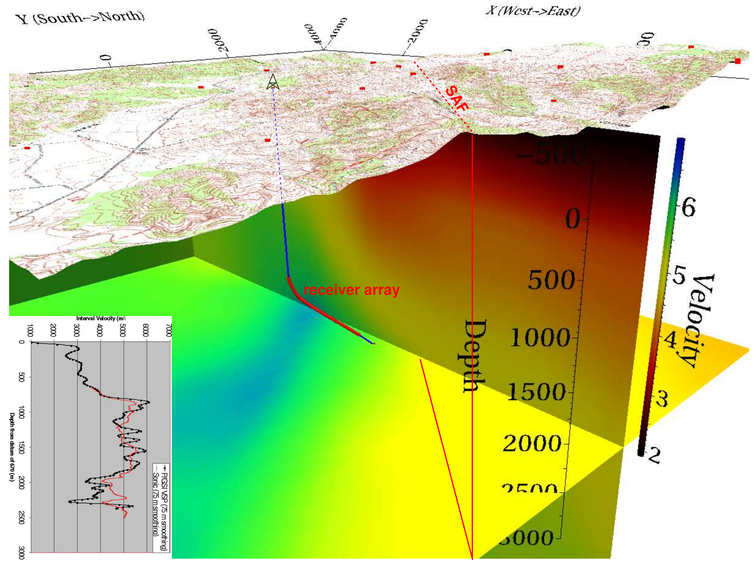

Figure 5: *Aerial view of the SAFOD drill site. The borehole trajectory is shown in blue, and the location of the 80-level receiver array is indicated in red. Background colors denote P-wave velocity values from Thurber et al. (2004).*

Figure 6 shows an example 3C shot gather for one of the calibration shots. Whereas the orientation of the axial component (left panel) is known from the borehole deviation survey, the two radial components are oriented randomly and need to be rotated to a common (true XYZ) coordinate system. After this initial rotation, we can rotate the two horizontal components towards the source (Figure 7). Any shear wave energy is then maximized on one of the horizontal components (right panel in Figure 7), whereas the vertical component (left panel) contains mostly P-wave energy.

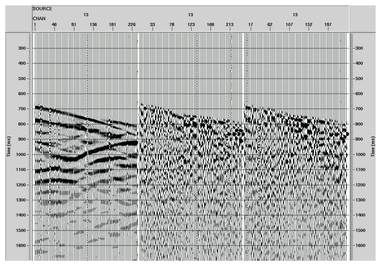

Figure 6: *Raw shot gather of one of the calibration shots (TANK) at an offset of about 1.8 km from the well head. Left panel denotes the axial component and the middle and right panel the raw (unrotated) radial components.*

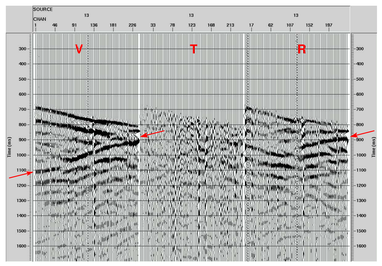

Figure 7: *Same shot than Figure 6 after rotation of the components to true XYZ, and a subsequent rotation of the horizontal components towards the source. Upgoing reflected energy from the fault zone is denoted by arrows.*

Recordings of the calibration shots display distinct upgoing energy which are interpreted to be reflections from the core of the fault zone. Although only sparse coverage is available with 13 shots, these data can be used to obtain a structural image of the core of the fault zone. Such an image will be of great benefit to resolve critical questions about the structure of the fault zone at the depth of the drilling target.

Microseismic monitoring

During the monitoring phase of the experiment, more than 85 micro-earthquakes were recorded from the fault zone, ranging in magnitude from < 0.0 to 2.7. The data example below shows one M0.0 event that happened in the proposed target area for drilling (Figure 8 and Figure 9), and a larger M2.7 event that was actually felt at the wellhead (Figure 10 and Figure 11). The high-resolution data acquired with the long borehole array enables a location of these target events with high precision in order to direct the drilling towards the target hypocentral area.

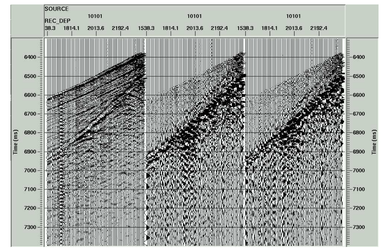

Figure 8: *Raw data of a M0.0 micro-earthquake close to the array. Left panel shows the axial component, and the middle and right panel show the two radial components.*

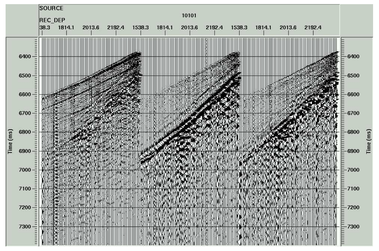

Figure 9: *Same event after rotating the components to vertical (left panel), transverse to the source (middle panel) and towards the source (right panel).*

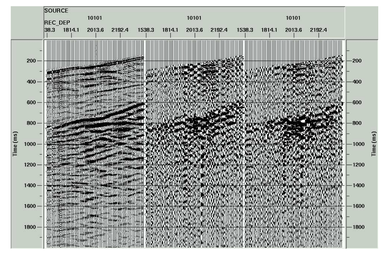

Figure 10: *Raw data of a M2.7 micro-earthquake that was actually felt at the site. Components are displayed as in Figure 8.*

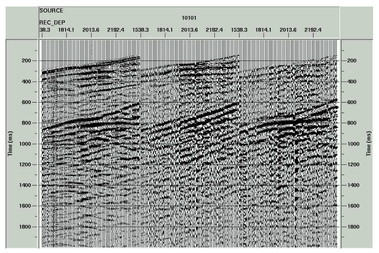

Figure 11: *Same event after rotating the components to vertical and towards the source. Components are displayed as in Figure 9.*

References

Paulsson, B., Karrenbach, M., Milligan, P., Goertz, A., and Hardin, A., 2004, High resolution imaging using 3C data from large borehole seismic arrays: First Break, **23**, 59–69.

Thurber, C., Roecker, S., Zhang, H., Baher, S., and Ellsworth, W., 2004, Fine-scale structure of the San Andreas fault zone and location of the SAFOD target earthquakes: GRL, **31**, L12S02.

Conclusions

A high-resolution image of the surrounding of the main hole is necessary to decide where to place side track drill holes during stage 3 of SAFOD. As shown by the preliminary results from the recent data acquisition, a long borehole array provides the means to obtain a direct reflection image of the vertical fault zone. In addition, the recording of microseismic events will prove most valuable for identifying the exact absolute location of target earthquakes. The deviation of the location of these events from the projected borehole trajectory will directly translate into steering directives for the driller.

DE-FC01NT41234

High resolution 3D seismic imaging using 3C data from large downhole seismic arrays

Björn Paulsson, Martin Karrenbach, Paul Milligan, Alex Goertz, and Alan Hardin of Paulsson Geophysical Services, with John O'Brien and Don McGuire of Anadarko Petroleum Corporation explain why recording multi-component seismic data using receivers positioned deep in the earth, and closer to the target zone, can overcome many of the limitations experienced by surface 3D seismic methods

Borehole seismic surveys, commonly known as Vertical Seismic Profiling (VSP), have been an industry standard technique for several decades. In the past, however, these data have been used primarily for check-shot type velocity surveys and for reflection mapping at the well location in a one-dimensional fashion. This 1D measurement can be extended to 2D by using one or more walk-away lines of surface source points. The 2D method works well enough for imaging simple layered stratigraphy, but in a complex reservoir a full 3D data acquisition and imaging solution needs to be pursued.

Inserting seismic sensors deep into oil and gas wells, as shown in Figure 1, allows the recording of much higher frequencies as compared to placing sensors at the Earth's surface. The reason for this is simple: seismic waves have to propagate only once through the weathered layer in a confined zone near the source. In contrast, during surface seismic surveys, waves must travel through the weathered layer twice. Each traversal of the weathered layer attenuates high frequencies much more than the low frequencies, thus reducing the image resolution. The frequency content of borehole seismic data is typically more than twice that of surface seismic data, which provides an increase in subsurface resolution.

In addition to recording higher frequency data, borehole seismic sensors provide a number of other advantages: borehole seismic data typically achieve a much higher signal-to-noise ratio than surface seismic data. The combination of a quiet borehole environment and strong sensor coupling to the borehole wall enables such high signal-to-noise ratio. Surface geophones, on the other hand, are generally poorly coupled in weathered rock and exposed to cultural and environmental noise at the surface. Good sensor coupling in the borehole enables three-component (3C) seismic data to be recorded with high vector fidelity. This ultimately allows shear and converted-wave imaging as well as the determination of anisotropy by shear wave splitting analysis (see, e.g., Maultzsch, 2003). Combining P and S wave images allows for attribute inversions of rock properties, such as fluid content, pore pressure, stress direction and fracture patterns. O'Brien et al. (2004b) use time lapse borehole seismic to map changes in such critical attributes for production monitoring purposes. Another advantage of borehole seismic surveys is a favourable geometry to illuminate complex structures such as sub-salt targets, salt flanks or steeply dipping faults.

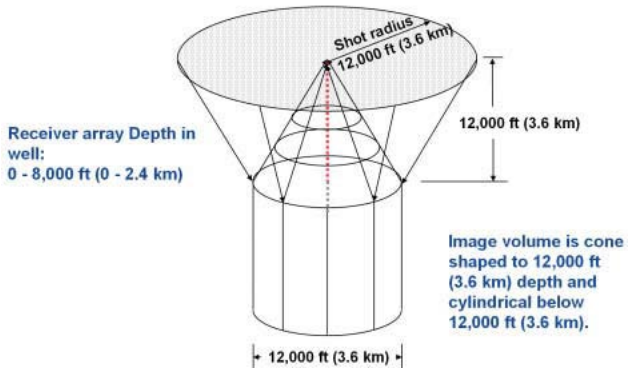

Figure 1 Schematic view of the volume imaged by a 3D borehole seismic survey using one large vertical receiver array and a circular source pattern on the earth's surface.

The 3D image volume that can be generated from a large downhole seismic array data is shown in Figure 1. The typical 3D borehole seismic image volume is cone shaped with the top of the cone coincident with the top receiver in the borehole array. The size of the base of the cone is determined by the depth of the image volume and the offset of the sources.

Wireline based borehole arrays

With all the advantages multi-component borehole seismic data has over surface seismic data, why has the petroleum industry not recorded more VSP data for the express purpose of 3D imaging? The answer is simple: so far, most borehole seismic arrays used on a seven-conductor wireline. Such arrays are too short and have too few channels to economically record the large data sets necessary for 3D seismic imaging. A standard seven-conductor wireline is limited to a maximum transmission bandwidth of about 500,000 bit/second, which limits the number of levels in the borehole to 16 3C levels (48 channels) if a 2 ms sampling rate is used. On the other hand, frequencies of 200 Hz or more can be recorded in a borehole from surface sources (McGuire et al.,

DE-FC26-01NT41234

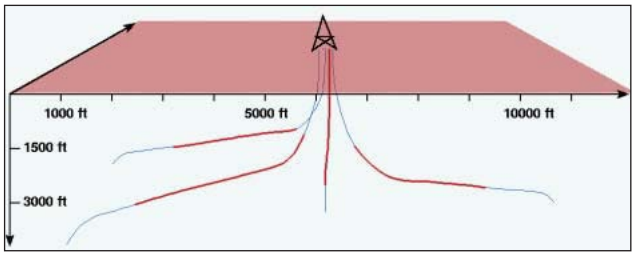

Figure 2 Example of four 80 level receiver arrays deployed simultaneously into four highly deviated wells, starting from a common well pad; active receiver sections are shown in red, and well trajectories are shown in blue.

Figure 3 A work-over rig deploying the production tubing to which the downhole receiver array is attached.

2004). In such a setting, a sampling rate of 1 ms or smaller is required, thus, limiting the number of 3C geophone levels to eight or even to four, if a sampling rate of 1/2 ms is required.

Tubing deployed borehole seismic arrays.

In order to overcome the previous limitations in borehole array technology, both the number of channels simultaneously recorded, and the data transmission rate needed to be increased. These goals have been achieved with a proprietary method deploying 3C geophone sensors attached to downhole tubing and providing a dedicated channel for each sensor component at each receiver level. With the advent of large tubing-deployed arrays, 3D borehole seismic imaging has become a viable and economic option. Images created from these surveys usually surpass surface seismic images in terms of accuracy and resolution. Current tubing-deployed technology makes it possible to deploy up to 1200 channels in one or more wells (O'Brien, 2004). Furthermore, by distributing several large downhole arrays over a larger area, the image volume can be increased. This concept is shown in Figure 2, where four wells were occupied in a survey on the

Figure 4 A geophone pod inside the geophone pod housing. The geophone pod housings are spaced 50 ft, and connected by two tubing joints.

North Slope of Alaska (Sullivan et al., 2002). All wells in Figure 2 are deviated, some of them up to 75^0 from vertical, making it very difficult for cable array deployment without tractors. Tubing-deployed arrays on the other hand can be installed accurately and with ease in highly deviated wells.

The tubing is the structural element in the system and consists of standard production tubing joints that have been manufactured with a length tolerance of +/- 6 mm (+/-1/4 inch). The precise length tolerance and the known mechanical and thermal expansion properties of the tubing allow the precise placement of the receivers into both vertical and horizontal boreholes. The deployment of a long downhole array using a workover rig is shown in Figure 3. Figure 4 shows a close-up view of one geophone pod assembly on the production pipe.

Clamping of receivers is achieved by inflating a bladder located behind a 3C geophone pod. The pressure required for inflation is delivered through the tubing and typically reaches 0.6 - 0.7 MPa differential pressure. As an example of the resulting data quality, Figure 5 shows a raw vertical component shot gather from a survey recorded in July 2004 using the latest generation array technology. The data shown in Figure 5 are recorded from the surface down to a depth of 5500 ft using 25 ft spacing between receiver levels. This was achieved by using a 2000 ft long 80 level downhole array with a 25 ft receiver spacing. The entire array was moved three times and recorded a 2 lb shot of dynamite in 20 ft boreholes each time.

Survey design and pre-survey modelling

One of the challenges in designing a 3D borehole seismic survey is to ensure uniform illumination in the target volume around the receiver wells. As shown by Van Gestel et al.

DE-FC26-01NT41234

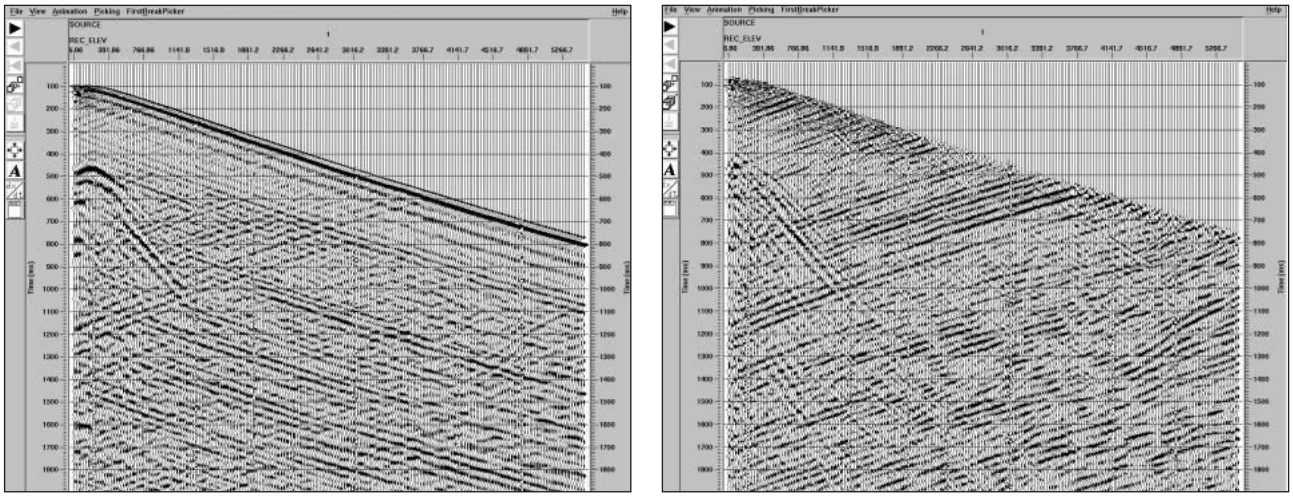

Figure 5 (a) raw unprocessed, and (b) up-going wavefield separated shot record of the vertical component recorded by a long downhole receiver array. There are 320 receiver levels, acquired with an 80-level array in four consecutive deployments. The source consisted of a 2 lb dynamite charge close to the well. Note the high signal to noise ratio on reflected energy in the raw data.

(2002, 2003), a sufficient receiver array aperture (i.e., array length) is critical to ensure artifact-free 3D imaging since the image size and resolution depend on the length and spacing of the borehole receiver array for a given source layout. Generally, the longer the array, the larger the volume over which good illumination can be achieved. At the same time, a dense receiver spacing is needed in order to avoid aliasing at the high frequencies obtained in the borehole environment.

In addition, the target illumination strongly depends on the distribution and spacing of the energy sources at the surface. An optimal placement of source points is necessary to achieve uniform fold coverage in the image volume around the receiver wells. Using the concept of Fresnel Volumes (Kravtsov & Orlov, 1980; Goertz et al. 2003) the minimum bin size is calculated and thus a minimum shot spacing is determined for non-aliased imaging at a given frequency. Given a uniform background velocity model and a single vertical receiver well, this optimization method results in a gradually increasing shot spacing away from the receiver well, as depicted in Figure 6. This adaptive shooting pattern requires approximately 30% fewer shot points compared to a conventional grid of equally spaced source locations while maintaining the same illumination and image resolution.

Figure 6 depicts the survey geometry and the target horizon in a gas reservoir. Pre-survey modelling of the expected hit count and angle coverage was carried out using wavefront ray tracing (Vinje et al., 1996) in an existing 3D velocity model. The hit count is obtained by counting the number of specular rays per bin cell on the target horizon (Figure 7a). Analyzing the hit count gives an estimate of the extent of the conical image volume at the reservoir level based on the

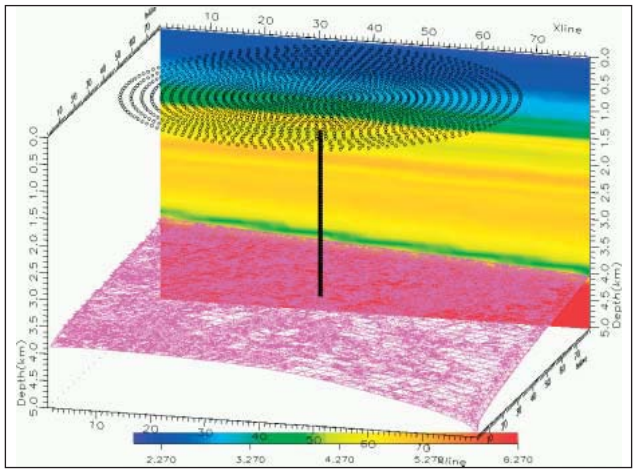

Figure 6 Optimized survey geometry for a single-well seismic survey. The reservoir horizon is located just below the receiver array. P-wave velocities from a 3D model are colour-coded on a slice through the volume. The shot spacing increases with offset from the well head as a consequence of the Fresnel zone coverage on the target horizon.

shape of the horizon and the 3D velocity model. As a rule of thumb, the image area at the target is about half the maximum shot offset (see Figure 1).

Of particular interest in borehole seismic reservoir characterization is the capability to invert the dynamic properties of the reflected wavefield by means of Amplitude versus Offset or Angle (AVO/AVA) analyses. Aside from a controlled recording environment and data processing for the proper handling of seismic amplitudes, this requires a sufficient and uniform aperture within the image volume in order

DE-FC26-01NT41234

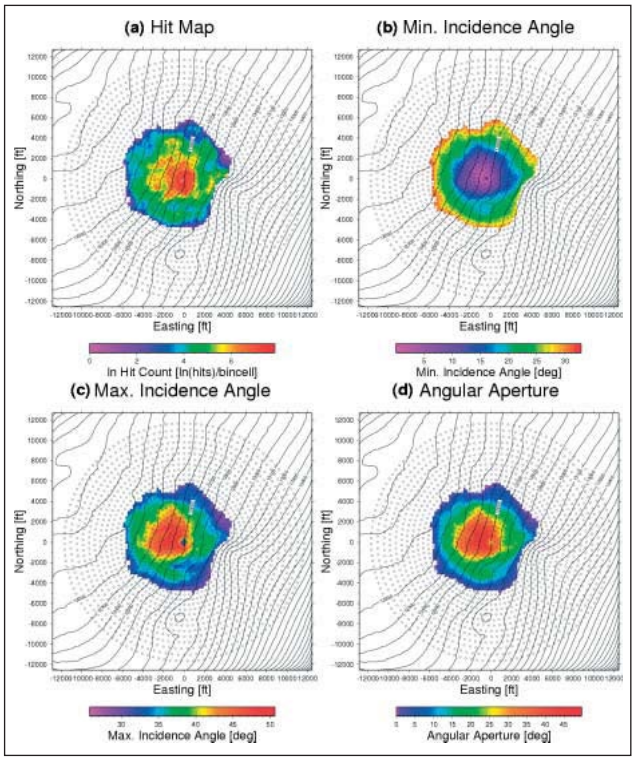

Figure 7 Result from pre-survey modelling for the acquisition geometry depicted in Figure 6. Open circles indicate source points at the surface, and black lines represent depth contours of the target horizon. Part (a) shows the hit distribution, (b) shows minimum incidence angle, (c) shows maximum incidence angle, and (d) shows angular aperture on the target horizon.

to extract AVO gradients over a range of incidence angles. In a borehole, reflection amplitudes are generally measured more reliably than at the surface since the reflected wavefield is not distorted by the weathering layer and often the receivers are clamped to a cemented borehole casing. However, the angular illumination for a 3D borehole seismic survey is typically less uniform than for a surface seismic grid. Therefore, the range of incidence angles observed at each image point has to be assessed beforehand. For such detailed studies, Figures 7b) and c) depict the minimum and maximum incidence angles at which an image point on the target horizon is illuminated. By subtracting the minimum and maximum incidence angle we obtain an angular aperture (Figure 7d), which gives an estimate of the range of angles over which AVA information can be gathered.

Pre-survey modelling is a critical step for ensuring that the 3D reservoir imaging objectives will be met. The parameters that need to be determined in the survey design phase are the receiver array spacing, the receiver array aperture and the source layout needed to image a target reliably with a desired resolution.

3D imaging of large downhole array 3C data

The use of large tubing-deployed downhole receiver arrays enables sufficient aperture and sampling density for high-resolution imaging in 3D. Seismic data using long downhole arrays may have been simultaneously recorded from multiple wells equipped with several hundreds of channels, and these wells may be highly deviated from vertical. Keeping in mind the massive amount of data created from such surveys, it becomes obvious that there must be some departures from traditional VSP data processing.

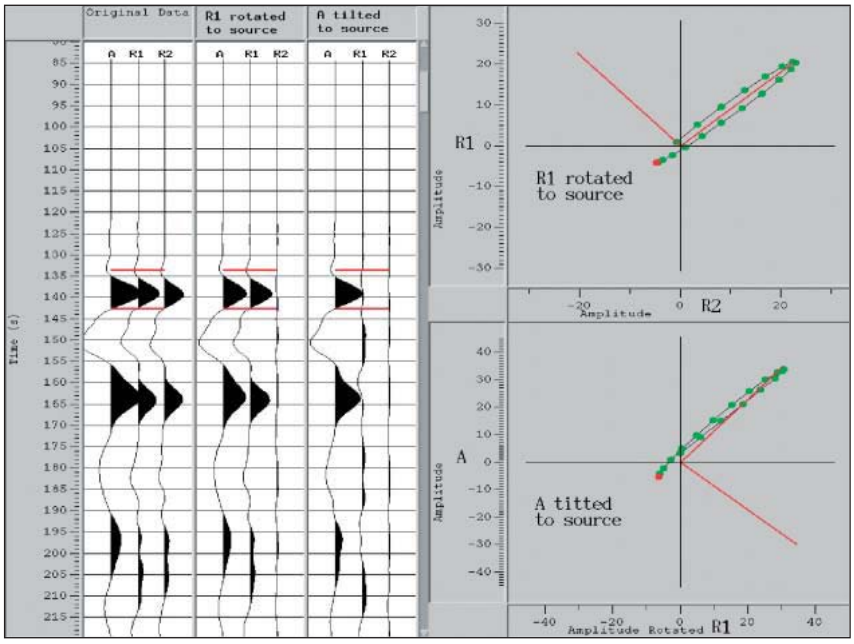

Figure 8 Hodogram analysis is used to determine receiver component orientation. Left trace panel is raw 3C data, with Axial, first radial (R1), and second radial (R2) components respectively. Centre trace panel is after rotation of the R1 component towards the source in the plane perpendicular to the borehole. Right trace panel is after rotating the R1 component, and after tilting the Axial component towards the source. Since the axial component's orientation is known from the well deviation survey, we only need the rotation angle required to maximize source energy in the R1 component, corresponding to the upper hodogram. The Hodograms on the right show excellent vector fidelity.

DE-FC26-01NT41234

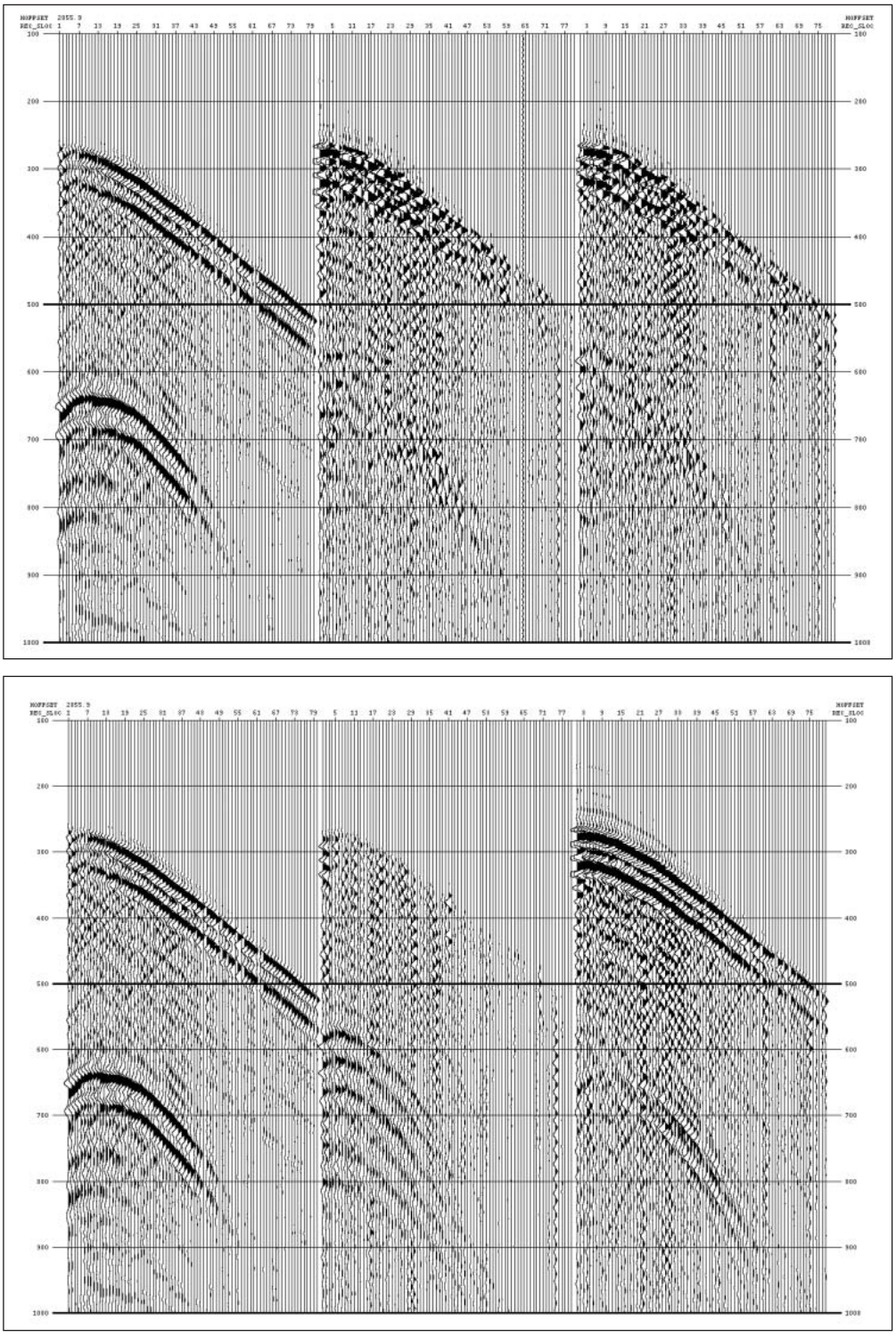

Figure 9 Raw 3C shot record (a) before rotation; components are Axial, Radial1, Radial2; (b) after rotation to true XYZ; the axial component is now vertical (Z), the radial1 component is now pointing due east (X), and the radial2 component is pointing due north (Y). We may re-label these components as V, H1, H2 respectively. This particular source was located 2055 ft due east of the receiver well, so there is maximum direct wave arrival energy on the H2 component, and minimal on the H1 component (which points due north).

DE-FC26-01NT41234

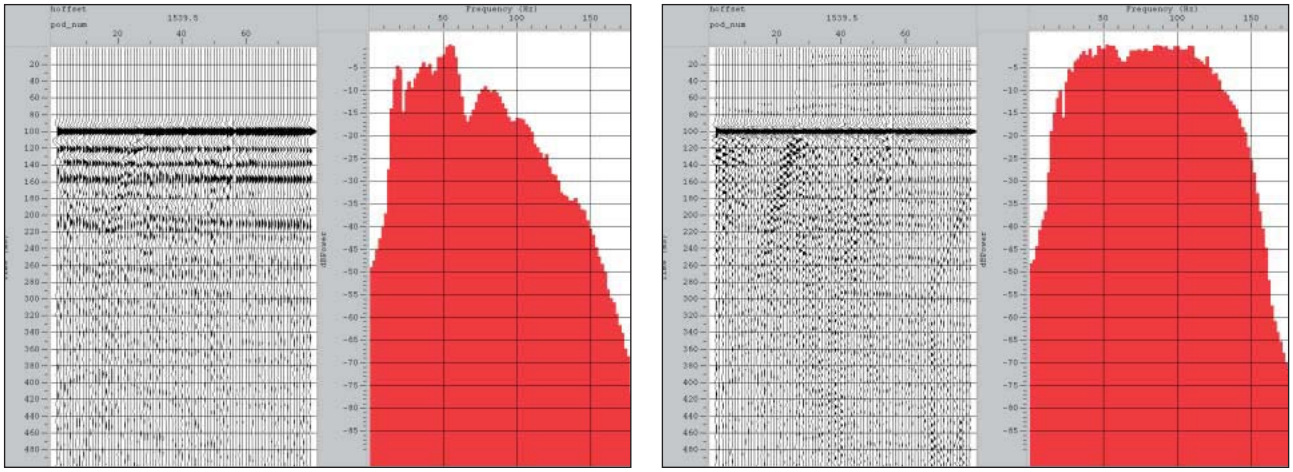

Figure 10 Spectra of a shot record's vertical component rotated towards source and aligned on FB picks; (a) before source signature deconvolution; (b) after source signature deconvolution. In this case we used a zero phase wavelet inversion method based on the first 200 ms.

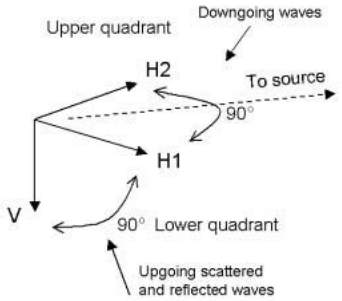

Figure 11 Geophone component orientation used for 3D-3C wavefield separation. The 3-components are oriented so as to split the source azimuth equally between the H1 and H2 components, while the vertical (V) component remains vertical. The desired upgoing wave mode is expected to arrive from anywhere in the lower 3D quadrant in the source direction.

Multi-component orientation

The first departure from traditional VSP processing is the computation of receiver geophone vector orientations. Since arrays do not use gimbal-mounted geophones, the two radial components are randomly oriented after deployment and clamping in the well. However, once deployed and clamped, the long downhole arrays remain in place for the duration of the 3D survey, allowing the orientation of the radial components to be obtained accurately by averaging over a subset of shotpoints.

The orientation of the two radial receiver components is determined with a hodogram analysis on the first-break arrivals for a subset of shot points. For a vertical well, a circle of shot points at similar offset to receiver depth is chosen. Using a full circle helps mitigate the possibility of ray bending caused by lateral velocity changes. However, for a highly deviated well, it is possible to place a walk-over line of shot points directly over the receivers. The advantage of using a walk-over line for hodogram analysis is the relatively straight direct ray paths taken by the first arrivals, leading to less ambiguity in radial component orientation. Figure 8 shows a typical hodogram analysis for receiver component orientation from a single shot point.

Once the hodogram analysis is complete, and all receiver orientations are known, the next major processing step is to rotate the entire 3C raw data set into true XYZ orientation. This results in a new 3C data set with components orientated due east, due north, and vertical, respectively. The separate components of a typical shot gather are shown in Figure 9a before rotation (Axial, radial1 and radial2), and in Figure 9b after rotation to true XYZ (H1, H2, V).

Processing continues with first-break (FB) time picking followed by source signature analysis and deconvolution filter computations. To facilitate both FB picking and source signature analysis, the 3C data are rotated to enhance either the direct P-wave component, or the direct S-wave component. The resulting deconvolution filters are both surface-consistent and deterministic, and result in a common wavelet suitable for pre-stack depth migration (PreSDM). Figure 10 shows an example comparing a typical shot-gather before (a) and after (b) deconvolution and bandpass filtering. The FB pick times are used later for velocity model construction and for computing 3D source statics.

Multi-component wavefield separation

The second main departure from traditional 2D VSP data processing is the method for wavefield separation prior to 3D imaging. Wavefield separation attempts to isolate reflected up-going and scattered energy, which is then used as input to scalar Kirchhoff pre-stack depth migration (PreSDM).

Traditionally, wavefield separation for 2D VSP reflection

DE-FC26-01NT41234

imaging has been done by focusing on primary reflections within the source-receiver vertical plane, either directly by maximizing reflected signal strength, or indirectly by maximizing signals arriving at the expected angle of primary reflections from horizontal layers. Both 3C rotation and array beam steering methods can be used to achieve this.

However, reflection and diffraction energy arrives from many different angles within the volume to be imaged, and all of these arrivals should be used to construct the image. Thus it is desirable to keep the receiver antenna aperture open as wide as possible in all three dimensions to enable recovery of all possible scattered/reflected events. Consequently, the 3D-3C wavefield separation technique accepts the desired up-going wave mode from as wide an incidence angle range as possible (ideally with an isotropic response), while also attenuating the undesired down-going wave mode.

The 3D-3C wavefield separation process begins by rotating the horizontal components towards the source (see Figure 11). The three components are then mathematically combined to accept the desired up-going wave mode with unit response regardless of angle of arrival within the lower 3D quadrant, while also attenuating the undesired down-going wave mode arriving in the upper quadrant. The attenuation is at a maximum if the undesired down-going wave arrives with a 45^0 incidence angle, otherwise it is attenuated with a dipole response curve (see Figure 12). Remaining down-going direct arrival energy is maximized on the first break after deconvolution and can be muted. The polarity of the components are then switched to select the up-going wave mode, i.e., up-going P, or up-going SV, while the complementary down-going wave mode is attenuated. In areas with strong wave mode conversions, there is one caveat: separation of upgoing P-P events can be contaminated by down-going P-S events, and vice versa. If these unwanted wave modes are producing image artifacts after stacking, then tau-p filtering is necessary to suppress them before migration.

In addition, this 3D-3C wavefield separation technique allows the tilting of all 3C axes while maintaining orthogonality, allowing it to deal with the case of a deviated (non vertical) well where a receiver may be directly below a surface source point. At this vertical angle, traditional 3C VSP wavefield separation must resort to velocity filtering, or beam-steering the receiver array, which effectively narrows the receiver antenna aperture and adversely attenuates reflection/diffraction arrivals from elsewhere. This can be detrimental for imaging complex structures in 3D, such as small stratigraphic faults, pinch-outs, or channel edges.

Surface-borehole 3D statics

3D statics for surface-to-borehole seismic are an inherent problem without an accurate shallow layer velocity model. Because all the receivers are usually below the weathered layer and only occupy a small lateral area it is impossible to use established methods, such as refraction arrival move-out or turning ray tomography to map weathered layer velocity or thickness changes over the area covered with source points. Instead, ray-tracing is used to compute the source-receiver direct arrival times in an estimated velocity model. The computed arrival times are compared to the actual FB pick times. Filtered differences between picked and computed arrival times for any one source can be averaged and applied as a static correction, as illustrated in Figure 13.

This model-driven static solution may include corrections for imperfections in the velocity model located between the source and receiver well, instead of being strictly local to the source point. Therefore, a static solution is obtained that is intrinsically tied to a given velocity model, and any velocity model update automatically requires a statics solution update.

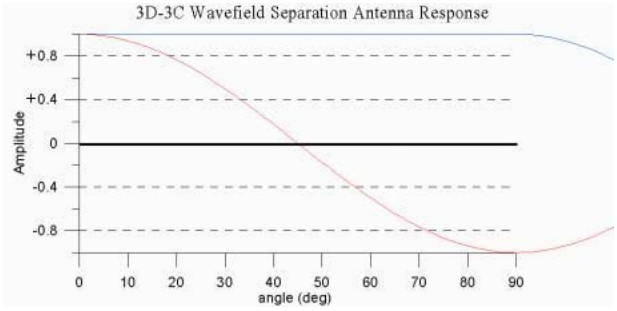

Figure 12 The resulting receiver antenna angular response after wavefield separation. The 0-90° scale represents either the horizontal or vertical plane in the lower or upper 3D quadrant pointed towards the source. The red curve is the attenuation response of the unwanted (down-going) wave. The blue curve is the desired (up-going) wave mode response. It can be seen that at an incidence angle of exactly 45^0, there is maximum attenuation of the down-going wave.

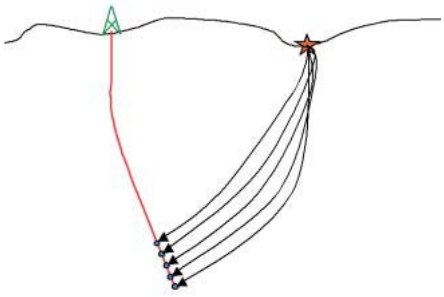

Figure 13 Surface-to-borehole shot statics takes the average of several travel time differences between ray traced arrival times and picked first break arrival times, common to a shot, into a group of (n) lower receiver levels. Static value is a function of the average difference: 1/n (FB computed … FB picked).

DE-FC26-01NT41234

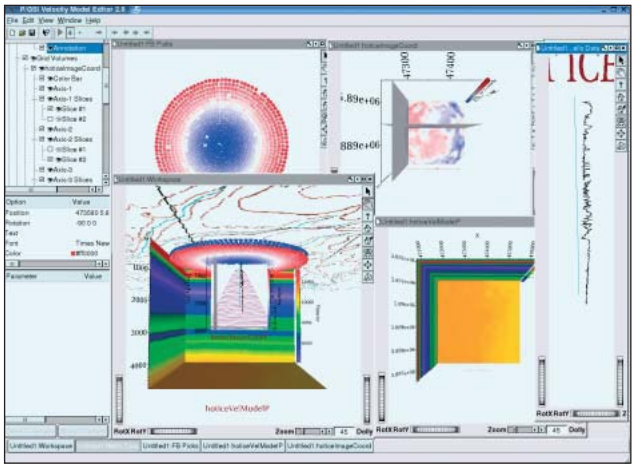

Figure 14 Composite 3D display and detailed views of integrated data sets for velocity model building. Auxiliary information is combined with data and processing results to enable interactive model changes and quality control.

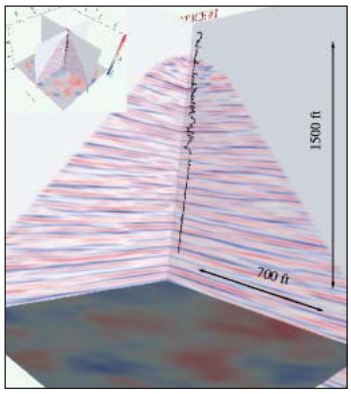

Figure 15 3D view into a high-resolution image of a methane hydrate target from the North Slope of Alaska, including an integrated well log. The well was cased in the upper part and uncased in the lower part. The 3D depth image accurately ties with the well log in minute detail, and allows detailed interpretation away from the well.

Velocity estimation and pre-stack depth migration

Following these pre-processing steps, the wavefield-separated and amplitude-balanced data are pre-stack depth-migrated using a Kirchhoff imaging method. Due to the illumination pattern for a 3D borehole seismic survey, it is favourable to parameterize the migration algorithm in terms of incidence angle at the image point. This allows re-sorting the migrated data into the incidence angle domain such that common-angle gathers can be obtained for both velocity model update as well as AVA studies. For a kinematic structural image, partial pre-stack depth-migrated images are combined to form complete P-P or P-S reflection image volumes.

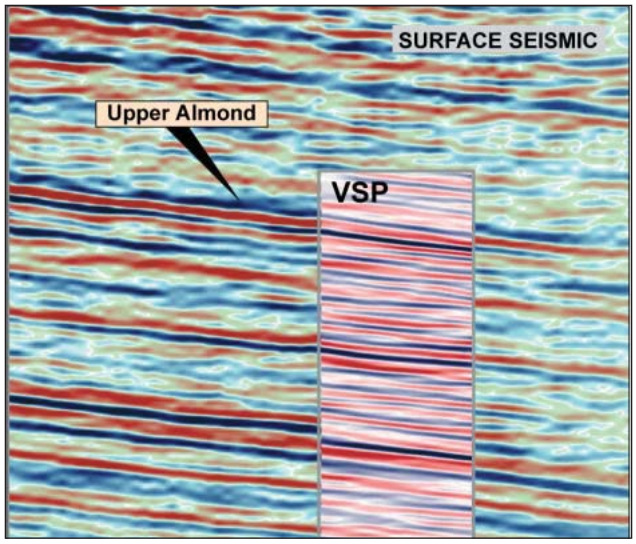

Figure 16 Comparison depth slice of a 3D surface seismic image, with a 3D VSP image slice at the same location. Note the increased resolution and detail of the 3D VSP image.

Depth imaging is sensitive to the velocity model, and great care must be taken in building the 3D velocity volume. An interactive velocity model building tool is used to achieve this in an iterative manner. Both VSP data and geological constraint data are used. Interpreted horizons or other a priori constraints can also be imposed. Both direct-wave and reflected-wave tomography and event move-out analysis in the depth domain are used. Common angle gathers at an image point in the depth domain are used for this move-out analysis.

The velocity model estimation is iterative in nature and uses interactive velocity model manipulation tools (see Figure 14) to produce model updates. It is important to use all auxiliary information available from the survey site, including well logs, formation tops, horizon information, ray path computations, velocity models and migrated image volumes, and to analyze them within a common framework. Only then can the interpretive processing procedures be used efficiently to obtain a velocity model accurate enough for PreSDM. In the following, we illustrate the 3D VSP methodology with two case studies that demonstrate the range of applications this technology is suited for.

High-resolution 3D imaging for methane hydrates exploration

A 3D VSP survey was recorded in February 2004 in conjunction with a continuously cored hydrate exploratory well (Hot Ice #1) on the North Slope of Alaska (McGuire et al., 2004). The purpose of the VSP was to identify and delineate lateral variations in the subsurface within the hydrate stability zone (HSZ) by using high frequency seismic sources arrayed in a 3D surface pattern and a large receiv-

DE-FC26-01NT41234

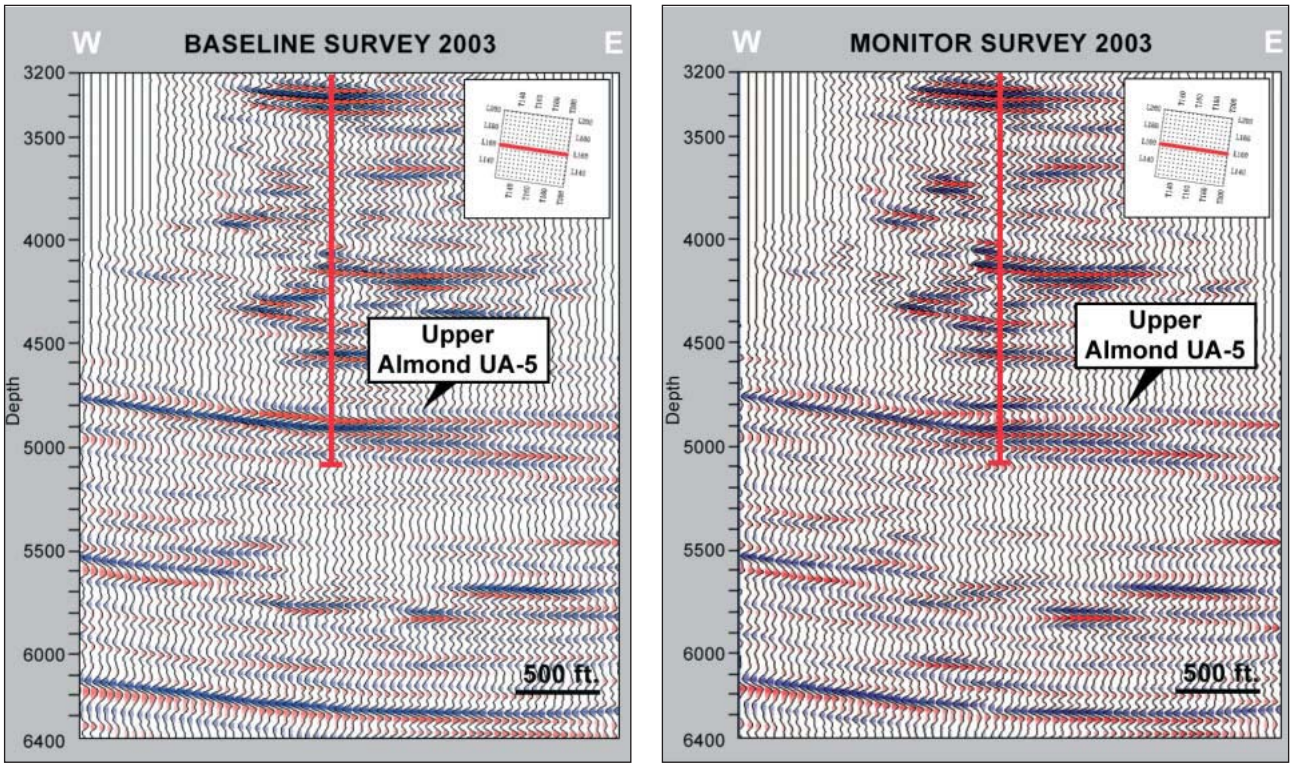

Figure 17 A vertical depth slice through a 3D VSP image from (a) the baseline survey before CO2 injection into the Upper Almond formation, and (b) after CO_2 injection. Note the distinct change in reflectivity around the well.

er array in the wellbore. Pre-survey modelling indicated that only a 3D downhole seismic survey would yield a high enough dominant frequency to successfully image the thin hydrate bearing layers.

The seismic source signal was composed of two 10 second linear sweeps from 8-220 Hz transmitted from each of 1185 surface locations. The seismic data were recorded by an 80-level 3C borehole array with a geophone spacing of 25 ft.

In Figure 14, an integrated, interactive velocity model-building tool has been used to analyze the Hot Ice #1 data. The main window shows the high resolution 3D image volume immersed in the 3D velocity model that was used for the PDSM. The circular source pattern shows colour-coded first arrival times and is displayed together with the sonic log. Figure 15 selects an overall view of the 3D image volume. The sonic log is draped in the centre of the cone shaped 3D image. The depth slice at about 2200 ft depth below the earth surface shows in detail the patchy nature of the amplitude distributions at this target level.

The close-up view into the volume shown in Figure 15 shows the excellent correlation between the well log sonic curve and the depth image. The well log shows two sections of distinct character. The upper section corresponds to the cased portion of the borehole, and the lower section representing the un-cased part of the borehole. The high-resolution 3D image proves consistent over the entire borehole range and correlates very well with the velocity contrasts seen in the sonic curve.

High-resolution time-lapse 3D imaging

In 2001 Anadarko Petroleum Corp initiated a miscible CO_2 enhanced oil recovery project in the Monell Unit of the Patrick Draw field in Wyoming, as reported in O•Brien et al. (2004). The objectives of this project were to test the injection process and the response of the reservoir to CO_2 injection. As part of the project, movement of the CO_2 front was monitored by time-lapse 3D VSP using a large downhole array.

A baseline 3-D VSP survey was acquired in the Monell 180 ST-1 well in January 2002 using a large downhole array, and the survey was repeated in June 2003 after 18 months of CO_2 injection. For both the baseline and monitoring surveys, a borehole array consisting of 80 receiver levels at 50 ft spacing was placed from the near-surface to a depth of approximately 4300 ft depth. A vibroseis source generated a source signal from 8 -180 Hz. Source locations extended with full azimuthal coverage to a maximum offset of about 5000 ft away from the well.

Figure 16 shows a data comparison between a surface seismic image and the 3D VSP image. While the surface seismic data have good bandwidth up to 60 Hz at these shallow

DE-FC26-01NT41234

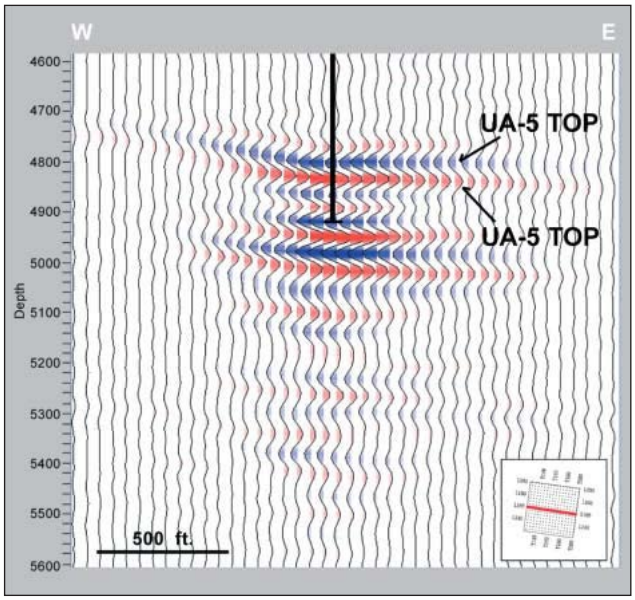

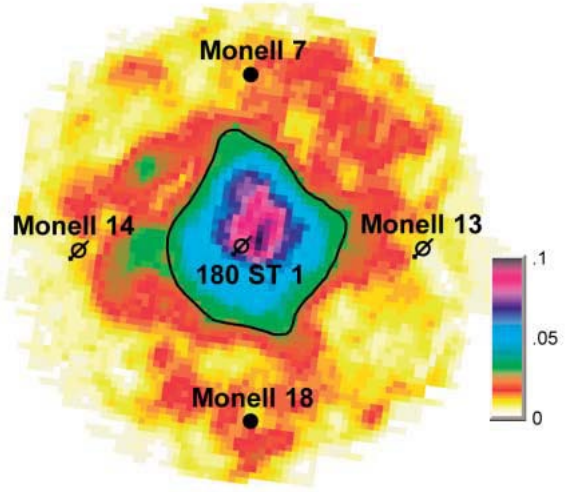

Figure 18 a) A vertical slice at the well through the 4D cross-equalized difference between the baseline survey and post CO2 injection survey images. Note that in addition to the changes in reflectivity in the Upper Almond layer, there are also apparent changes in lower layers, and these are caused by •push-downŽ of these reflection events because of the post-CO2 injection velocity changes. b) A horizontal amplitude map along the Upper Almond Top UA-5 delineates in great detail and with high-signal to noise ratio the extent and direction of the CO2 flooding that occurred within 18 months.

depths, the VSP data have a significantly higher frequency content and vertical resolution that provide more detailed imaging.

Figure 17a and b show the resulting vertical east-west slices through the 3D image volume for the baseline and monitoring surveys respectively. The images provide an excellent view of Upper Almond UA-5 reservoir and allow a detailed comparison of amplitude changes due to CO_2 injection. In Figure 18a the monitor data were cross-equalized and subtracted from the baseline data clearly delineating changes within the 42 ft reservoir interval which are attributed to the CO_2 flood. Figure 18b shows a map view of the time-lapse amplitude difference at the reservoir level. The CO_2 injection occurred in the Monell 180 well in the center. The acoustic properties of the reservoir are changed slightly as the CO_2 flood advances through the formation, giving rise to seismic amplitude changes in the 3D image. The time-lapse 3D VSP clearly documents the advance of the CO_2 flood into the reservoir providing information on the rate of advance and the azimuthal uniformity of the flood and also implying that no areas have been left unswept.

Conclusions

The use of large 3C borehole seismic arrays has evolved into a powerful technology for 3D imaging and reservoir characterization. 3D-3C borehole seismic surveys provide data with high vector fidelity and the high frequency content of the data provides imaging detail with superior vertical and lateral resolution. The excellent survey repeatability and the high signal/noise quality enable the implementation of sophisticated dynamic reservoir monitoring techniques. The ability to tie depth seismic data directly with well logs ensures accuracy and reduces uncertainties in 3D images. In contrast to surface seismic data, wave field quantities can be determined directly in depth. Several examples presented in this paper show how this technology is increasingly employed in a target-oriented fashion for the characterization of complex reservoirs that cannot be effectively imaged using surface seismic. Many stratigraphically complex areas require high resolution imaging that can be achieved only by acquiring high-frequency, high-fidelity seismic data within a borehole.

Acknowledgements

We wish to thank Paulsson Geophysical and Anadarko Petroleum Corp for permission to publish imaging results. The surface seismic data are shown courtesy of PGS Onshore. The large downhole receiver technology was supported through co-operative grant DE-FC26-01NT41234 and acquisition of the Hot Ice Methane Hydrate data through co-operative grant DE-FC26-01NT4133 by the US Department of Energy National Energy Technology Laboratory.

References

Bredbeck, T. and Buehring, R. [2003] 3D Vertical Seismic Profiles - Implications for Reservoir Characterization, Lithology and Fluid Detection. EAGE Workshop, Stavanger, Norway.

DE-FC26-01NT41234

Chopra, S., Alexeev, V., Manerikar, A. and Kryzan, A., [2004] Acquisitions/Processing-Processing/integration of simultaneously acquired 3D surface seismic and 3D VSP data. The Leading Edge, 23, 5, 422.

Goertz, A., Mueller, C., Buske, S. and Lueth, S. [2003] Elastic Fresnel-Volume True-amplitude Multicomponent Migration. 65th EAGE Annual Conference, Stavanger, Norway.

Kravtsov, J. A. and Orlov, J. [1980] Geometrical Optics in inhomogeneous media. Springer Verlag.

Maultzsch, S., Liu, E., Li, X.-Y., Daley, T., Queen, J., Cox, D. [2004] Shear-wave splitting analysis of a 3D VSP from the San Juan Basin. 65th EAGE conference, Stavanger, Norway.

McGuire, D., Runyon, S., Williams, T., Paulsson, B., Goertz, A. and Karrenbach, M., [2004] Gas Hydrate Exploration with 3D VSP Technology, North Slope, Alaska. SEG 74th Annual International Meeting.

O'Brien, J., Kilbridge, F. and Lim, F. [2004] Time-Lapse 3-D VSP Monitoring of a CO_2 EOR Flood. SEG 74th Annual International Meeting.

O'Brien, J., Kilbridge, F. and Lim, F. [2004] Time-Lapse VSP Reservoir Monitoring. Submitted to The Leading Edge.

Sullivan, C., Ross, A., Lemaux, J., Urban, D., Hornby, B., West, C., Garing, J., Paulsson, B., Karrenbach, M. and Milligan, P. [2002] A massive 3D VSP in Milne Point, Alaska. SEG 72nd Annual International Meeting.

Van Gestel, J. and Ray, A. [2002] VSP survey design using finite difference modeling, SEG 72nd Annual International Meeting, Expanded Abstracts, 2361-2364.

Van Gestel, J., Hornby, B., Ebrom, D., Sharp, J. and Regone, C., 2003, Effects of changing the receiver array settings on VSP images. SEG 73rd Annual International Meeting, Expanded Abstracts, 2278-2281.

Vinje, V., Iversen, E., Åstebøl, K. and Gjøystdal, H. Estimation of multivalued arrivals in 3D models using wavefront construction …Part I. Geophysical Prospecting, 44, 819-842.

DE-FC26-01NT41234

EDITED REFERENCES

Note: This reference list is a copy-edited version of the reference list submitted by the author. Reference lists for the 2005 SEG Technical Program Expanded Abstracts have been copy edited so that references provided with the online metadata for each paper will achieve a high degree of linking to cited sources that appear on the Web.

Optimized 3D VSP survey geometry based on Fresnel zone estimates

References

Goertz, A., C. Muller, S. Buske, and S. Luth, 2003, Elastic Fresnel-volume true-amplitude multicomponent migration: 65th Annual Conference, EAGE, Extended Abstracts.

Kravtsov, J. A., and J. Orlov, 1980, Geometrical optics in inhomogeneous media: Springer Verlag.

Luth, S., S. Buske, R. Giese, and A. Goertz, 2005, Fresnel volume migration of multicomponent data: submitted to Geophysics.

McGuire, D., S. Runyon, T. Williams, B. Paulsson, A. Goertz, and M. Karrenbach, 2004, Gas hydrate exploration with 3D VSP technology, North Slope, Alaska: 74th Annual International Meeting, SEG, Expanded Abstracts, 2489-2492.

Paulsson, B., M. Karrenbach, P. Milligan, A. Goertz, A. Hardin, J. O'Brien, and D. McGuire, 2004, High resolution 3D seismic imaging using 3C data from large downhole seismic arrays: First Break, **23**, 73-83.

Cerveny, V., and J. Soares, 1992, Fresnel volume ray tracing: Geophysics, **57**, 902-915.

EDITED REFERENCES

Note: This reference list is a copy-edited version of the reference list submitted by the author. Reference lists for the 2006 SEG Technical Program Expanded Abstracts have been copy edited so that references provided with the online metadata for each paper will achieve a high degree of linking to cited sources that appear on the Web.

REFERENCES

Baer, M., and U. Kradolfer, 1987, An automatic phase picker for local and teleseismic events: Bulletin of the Seismological Society of America, **77**, 1437–1445.

Hickman, S., M. Zoback, and W. Ellsworth, 2004, Introduction to special section: Preparing for the San Andreas Fault observatory at depth: Geophysical Research Letters, **31**, doi:10.1029/2004GRL020688.

Ishimaru, A., 1978, Wave propagation and scattering in random media: Academic Press.

Jurkevics, A., 1988, Polarization analysis of three component array data: Bulletin of the Seismological Society of America, **78**, 1725–1743.

Kravtsov, Y. A., and Y. I. Orlov, 1990, Geometrical optics of inhomogeneous media: Springer-Verlag.

Rentsch, S., S. Buske, S. Lüth, and S. Shapiro, 2004, Location of seismicity using Gaussian beam type migration: 74th Annual International Meeting, SEG, Expanded Abstracts, 354–357.

———, 2005, Passive seismic monitoring using a migration technique: 67th Annual Conference and Exhibition, EAGE, Extended Abstracts, C023.

Thurber, C., S. Roecker, H. Zhang, S. Baher, and W. Ellsworth, 2004, Fine-scale structure of the San Andreas fault zone and location of the safod target earthquakes: Geophysical Research Letters, **31**, doi:10.1029/2003GL019398.

DE-FC26-01NT41234